NASA TECHNICAL NOTE

NASA TN D-6258

NASA TN D-6258

A DIFFERENTIAL CORRECTION TECHNIQUE FOR DETERMINING PHYSICAL PROPERTIES OF THE MARTIAN ATMOSPHERE BY USE OF SOLAR OCCULTATION AS SEEN FROM AN ARTIFICIAL SATELLITE

by James R. Williams and H. Andrew Wallio

Langley Research Center
Hampton, Va. 23365

NATIONAL AERONAUTICS AND SPACE ADMINISTRATION • WASHINGTON, D. C. • MAY 1971

1. Report No.	2. Government Accession No.	3. Recipient's Catalog No.
NASA TN D-6258		

4. Title and Subtitle	5. Report Date
A DIFFERENTIAL CORRECTION TECHNIQUE FOR DETERMINING PHYSICAL PROPERTIES OF THE MARTIAN ATMOSPHERE BY USE OF SOLAR OCCULTATION AS SEEN FROM AN ARTIFICIAL SATELLITE	May 1971
	6. Performing Organization Code
7. Author(s)	8. Performing Organization Report No.
James R. Williams and H. Andrew Wallio	L-7601
	10. Work Unit No.
9. Performing Organization Name and Address	125-17-06-04
NASA Langley Research Center Hampton, Va. 23365	11. Contract or Grant No.
	13. Type of Report and Period Covered
12. Sponsoring Agency Name and Address	Technical Note
National Aeronautics and Space Administration Washington, D.C. 20546	14. Sponsoring Agency Code

15. Supplementary Notes

16. Abstract

A least-squares differential correction technique has been developed to determine the physical properties of the Martian atmosphere by use of solar occultation data. The surface pressure, surface temperature, and temperature lapse rate in the atmosphere can best be determined, for a wide range of initial estimates of the parameter values, by observing a wavelength of about 5500 Å (1 Å = 10^{-10} m). This wavelength appears to provide the best and the most rapid convergence in the curve-fitting process for the three atmospheric parameters that were used in the analysis.

17. Key Words (Suggested by Author(s))	18. Distribution Statement
Martian atmospheres Solar occultation Satellites	Unclassified – Unlimited

19. Security Classif. (of this report)	20. Security Classif. (of this page)	21. No. of Pages	22. Price*
Unclassified	Unclassified	70	$3.00

*For sale by the National Technical Information Service, Springfield, Virginia 22151

A DIFFERENTIAL CORRECTION TECHNIQUE FOR DETERMINING PHYSICAL PROPERTIES OF THE MARTIAN ATMOSPHERE BY USE OF SOLAR OCCULTATION AS SEEN FROM AN ARTIFICIAL SATELLITE

By James R. Williams and H. Andrew Wallio
Langley Research Center

SUMMARY

A satellite in a circular orbit about Mars is assumed to be equipped with instrumentation capable of observing the diminution of sunlight passing through the atmosphere at grazing incidence to the Martian surface. A differential correction technique utilizing a least-squares method of data fitting has been used in conjunction with a model of the Martian atmosphere to determine the surface pressure, surface temperature, and temperature gradient. In the visible spectrum a wavelength of 5500 Å (1 Å = 10^{-10} m) produces the quickest convergence for the widest range of varied initial conditions of the three parameters under consideration.

INTRODUCTION

Before a scientific payload can be soft-landed on Mars at precise locations, a better knowledge of the physical properties of the Martian atmosphere is required. One technique which could serve as an independent method in determining such atmospheric properties as pressure scale height, surface pressure, surface temperature, and temperature lapse rate (defined as the negative of the temperature gradient) is outlined in reference 1. This technique utilizes a photometer aboard an artificial satellite to measure the variation in light intensity from the sun as the light passes at grazing incidence through the Martian atmosphere.

Reference 1 demonstrates that the occultation technique allows ready discernment of differences in the curves of light intensity variation for various models of the atmosphere. The present paper investigates the problem of extracting the atmospheric properties of surface pressure, surface temperature, and temperature lapse rate if a measured curve of the light intensity variation is given. The purpose of this study is to determine whether a first-order differential correction technique is adequate to determine these physical properties of the Martian atmosphere.

In order to accomplish this a Taylor expansion of the equation of light intensity variation is truncated after the first-degree terms, and a least-squares fit is made to the data on the basis of an initial estimate, to determine the increments for the atmospheric properties that are to be used as the input conditions for the second iteration. This process is repeated until convergence criteria are met.

As in reference 1, the factors which determine the mathematical model for the light intensity variation are hydrostatic equilibrium in the atmosphere, refraction through the atmosphere, limb darkening and finite size of the sun, and Rayleigh scattering in the atmosphere. A model using these factors appears to be adequate since recent findings of Mariners VI and VII (ref. 2) indicate that clouds and fog are not prominent in the Martian atmosphere, and therefore multiple and Mie scattering can be neglected.

The technique presented in this paper can be used as a method to determine surface pressure and temperature, pressure scale height, and temperature lapse rate in the atmosphere. The advantage of using this occultation data is that with an attitude control system and cruise orientation similar to that used on the Lunar Orbiter and Mariner spacecraft, one spacecraft axis would be nominally pointed toward the sun, and a properly mounted solar sensor would require no additional attitude control.

SYMBOLS

A	matrix of partials
D	distance from satellite to planet, 8700 km
E	error
g	acceleration due to gravity, 3.7 m/sec^2
h	pressure scale height, TR/mg, km
I(x)	intensity of sunlight passing through Martian atmosphere
I_0	intensity of sunlight in free space
I_x	ratio of I(x) to I_0
$I_{x,i}$	value of I_x at ith point

$l(y)$	factor determining limb darkening and finite sun size
m	average mass of gas, kg/mol
p	surface pressure, mb
R	universal gas constant
r	radius of Mars, km
T	surface temperature, K
V	variable limit of integration
x	coordinate of satellite trajectory, km
y	dummy variable of integration
z	altitude above Martian surface, km
z_{max}	maximum value of z
α	half-angle subtended by sun as seen from satellite, radians
β	Rayleigh scattering coefficient, km^{-1}
Γ	temperature gradient parameter, km^{-1}
λ	wavelength, Å (1 Å = 10^{-10} m)
ω	deviation of light ray from straight line at Martian surface, radians

Primed parameters are estimated values. Parameters prefixed with Δ represent the difference between data and estimate.

ASSUMPTIONS AND ANALYSIS

In this paper the major effects on the variation of the light intensity are differential refraction through the Martian atmosphere, limb darkening of the sun, and Rayleigh

scattering due to the gas molecules in the atmosphere. The mathematical model of these effects is derived in reference 1. Mie scattering and multiple scattering due to clouds or fog are neglected (see ref. 2).

Differential refraction is the divergence of two infinitesimally separated parallel rays which traverse an atmosphere whose index of refraction is a function of altitude.

Limb darkening of the sun occurs because the light which reaches the satellite is the sum of rays from the various parts of the disk of the sun, each ray passing through a different layer of the Martian atmosphere. The effect is a spreading of the curve of light intensity variation and a smoothing of the discontinuities due to the fine structure of the atmosphere. Implicit in limb darkening effects is the consideration of the finite size of the sun.

Rayleigh scattering is the scattering of light by the gas molecules in the atmosphere, where the wavelength of the incident radiation is long in comparison to the dimensions of the molecule. The scattering is dependent on the fourth power of the wavelength and the number and type of gas molecules in the atmosphere.

Thus, for reference 1, the ratio of the light intensity of the sun received through the atmosphere to the light intensity of the sun in free space is given by combining the effects of refraction, limb darkening, and Rayleigh scattering as follows:

$$\frac{I(x)}{I_o} = \frac{\exp\left\{-\beta\sqrt{2\pi r h}\left[\exp\left(\frac{-z}{h}\right)\right]\right\}}{1 + \frac{\omega D}{h}\left(1 + \frac{3}{2}\Gamma h - \frac{5}{2}\Gamma z\right)\exp\left(\frac{-z}{h}\right)} \int_{-1}^{V} l(y)\,dy \qquad \left(0 < z < z_{max}\right) \quad (1)$$

with the auxiliary equation

$$x + \alpha D y = -z + \omega D\left(1 + \frac{3}{2}\Gamma h - \frac{5}{2}\Gamma z\right)\exp\left(\frac{-z}{h}\right) \quad (2)$$

and the variable limits of integration given by

$$V = \begin{cases} 1 & \left(1 \leqq \frac{1}{\alpha D}\left[\omega D\left(1 + \frac{3}{2}\Gamma h\right) - x\right]\right) \\ \frac{1}{\alpha D}\left[\omega D\left(1 + \frac{3}{2}\Gamma h\right) - x\right] & \left(-1 \leqq \frac{1}{\alpha D}\left[\omega D\left(1 + \frac{3}{2}\Gamma h\right) - x\right] \leqq 1\right) \\ -1 & \left(-1 \geqq \frac{1}{\alpha D}\left[\omega D\left(1 + \frac{3}{2}\Gamma h\right) - x\right]\right) \end{cases} \quad (3)$$

For brevity of notation, the following definition is introduced:

$$I_x = \frac{I(x)}{I_o} \tag{4}$$

In this paper it is assumed that the atmosphere is composed of 90 percent carbon dioxide and 10 percent argon. (See ref. 2.) The remaining assumptions are the same as in reference 1.

The dashed curve in figure 1 represents a typical variation of light intensity with distance into the geometric shadow of the planet. Since the constituents of the Martian atmosphere have been assumed, I_x is a function of Γ, p, and T only:

$$I_x = I_x(\Gamma,p,T) \tag{5}$$

The functions Γ, p, and T are the unknown physical parameters that characterize the Martian atmosphere. The technique used in this paper to solve for these parameters consists of assuming a light curve which approximates the observed light curve and for which the parameters Γ', p', and T' are known. (Primed parameters are estimated values.) Now from Taylor's theorem,

$$I_x(\Gamma,p,T) = I_x'(\Gamma',p',T') + \frac{\partial I_x'}{\partial \Gamma'}(\Gamma - \Gamma') + \frac{\partial I_x'}{\partial p'}(p - p') + \frac{\partial I_x'}{\partial T'}(T - T') + \ldots \tag{6}$$

where second and higher order terms have been dropped. By definition,

$$\Delta I_x = I_x - I_x' \tag{7}$$

$$\Delta \Gamma = \Gamma - \Gamma' \tag{8}$$

$$\Delta p = p - p' \tag{9}$$

$$\Delta T = T - T' \tag{10}$$

Equation (6) may be rewritten in a matrix notation as

$$\Delta I_x \approx \left(\frac{\partial I_x'}{\partial \Gamma'} \frac{\partial I_x'}{\partial p'} \frac{\partial I_x'}{\partial T'}\right)\begin{pmatrix}\Delta\Gamma \\ \Delta p \\ \Delta T\end{pmatrix} \tag{11}$$

For brevity let

$$A = \left(\frac{\partial I_x'}{\partial \Gamma'} \frac{\partial I_x'}{\partial p} \frac{\partial I_x'}{\partial T'} \right) \tag{12}$$

Solving equation (11) $\left(\text{under the constraint that } \sum_i \Delta I_{x,i} \text{ is a minimum} \right)$ for $\Delta\Gamma$, Δp, and ΔT yields the least-squares solution

$$\begin{pmatrix} \Delta\Gamma \\ \Delta p \\ \Delta T \end{pmatrix} = \left[A^T A \right]^{-1} A^T \Delta I_x$$

The solid curve in figure 1 is a typical first estimate I_x' of I_x, the dashed curve. Now ΔI_x is computed at approximately 100 points from figure 1. These values, along with the elements of A, are substituted into equation (12) and values for $\Delta\Gamma$, Δp, and ΔT are computed in a least-squares sense. These results are substituted into equations (7), (8), (9), and (10) to obtain new values for Γ, p, and T which are used to generate a new estimate for the I_x' curve. The process is repeated for either 41 iterations or until the error is less than 10^{-7}. The error is defined as

$$E = \sum_{i=1}^{100} \left(\Delta I_{x,i} \right)^2$$

where $\Delta I_{x,i}$ is computed at the ith point.

DISCUSSION AND RESULTS

The values chosen for the assumed measured light-intensity curve are T = 240 K, $\Gamma = -5 \times 10^{-3}$ km^{-1}, and p = 10 mb (1 mb = 100 N/m^2). The surface temperature was arbitrarily chosen between that of an illuminated hemisphere (252 K) and a planet average theoretical temperature (213 K) calculated for solar radiant energy equilibrium (ref. 3). The surface pressure was chosen to be between a low of 5 mb measured by Mariner IV (ref. 2) and the value of 17 mb calculated from spectroscopic observation of the 1.6 μm CO_2 bands (ref. 4). The value of Γ, which is related to the temperature lapse rate $-T\Gamma$, was chosen between the values of -3×10^{-3} km^{-1} and -6.42×10^{-3} km^{-1} obtained from a least-squares fit to the temperature curves of the Martian atmospheric engineering models used by the Viking Project Office.

For the initial conditions, only one of the three parameters was varied while the other two were started at the desired convergence values. The question of varying the three parameters simultaneously for input is essentially considered, because in the second iteration all three parameters are displaced from the desired conditions. Therefore, if the second iteration is considered as the first, all three parameters are varied simultaneously.

Reference 1 pointed out that the shorter visible wavelengths (3500 Å) produced the most readily discernible effects of the light intensity variation. Because of the importance of wavelength and its effect on the results, this paper considers four wavelengths: 3500 Å, 4700 Å, 5500 Å, and 6500 Å.

The results are presented in tables and graphs. The tables list the final convergence values of p, T, and Γ along with their relative errors, and thus provide a quick summary of the results. On the other hand, the graphs of p', T', and Γ' plotted against iteration number provide insight into the rate of convergence to the correct values and the convergence to local minimums.

In figures 2 to 6 the initial p' values range from 2 to 25 mb while the other initial values are $T' = 240$ K and $\Gamma' = -5 \times 10^{-3}$ km^{-1}. The parameters are plotted against iteration number for the four wavelengths under consideration.

Table I summarizes the results of figures 2 to 6.

Figures 2 and 3 illustrate the rate of convergence when p is estimated lower than the desired value. Figure 2 is for an initial value of $p' = 2$ mb, and figure 3 is for an initial value of $p' = 6$ mb. Figures 2(a), 2(b), and 2(c) converge within 3 percent of the desired values of p and T after 40 iterations. (See table I.) The desired value of Γ is being approached in figures 2(a), 2(b), and 2(c); however, its convergence rate is much slower than that of p and T. The temperature gradient parameter Γ is slowly converging in figures 2(a) and 2(b) but after 40 iterations its value is too great, by 20 percent and 25 percent, respectively. (See table I.) In figure 2(c), for $\lambda = 5500$ Å, the value of Γ after 40 iterations is within 1 percent. (See table I.) The same statements as were made about figures 2(a), 2(b), and 2(c) may be made about figures 3(a), 3(b), and 3(c), with 3(c) showing the best convergence after 40 iterations from the point of view of atmospheric physics. Figures 2(d) and 3(d), for $\lambda = 6500$ Å, do not converge to physically acceptable values of Γ and T.

Figures 4, 5, and 6 are plots of the convergence rate for initial p' values of 14 mb, 18 mb, and 25 mb, respectively. Except in figure 6(d), all the values are converging for initial estimates of p' which are too high; however, the case for $\lambda = 4700$ Å converges most slowly, as can be seen in figures 4(b) and 5(b). In figure 6(d) the three parameters are far from correct values after 40 iterations. For the three

cases studied with p' initially estimated too high, the wavelengths that converge best are 5500 Å and 3500 Å. (See table I.) These results, together with the results for the cases in which p' was estimated too low, indicate that 5500 Å is the most acceptable wavelength for determining an accurate p by using a linear estimation technique.

In figures 7 to 10 the initial T' values range from 160 to 320 K while the other initial values are $p' = 10$ mb and $\Gamma' = -5 \times 10^{-3}$ km^{-1}. The parameters are plotted against iteration number for the four wavelengths under consideration.

Table II summarizes the results of figures 7 to 10.

As was true of the first set of figures, Γ is the parameter which is the most difficult to converge. Figures 7 and 8 are convergence plots for the cases of T' estimated lower than T; here $T' = 160$ K and 200 K, respectively. For a T' of 160 K the best convergence for Γ is at a wavelength of 5500 Å. At the end of 40 iterations, figure 7(c) has Γ converged within 11 percent, p within 4 percent, and T within 8 percent. For these percentages and the final values of p, T, and Γ, see table II. For $T' = 160$ K, the p and T values after 40 iterations are better at 3500 Å than at 5500 Å, but Γ converges only within 32 percent at 3500 Å. (See table II.) In figure 8, for $T' = 200$ K, there is convergence within 2 percent of the desired value for all three parameters at both 5500 Å and 6500 Å.

Figures 9 and 10 are convergence plots for T' estimated higher than T; here T' is 280 K and 320 K, respectively. For a T' of 280 K there is convergence for all four wavelengths, with the best convergence for all three parameters occurring at 5500 Å as shown in figure 9(c). Figures 10(a), 10(b), and 10(c) show convergence for all parameters to within 10 percent of the desired value, but in figure 10(d) the parameters fail to converge. (See table II.) However, a wavelength of 5500 Å, shown in figure 10(c), again produces the quickest convergence for a given iteration. For a surface temperature that can be estimated within 33 percent (see table II), a wavelength of 5500 Å appears to be most suitable for obtaining convergence of p, T, and Γ.

In figures 11 to 15 the initial Γ' values range from -50×10^{-3} km^{-1} to 5×10^{-3} km^{-1} while the other initial values are $p' = 10$ mb and $T' = 240$ K. The parameters are plotted against iteration number for the four wavelengths under consideration.

Table III summarizes the results of figures 11 to 15.

Figure 11 presents plots for $\Gamma' = +5 \times 10^{-3}$ km^{-1}, which is of the desired magnitude but has the wrong sign. Only the case with $\lambda = 5500$ Å (fig. 11(c)) converges within 3.5 percent for all three parameters. (See table III.) Figure 12 presents plots for $\Gamma' = 0$ as the initial value. For this case both $\lambda = 5500$ Å and $\lambda = 6500$ Å converge within 2.6 percent for all three parameters. (See table III.) Figure 13 is for an

initial Γ' of -8×10^{-3} km^{-1}. For this case all parameters converge at all wavelengths except $\lambda = 3500$ Å, and even at $\lambda = 3500$ Å only Γ, with an error of 11.2 percent, is not close to the desired value. (See table III.) Figure 14 is for $\Gamma' = -12 \times 10^{-3}$ km^{-1} as the initial value. In figure 14 only the parameters at $\lambda = 3500$ Å do not converge to the desired values. In figure 15 the initial estimate of Γ' is in error by an order of magnitude, or $\Gamma' = -50 \times 10^{-3}$ km^{-1}. The only wavelength for which convergence is attained for all the parameters after 40 iterations is 5500 Å. Thus, for an estimate of Γ within 900 percent a wavelength of 5500 Å appears to be most suitable for convergence of p, T, and Γ.

The results of the convergence figures indicate that a wavelength of about 5500 Å should give the best overall convergence for a wide range of input conditions, when the linear estimation technique is used. At this wavelength the best convergence is obtained for p, the next best for T, and the worst for Γ. Thus, this technique is most sensitive to p, T, and Γ in that order. This is an interesting fact because in other investigations these parameters have been best observed and measured in the inverse order. In a great many studies Γ is taken, to a first approximation, as being zero; that is, an isothermal atmosphere is assumed. The surface temperature can be estimated fairly well by assuming thermal equilibrium of the planet and the sun, and it has also been well measured from polarization studies. The property that has yielded the widest range of measurements is the surface pressure, which varies from a calculated 5 mb (Mariner IV) to a calculated 87 mb (ref. 5).

CONCLUDING REMARKS

A first-order differential correction technique utilizing a least-squares method of data fitting has been applied to the sun occultation light curves to recover the surface pressure, surface temperature, and temperature lapse rate in the Martian atmosphere. The model of light passage in the atmosphere included the effects of refraction, limb darkening, finite sun size, and Rayleigh scattering. The results of this investigation demonstrate that the most suitable wavelength at which to obtain data for quick convergence, even when the initial estimates are in error by 150 percent for surface pressure p, 33 percent for surface temperature T, or 900 percent for temperature gradient parameter Γ, is in the 5500 Å region of the visible spectrum. At this wavelength, the order of best convergence was found to be (1) p, (2) T, and (3) Γ.

This technique of utilizing the occultation of sunlight as seen by an artificial satellite and the differential correction technique to recover atmospheric parameters can be used as an independent method to determine the Martian atmospheric parameters or to provide a check on any other data source.

Langley Research Center,
National Aeronautics and Space Administration,
Hampton, Va., March 29, 1971.

REFERENCES

1. Wallio, H. Andrew; and Williams, James R.: A Feasibility Study of Determining Physical Properties of the Martian Atmosphere by Use of Solar Occultation as Seen From an Artificial Satellite. NASA TN D-5443, 1969.

2. Anon.: Mariner-Mars 1969 – A Preliminary Report. NASA SP-225, 1969.

3. Moroz, V. I.: Physics of Planets. NASA TT F-515, 1968.

4. Owen, T. C.; and Kuiper, G. P.: A Determination of the Composition and Surface Pressure of the Martian Atmosphere. (Aug. 24, 1964.) Commun. Lunar Planetary Lab., Univ. of Arizona, vol. 2, no. 32, pp. 113-132.

5. Danielson, R. E.; Gaustad, J. E.; Schwarzschild, M.; Weaver, H. F.; and Woolf, N. J.: Mars Observations From Stratoscope II. Astron. J., vol. 69, no. 5, June 1964, pp. 344-352.

TABLE I.- SUMMARY OF RESULTS FOR VARIED INITIAL VALUES OF p'

Figure	Wavelength, Å	Initial conditions			Final conditions			Error, percentage		
		p', mb	T', K	Γ', km^{-1}	p, mb	T, K	Γ, km^{-1}	$\frac{p' - 10}{10} \times 100$	$\frac{T' - 240}{240} \times 100$	$\frac{\Gamma' + (5 \times 10^{-3})}{-5 \times 10^{-3}} \times 100$
2(a)	3500	2	240	-5×10^{-3}	9.97	240.4	-5.98×10^{-3}	0.3	0.2	19.6
(b)	4700	↓	↓	↓	9.87	243.6	-6.27×10^{-3}	1.3	1.5	25.4
(c)	5500				9.99	246.8	-5.05×10^{-3}	.1	2.9	1.0
(d)	6500				31.1	1634.6	-4.55×10^{-15}	211.0	581.1	100.0
3(a)	3500	6			9.97	240.5	-5.83×10^{-3}	.3	.2	16.6
(b)	4700	↓			9.90	241.8	-5.67×10^{-3}	1.0	.8	13.4
(c)	5500				9.99	242.4	-5.07×10^{-3}	.1	1.0	1.4
(d)	6500				31.1	1634.6	-4.55×10^{-15}	211.0	581.1	100.0
4(a)	3500	14			10.0	240.1	-4.87×10^{-3}	0	.1	2.6
(b)	4700	↓			10.1	238.2	-4.07×10^{-3}	1.0	.7	18.6
(c)	5500				10.1	236.0	-4.94×10^{-3}	1.0	1.7	1.2
(d)	6500				9.99	238.6	-5.10×10^{-3}	.1	.6	2.0
5(a)	3500	18			10.0	240.0	-4.44×10^{-3}	0	0	11.2
(b)	4700	↓			10.2	237.4	-3.61×10^{-3}	2.0	1.1	27.8
(c)	5500				10.2	231.5	-4.81×10^{-3}	2.0	3.5	3.8
(d)	6500				9.98	237.5	-5.16×10^{-3}	.2	1.1	3.2
6(a)	3500	25			10.0	240.1	-4.75×10^{-3}	0	.1	5.0
(b)	4700	↓			10.1	239.0	-4.48×10^{-3}	1.0	.4	10.4
(c)	5500				10.2	227.2	-4.66×10^{-3}	2.0	5.3	6.8
(d)	6500	↓	↓	↓	10.9	159.2	-14.2×10^{-3}	9.0	33.7	184.0

TABLE II.- SUMMARY OF RESULTS FOR VARIED INITIAL VALUES OF T'

Figure	Wavelength, Å	Initial conditions			Final conditions			Error, percentage		
		p', mb	T', K	Γ', km^{-1}	p, mb	T, K	Γ, km^{-1}	$\frac{p' - 10}{10} \times 100$	$\frac{T' - 240}{240} \times 100$	$\frac{\Gamma' + (5 \times 10^{-3})}{-5 \times 10^{-3}} \times 100$
7(a)	3500	10	160	-5×10^{-3}	10.0	239.8	-3.40×10^{-3}	0	0.1	32.0
(b)	4700				10.2	237.4	-3.58×10^{-3}	2.0	1.1	28.4
(c)	5500				10.4	221.2	-4.47×10^{-3}	4.0	7.8	10.6
(d)	6500		↓		9.97	196.4	-9.13×10^{-3}	.3	18.2	82.6
8(a)	3500		200		10.0	239.8	-3.51×10^{-3}	0	.1	29.8
(b)	4700				10.1	237.6	-3.77×10^{-3}	1.0	1.0	24.6
(c)	5500				10.1	236.5	-4.92×10^{-3}	1.0	1.5	1.6
(d)	6500		↓		10.0	238.5	-5.10×10^{-3}	0	.6	2.0
9(a)	3500		280		9.97	239.9	-5.31×10^{-3}	.3	0	6.2
(b)	4700				9.99	242.0	-5.46×10^{-3}	.1	.8	9.2
(c)	5500				9.97	240.5	-5.00×10^{-3}	.3	.2	0
(d)	6500		↓		10.0	240.4	-4.97×10^{-3}	0	.2	.6
10(a)	3500		320		10.0	240.0	-4.84×10^{-3}	0	0	3.2
(b)	4700				9.94	240.5	-5.48×10^{-3}	.6	.2	9.6
(c)	5500				9.97	241.5	-5.03×10^{-3}	.3	.6	.6
(d)	6500	↓	↓	↓	31.1	1634.6	-4.55×10^{-15}	211.0	581.1	100.0

TABLE III.- SUMMARY OF RESULTS FOR VARIED INITIAL VALUES OF Γ'

Figure	Wavelength, Å	Initial conditions			Final conditions			Error, percentage		
		p', mb	T', K	Γ', km^{-1}	p, mb	T, K	Γ, km^{-1}	$\frac{p' - 10}{10} \times 100$	$\frac{T' - 240}{240} \times 100$	$\frac{\Gamma' + (5 \times 10^{-3})}{-5 \times 10^{-3}} \times 100$
11(a)	3500	10	240	5×10^{-3}	10.1	239.6	-1.74×10^{-3}	1.0	0.2	65.2
(b)	4700			↓	10.2	236.2	-3.01×10^{-3}	2.0	1.6	39.8
(c)	5500				10.1	232.1	-4.83×10^{-3}	1.0	3.3	3.4
(d)	6500				9.95	232.0	-5.67×10^{-3}	.5	3.3	13.4
12(a)	3500			0	10.0	239.8	-3.46×10^{-3}	0	.1	30.8
(b)	4700			↓	10.1	238.5	-4.25×10^{-3}	1.0	.6	15.0
(c)	5500				10.0	238.0	-4.94×10^{-3}	0	.8	1.2
(d)	6500				9.99	238.5	-5.13×10^{-3}	.1	.6	2.6
13(a)	3500			-8×10^{-3}	9.93	239.8	-5.56×10^{-3}	.7	.1	11.2
(b)	4700			↓	10.0	240.5	-5.26×10^{-3}	0	.2	5.2
(c)	5500				10.0	240.6	-5.03×10^{-3}	0	.3	.6
(d)	6500				10.0	240.8	-4.99×10^{-3}	0	.3	.2
14(a)	3500			-12×10^{-3}	9.92	240.5	-6.39×10^{-3}	.8	.2	27.8
(b)	4700			↓	9.95	240.7	-5.41×10^{-3}	.5	.3	8.2
(c)	5500				10.0	241.3	-5.07×10^{-3}	0	.5	1.4
(d)	6500				9.99	240.8	-4.95×10^{-3}	.1	.3	1.0
15(a)	3500			-50×10^{-3}	9.69	241.1	-15.9×10^{-3}	3.1	.5	218.0
(b)	4700			↓	9.72	246.9	-7.83×10^{-3}	2.8	2.9	56.6
(c)	5500				9.95	244.8	-4.96×10^{-3}	.5	2.0	.8
(d)	6500	↓	↓	↓	31.1	1634.6	-3.96×10^{-14}	211.0	581.1	100.0

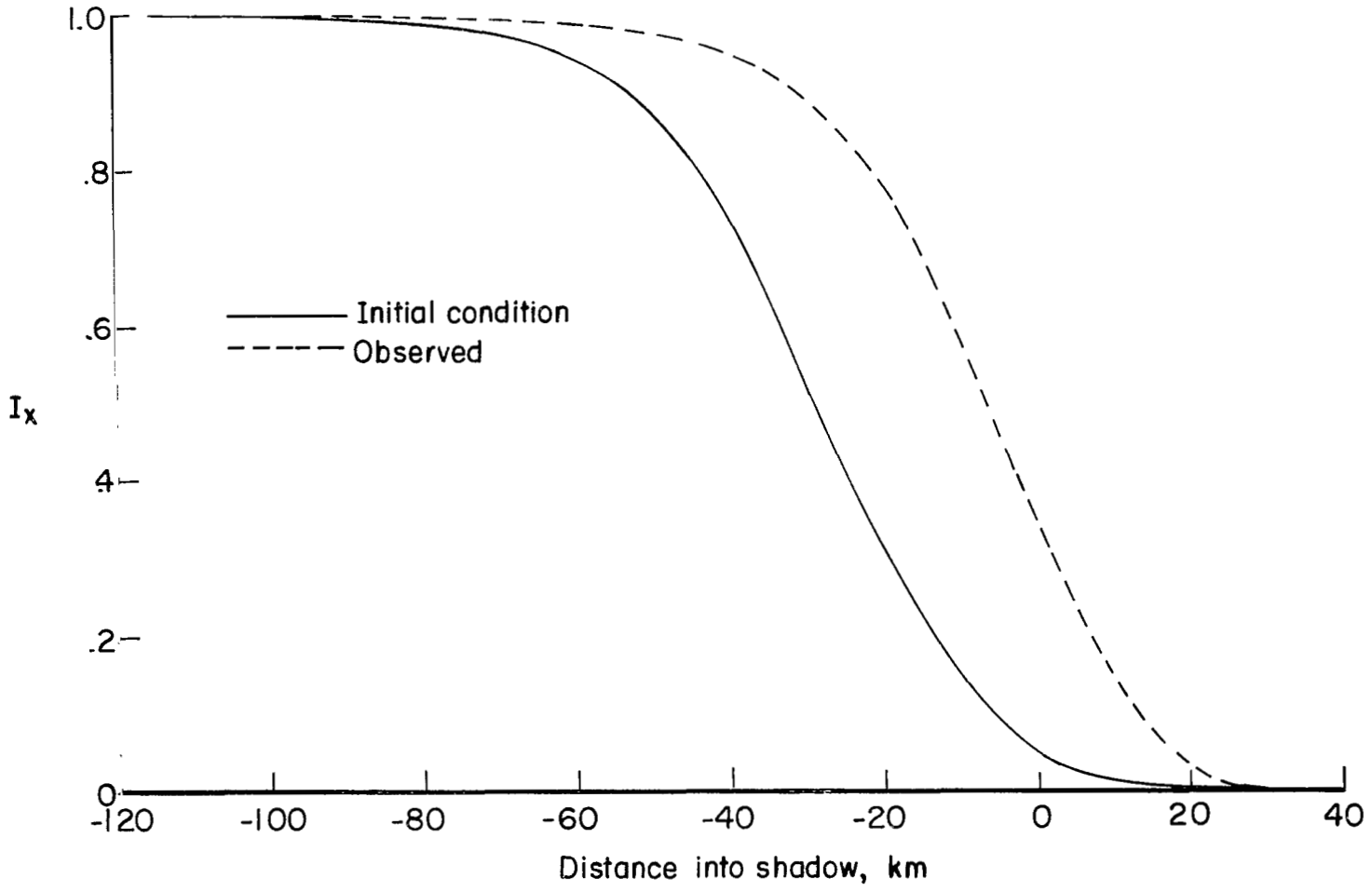

Figure 1.- Typical curves for observed and initial conditions.

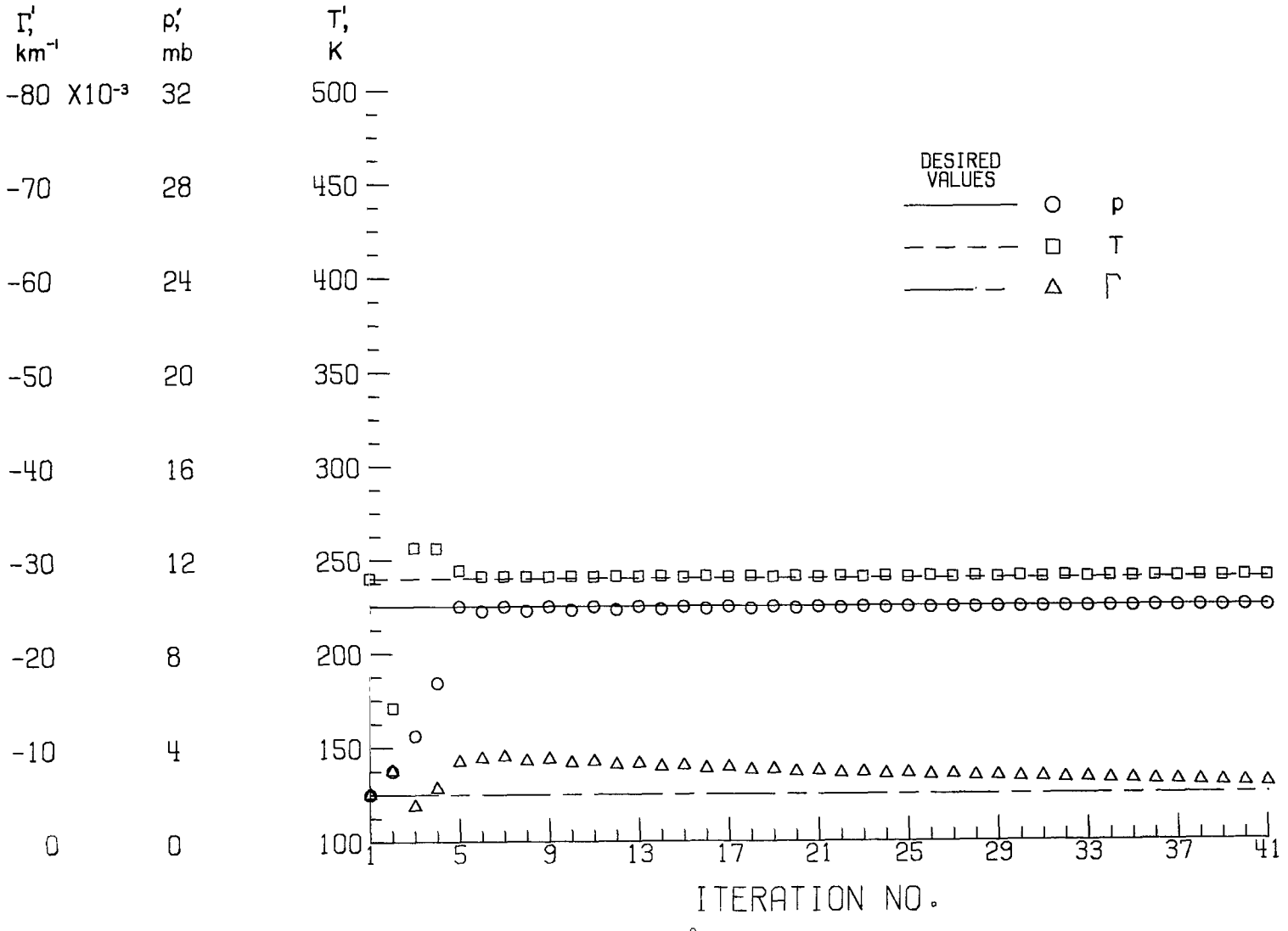

(a) λ = 3500 Å.

Figure 2.- Convergence plots for p' = 2 mb, T' = 240 K, and $\Gamma' = -5 \times 10^{-3}$ km^{-1}.

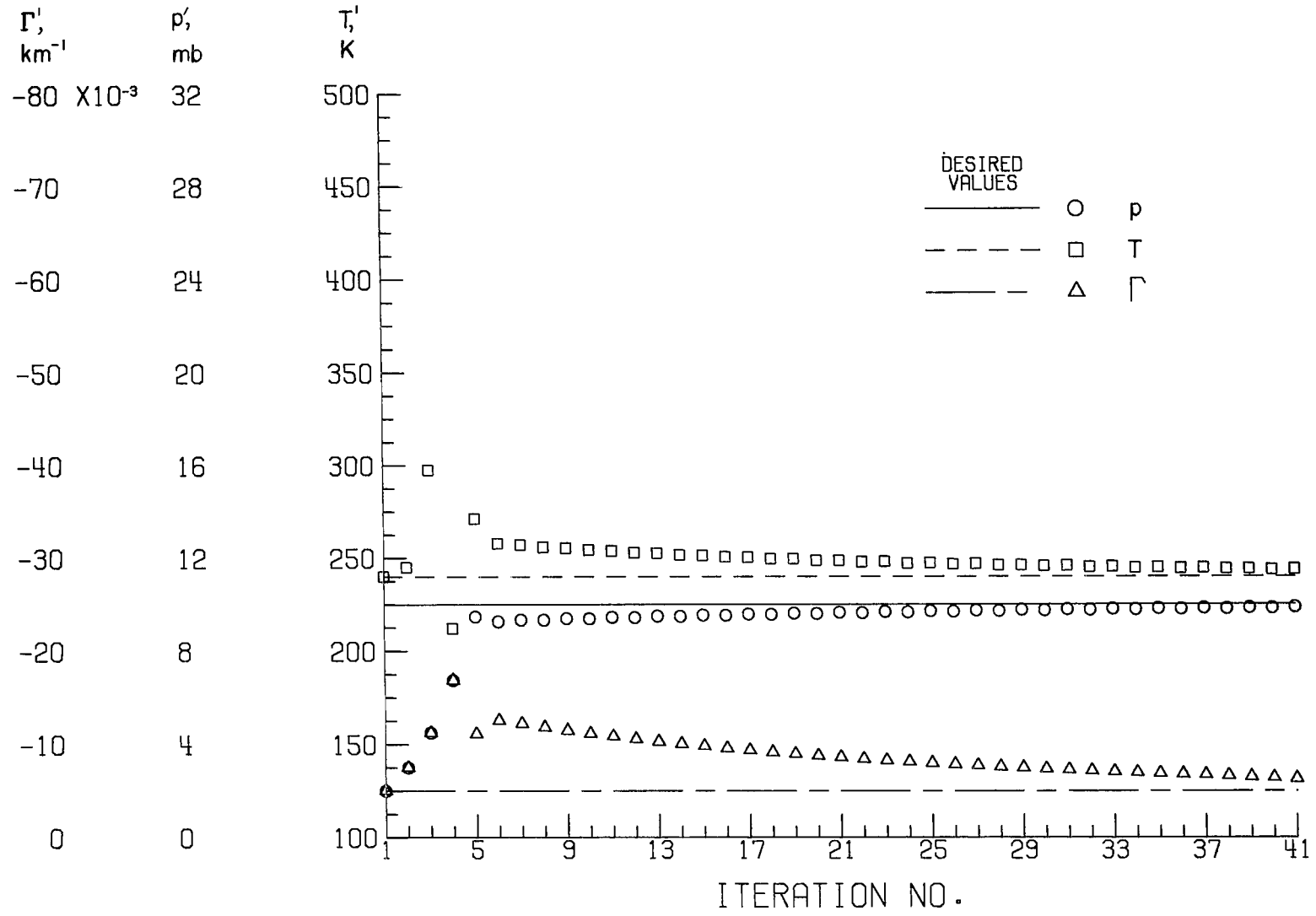

(b) $\lambda = 4700$ Å.

Figure 2.- Continued.

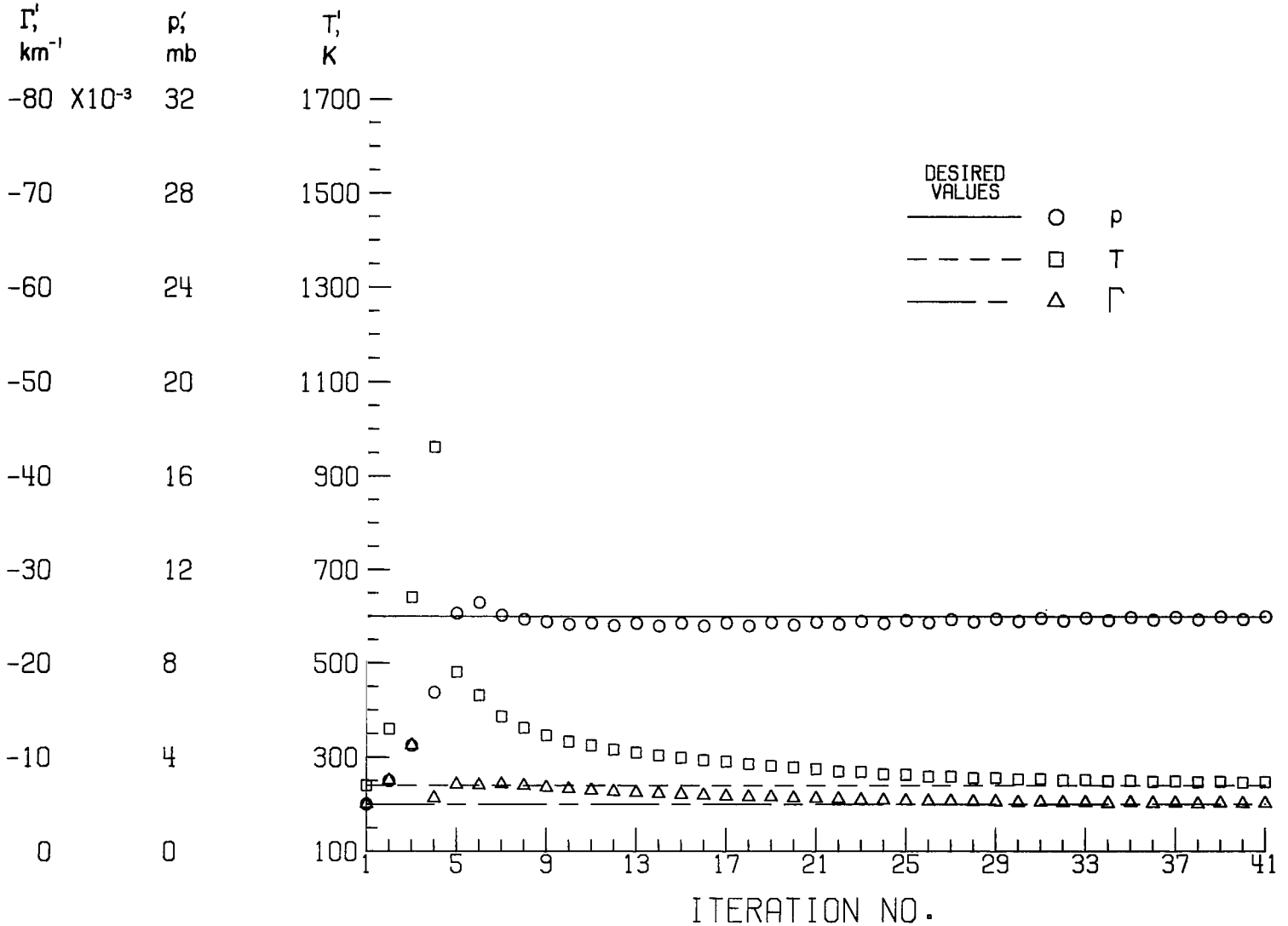

(c) $\lambda = 5500$ Å.

Figure 2.- Continued.

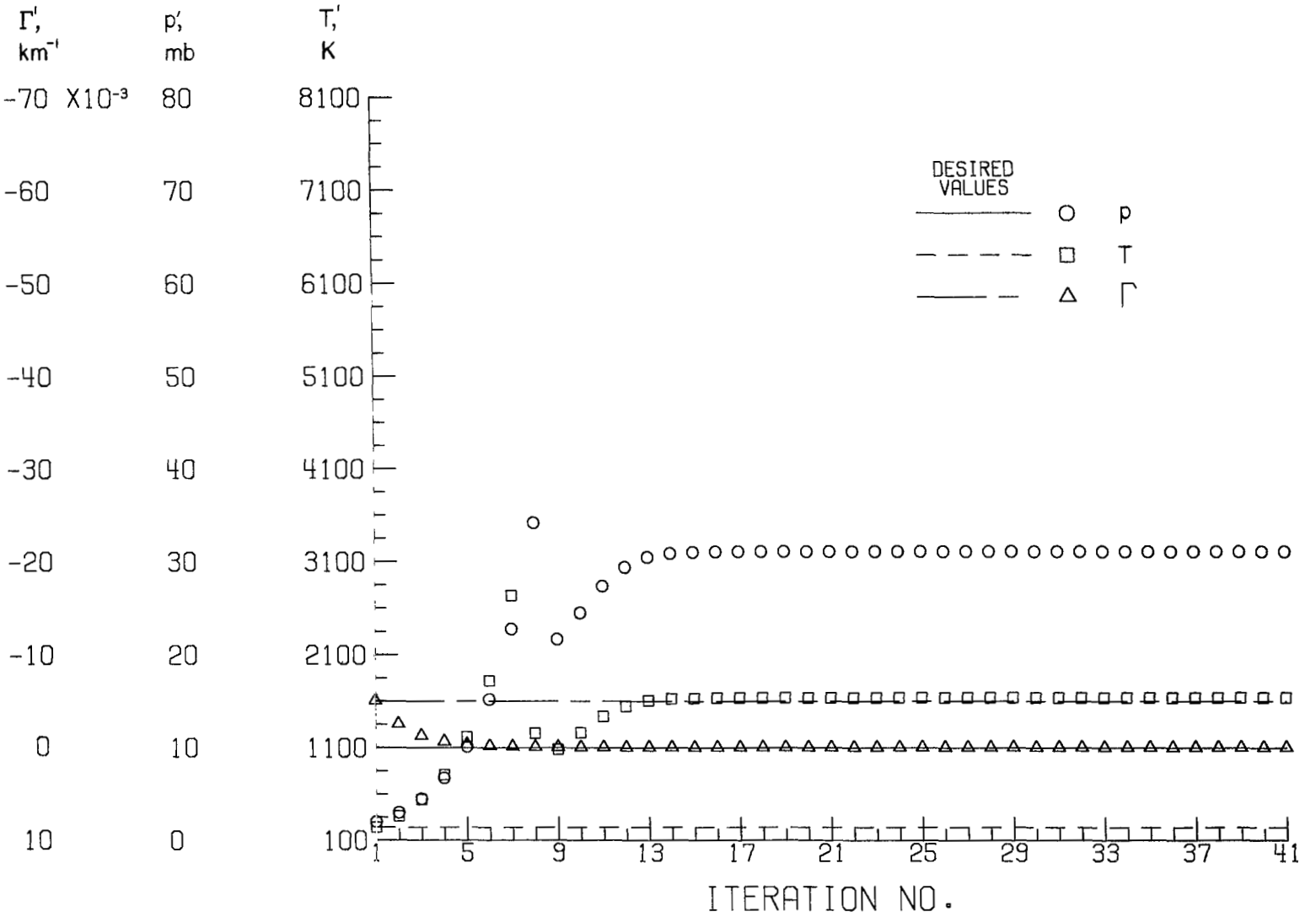

(d) λ = 6500 Å.

Figure 2.- Concluded.

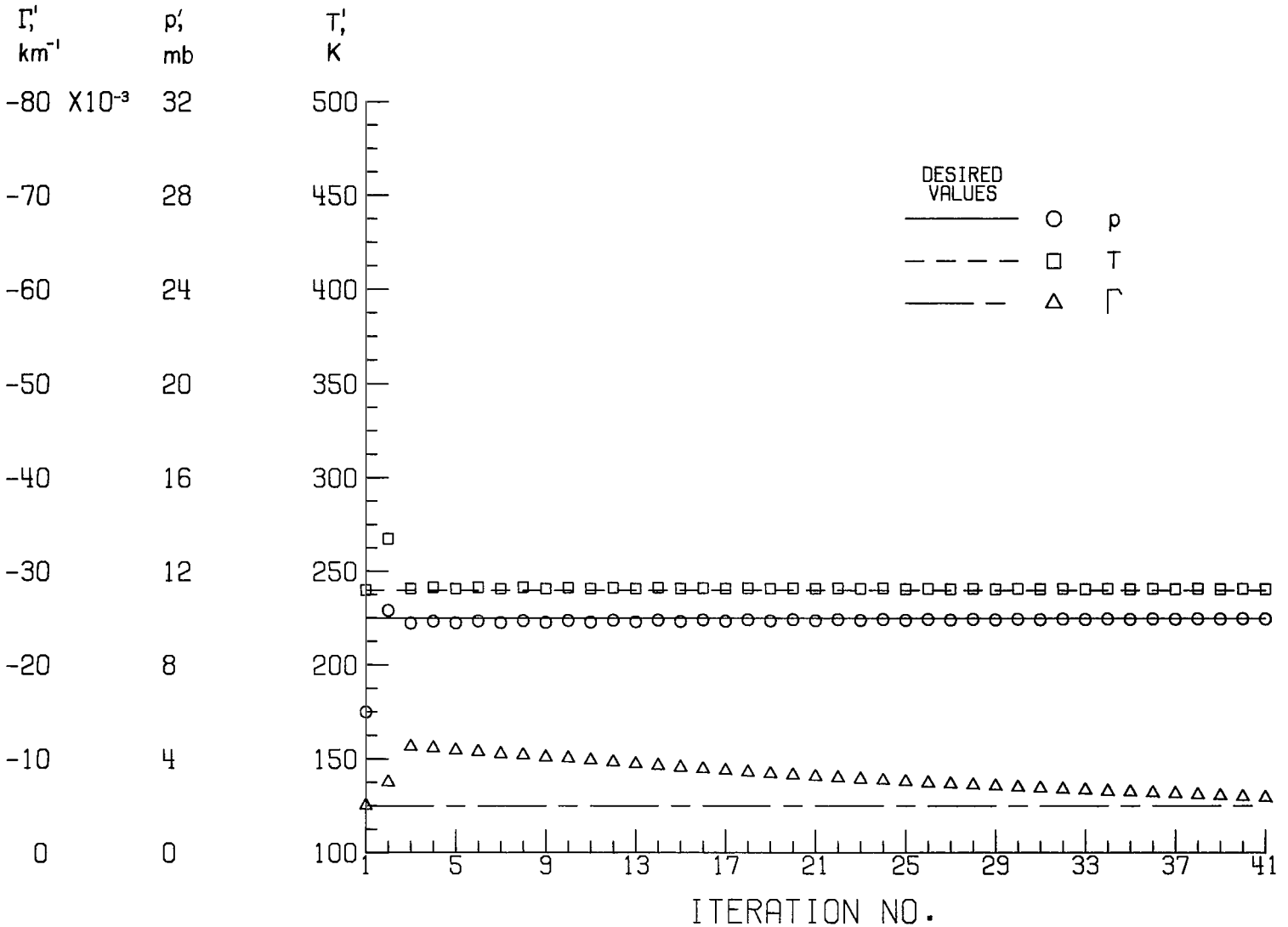

(a) λ = 3500 Å.

Figure 3.- Convergence plots for p' = 6 mb, T' = 240 K, and $\Gamma' = -5 \times 10^{-3}$ km^{-1}.

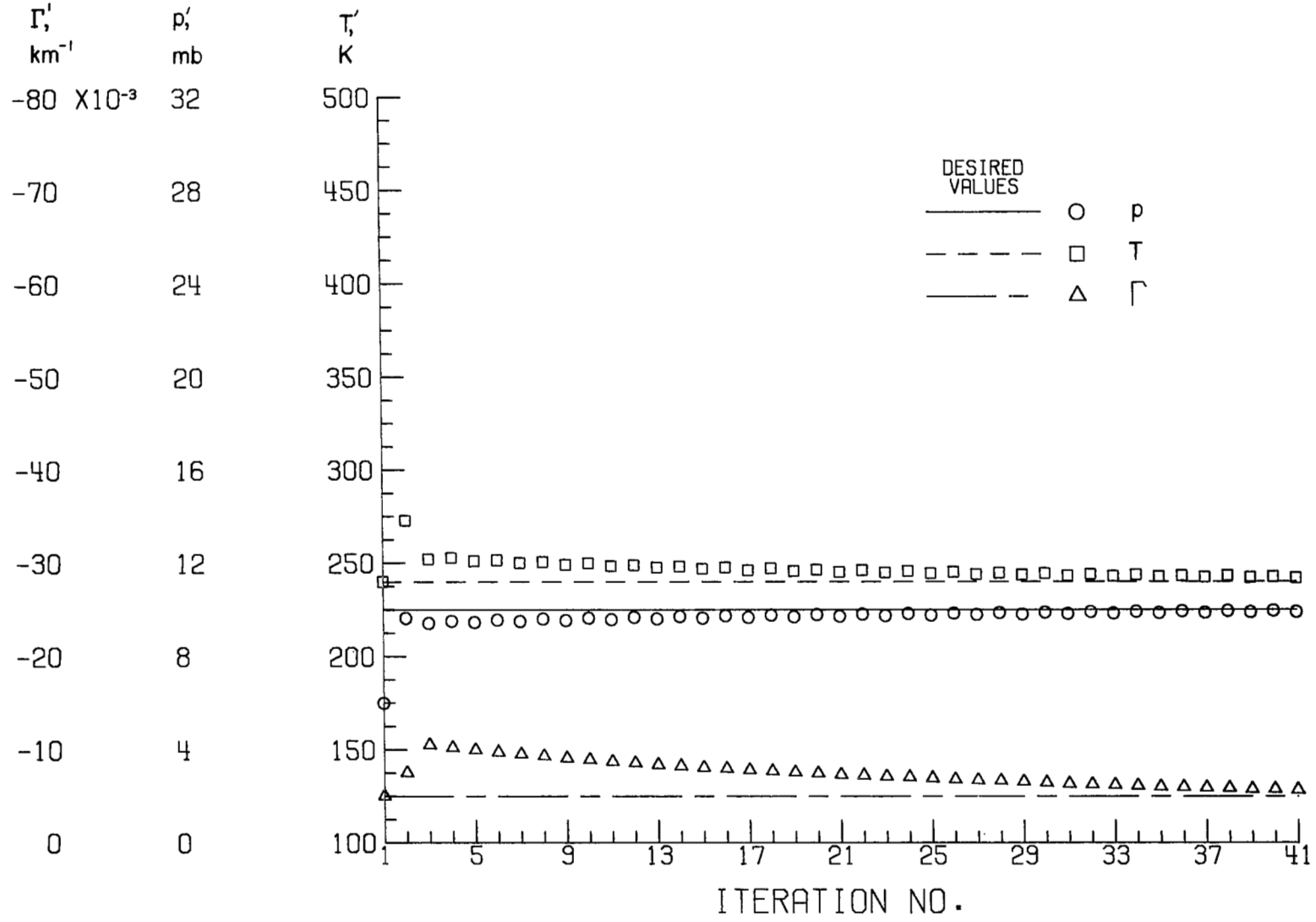

(b) $\lambda = 4700$ Å.

Figure 3.- Continued.

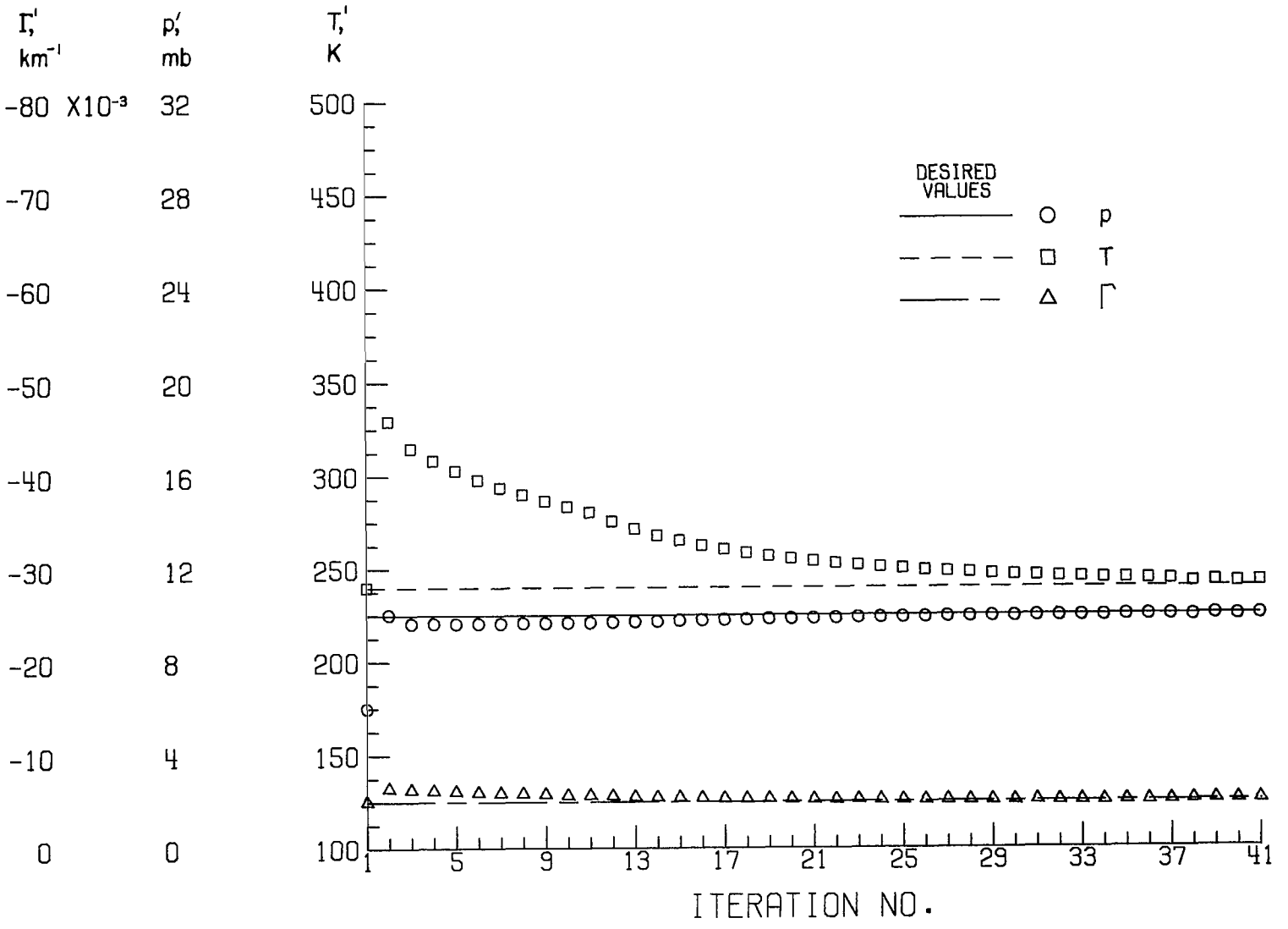

(c) $\lambda = 5500$ Å.

Figure 3.- Continued.

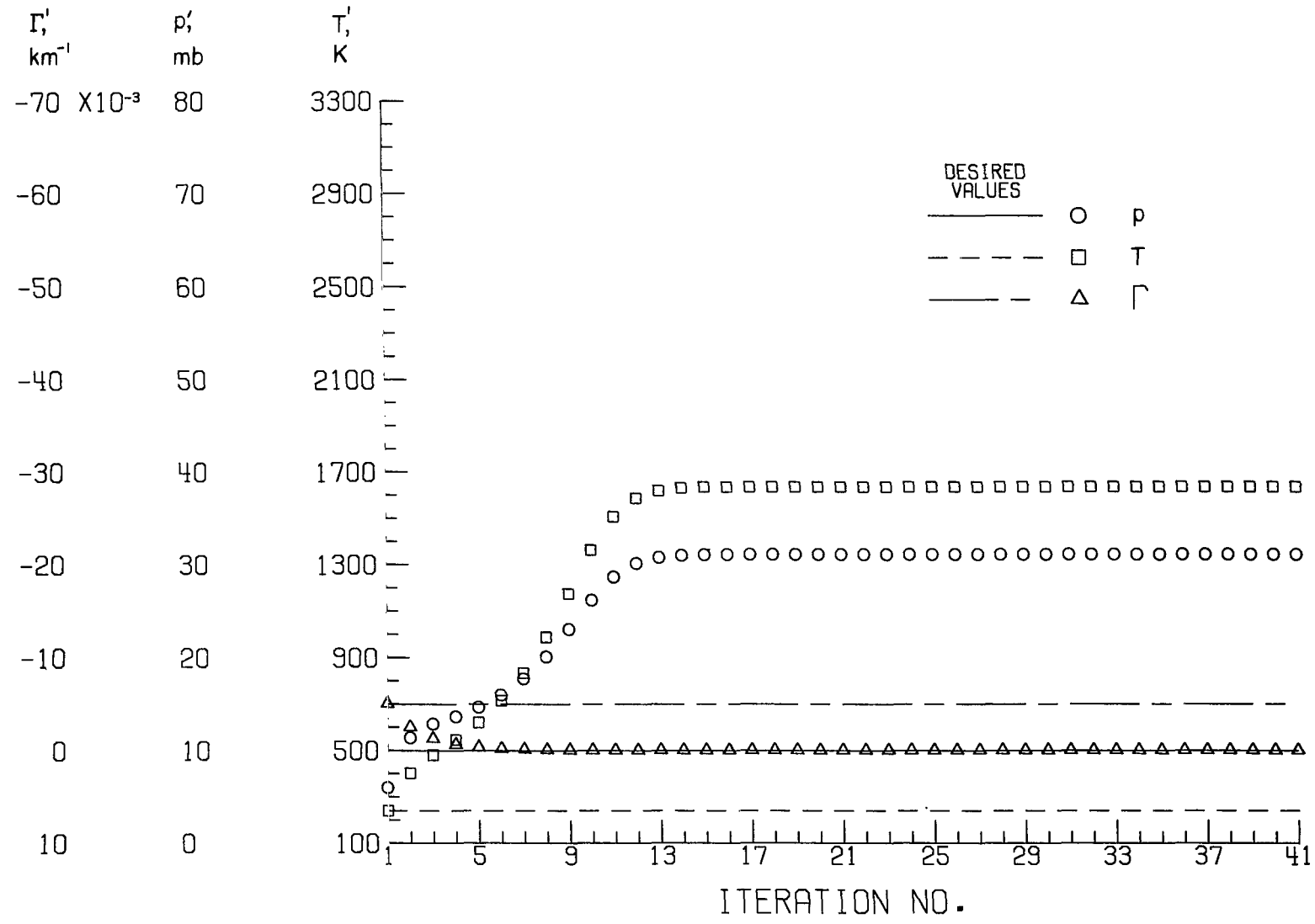

(d) $\lambda = 6500$ Å.

Figure 3.- Concluded.

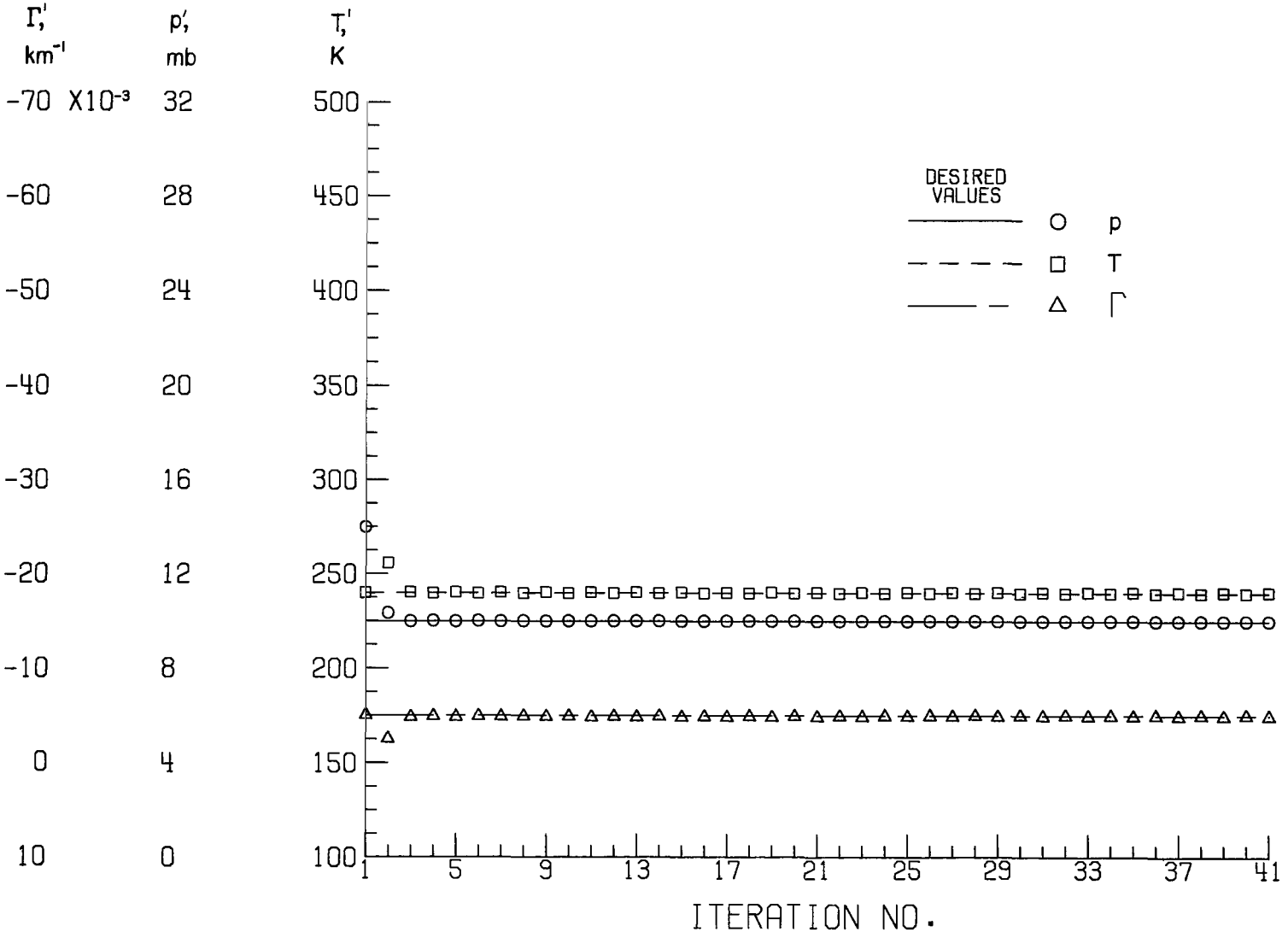

(a) $\lambda = 3500$ Å.

Figure 4.- Convergence plots for $p' = 14$ mb, $T' = 240$ K, and $\Gamma' = -5 \times 10^{-3}$ km^{-1}.

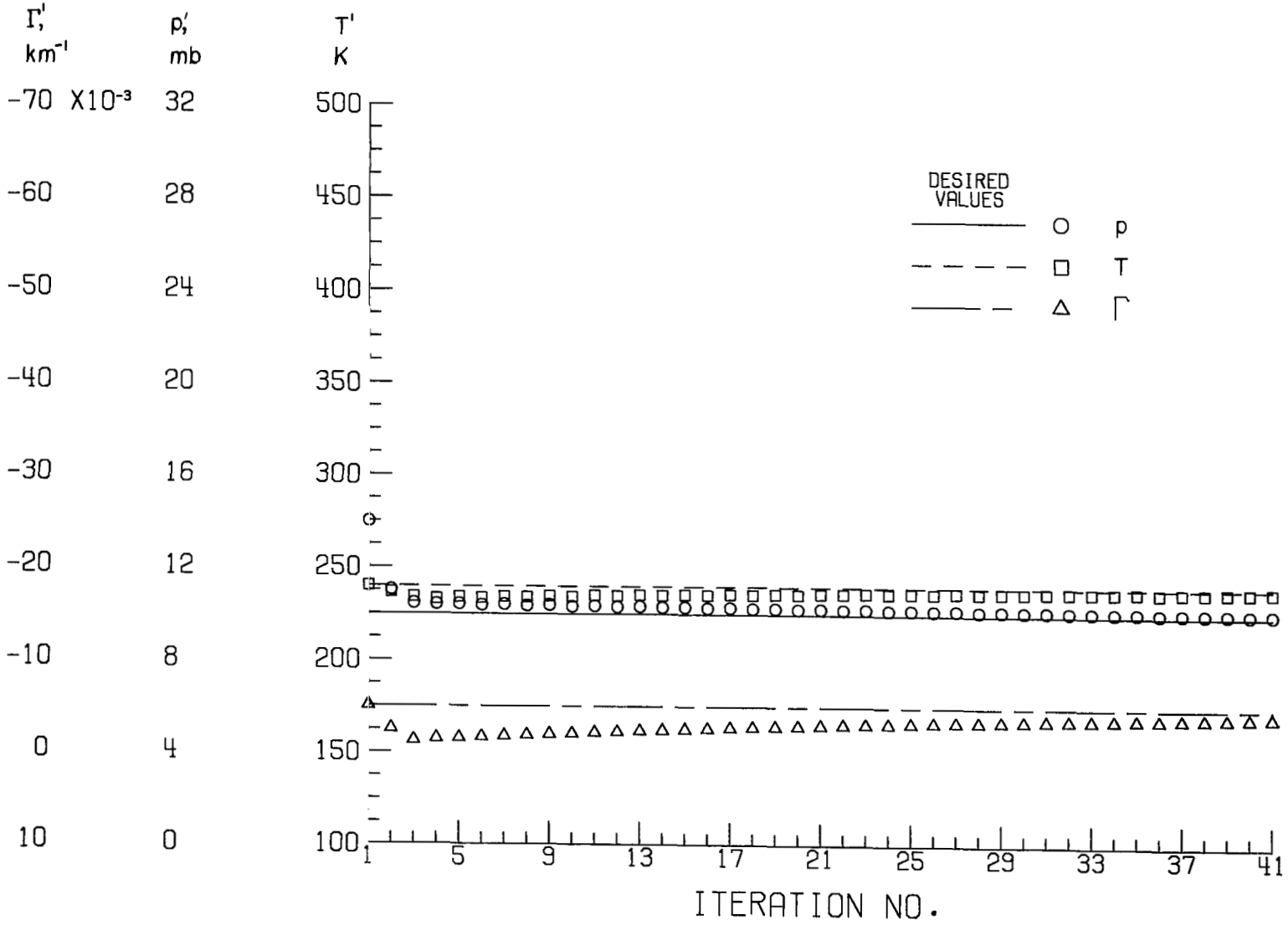

(b) $\lambda = 4700$ Å.

Figure 4.- Continued.

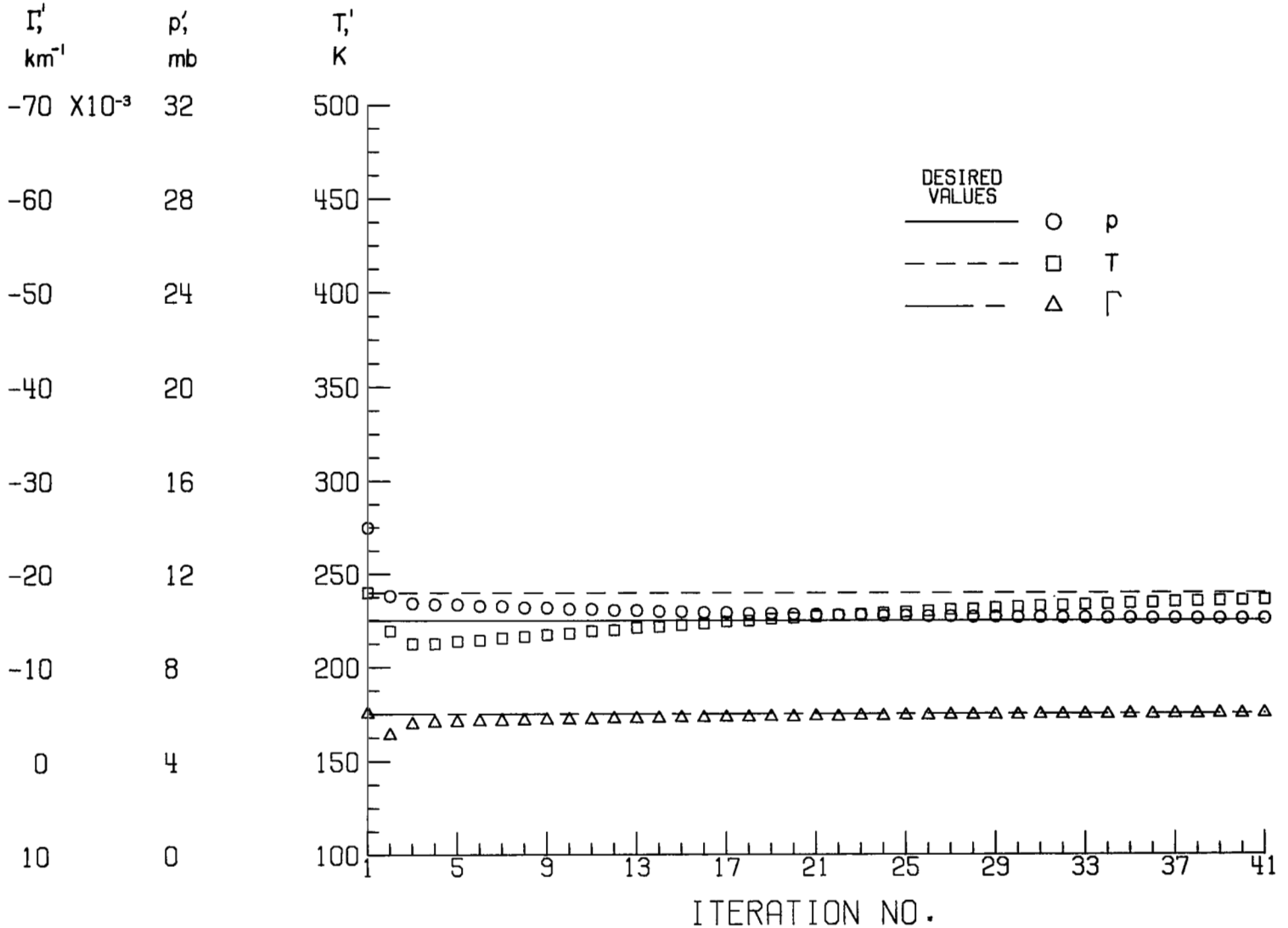

(c) λ = 5500 Å.

Figure 4.- Continued.

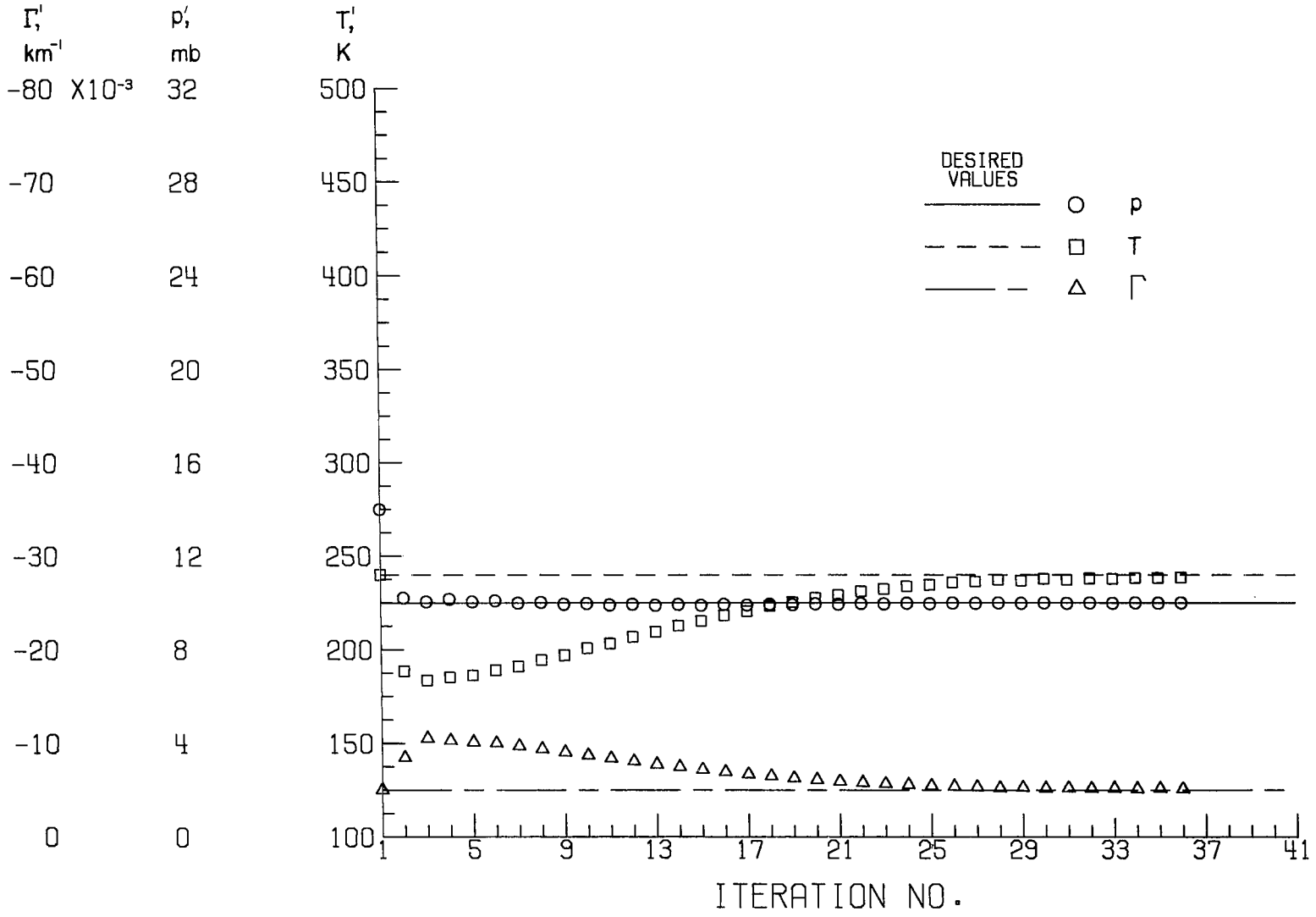

(d) λ = 6500 Å.

Figure 4.- Concluded.

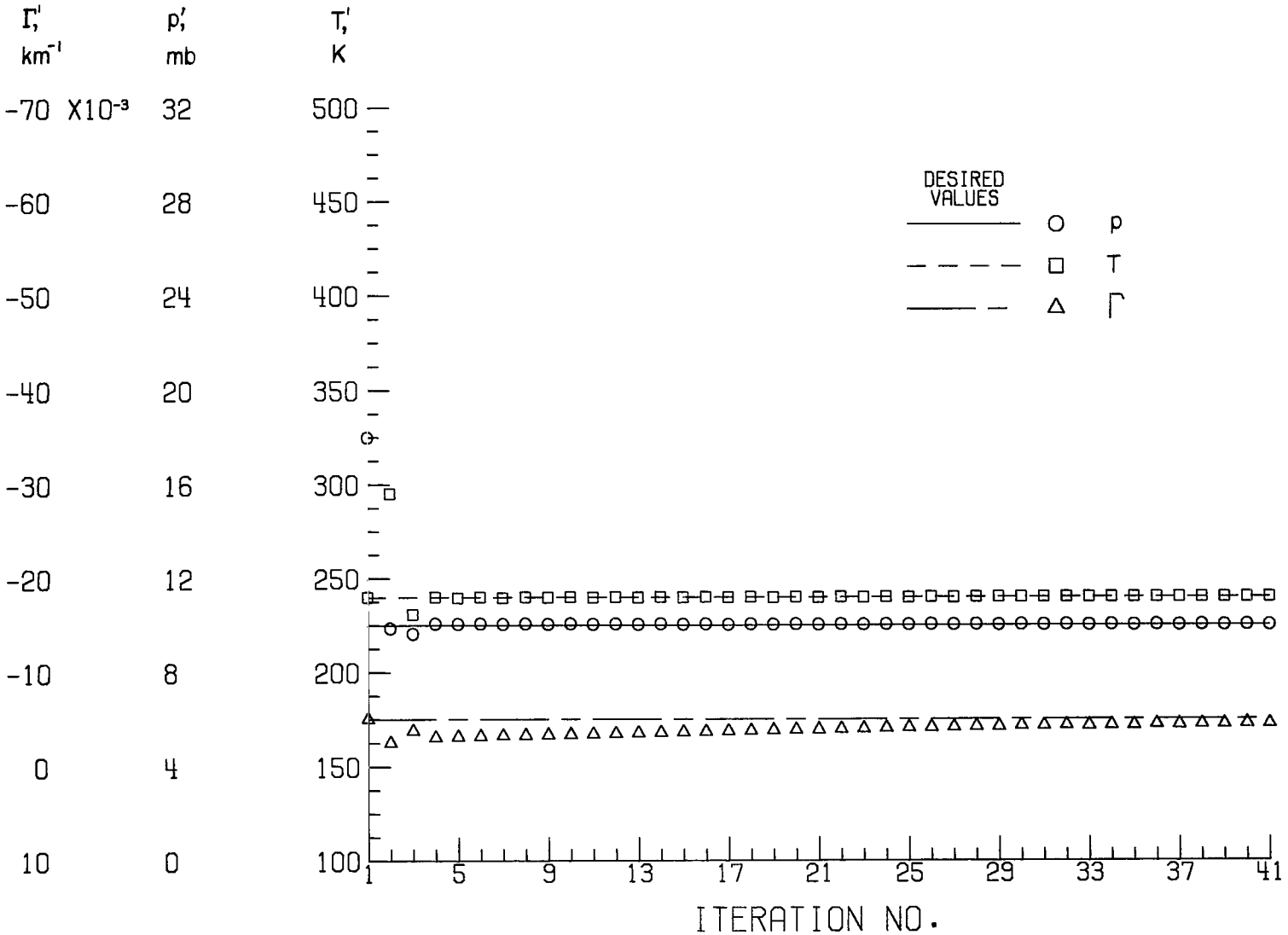

(a) $\lambda = 3500$ Å.

Figure 5.- Convergence plots for $p' = 18$ mb, $T' = 240$ K, and $\Gamma' = -5 \times 10^{-3}$ km^{-1}.

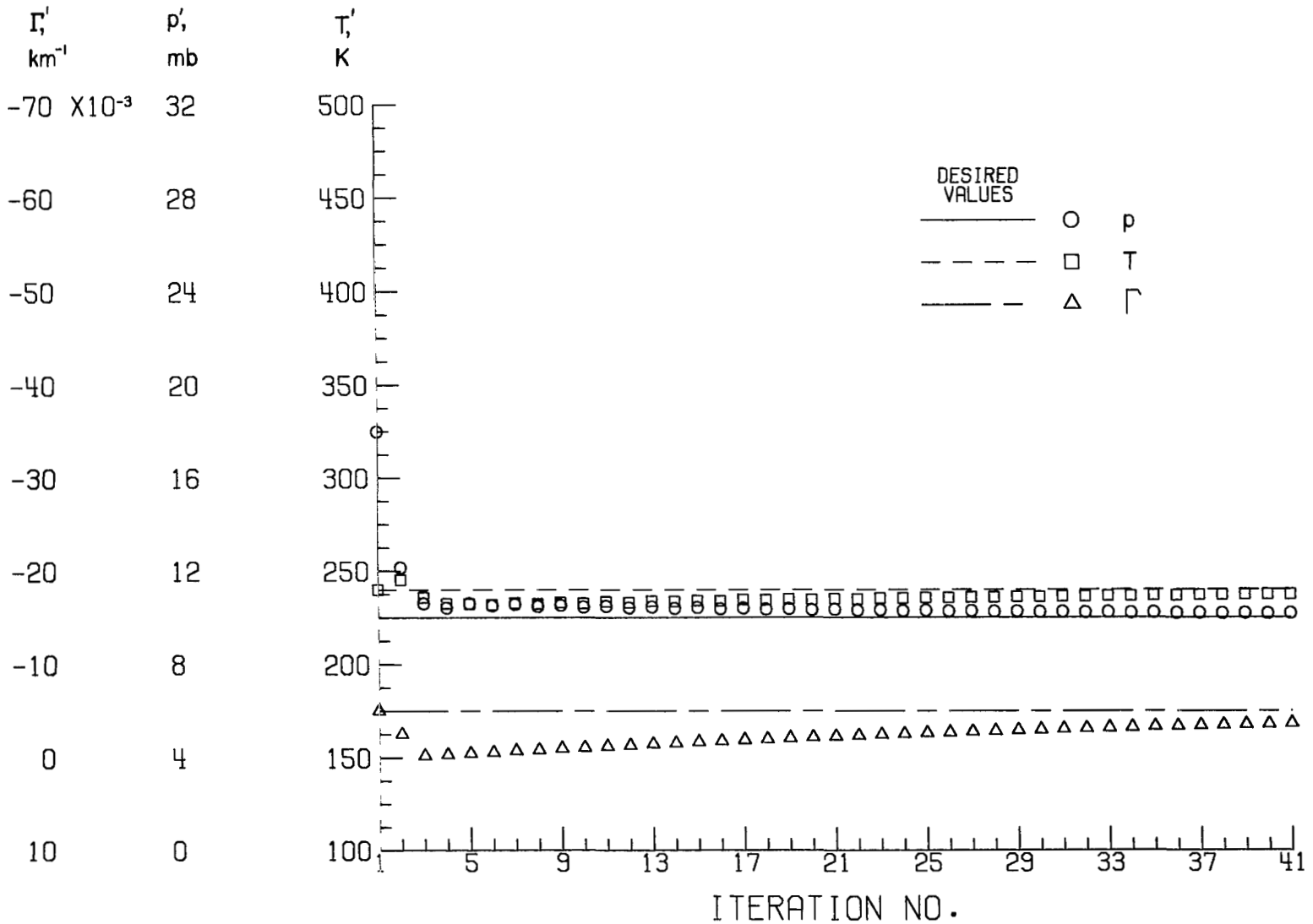

(b) $\lambda = 4700$ Å.

Figure 5.- Continued.

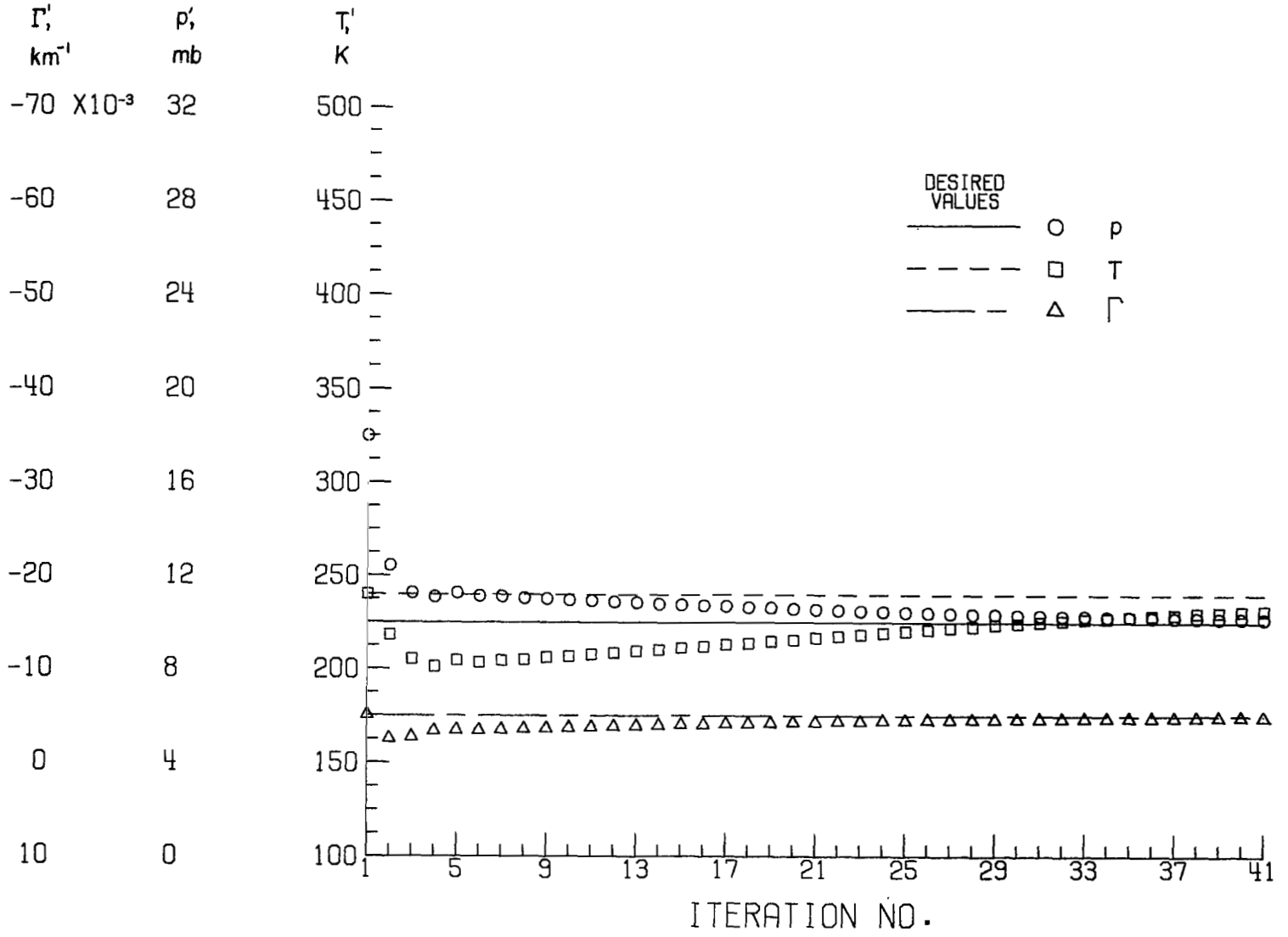

(c) $\lambda = 5500$ Å.

Figure 5.- Continued.

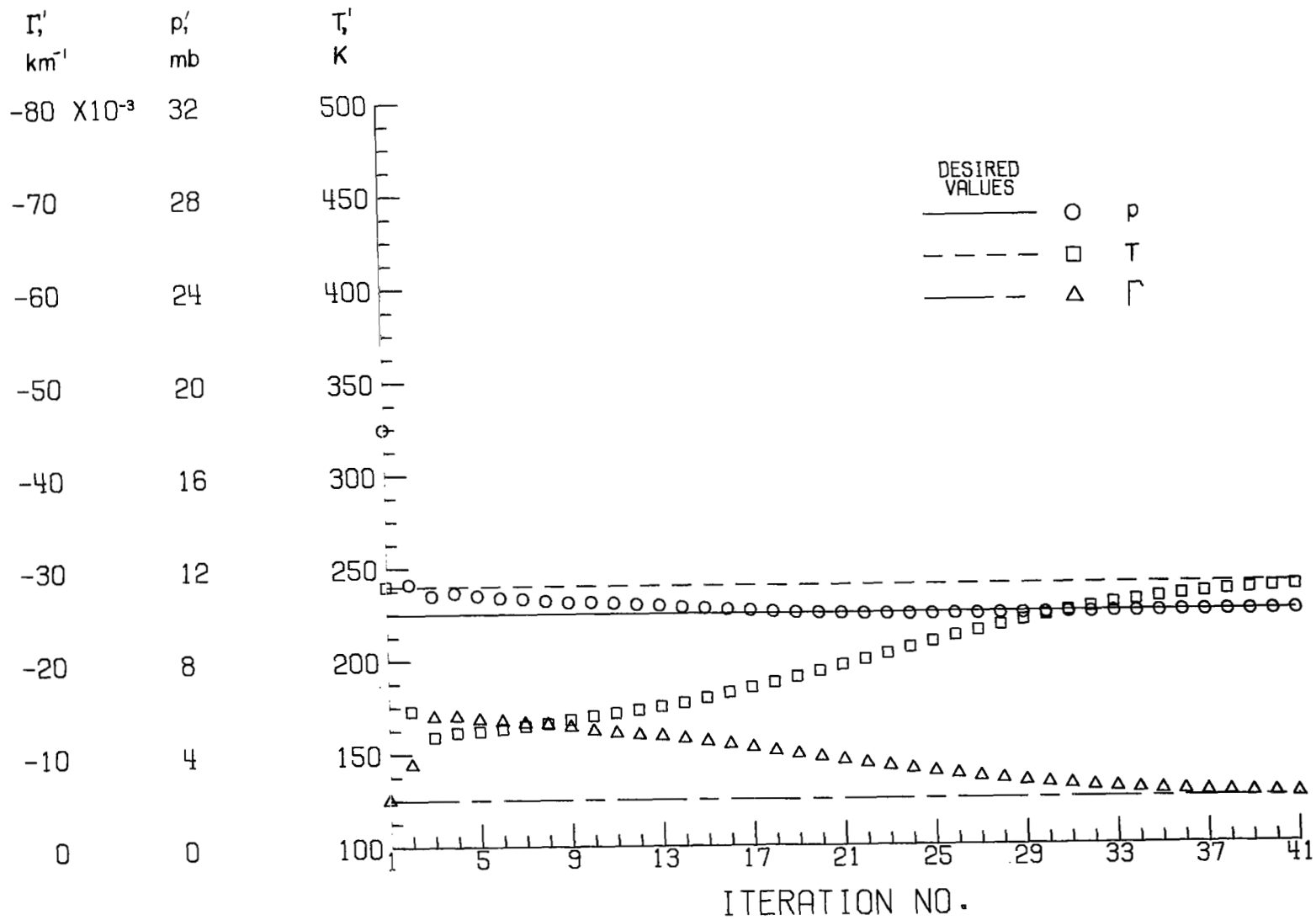

(d) λ = 6500 Å.

Figure 5.- Concluded.

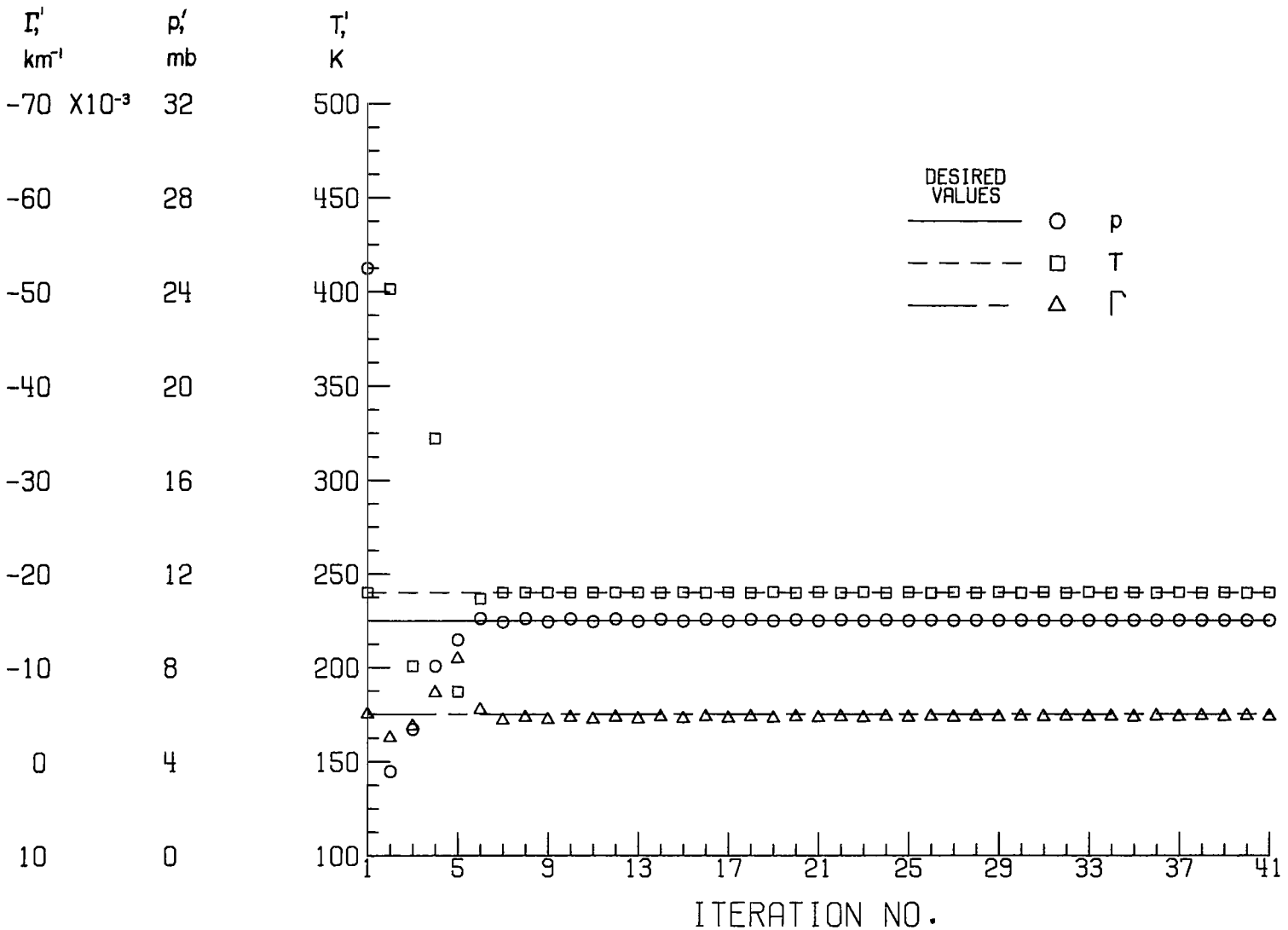

(a) $\lambda = 3500$ Å.

Figure 6.- Convergence plots for $p' = 25$ mb, $T' = 240$ K, and $\Gamma' = -5 \times 10^{-3}$ km^{-1}.

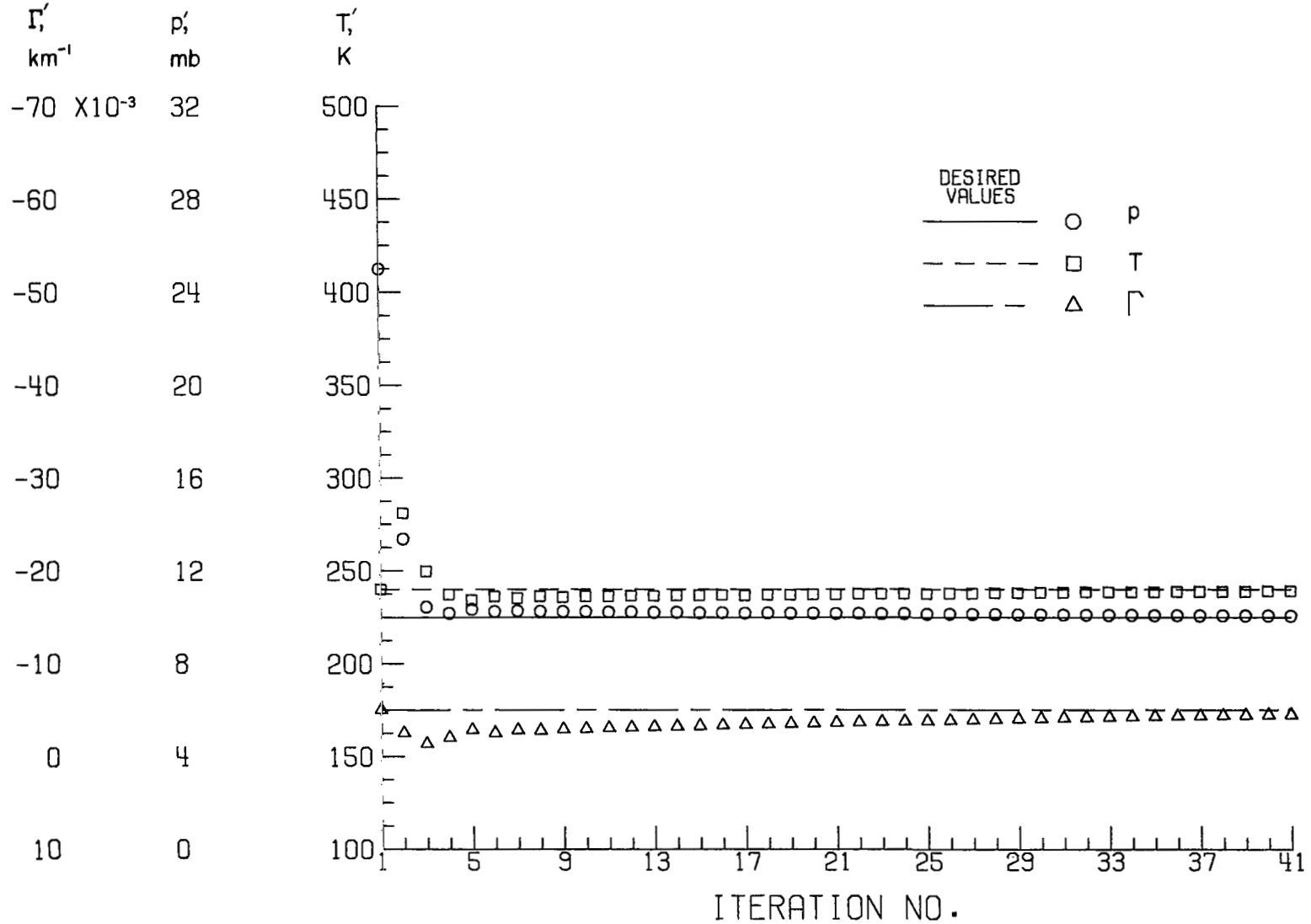

(b) $\lambda = 4700$ Å.

Figure 6.- Continued.

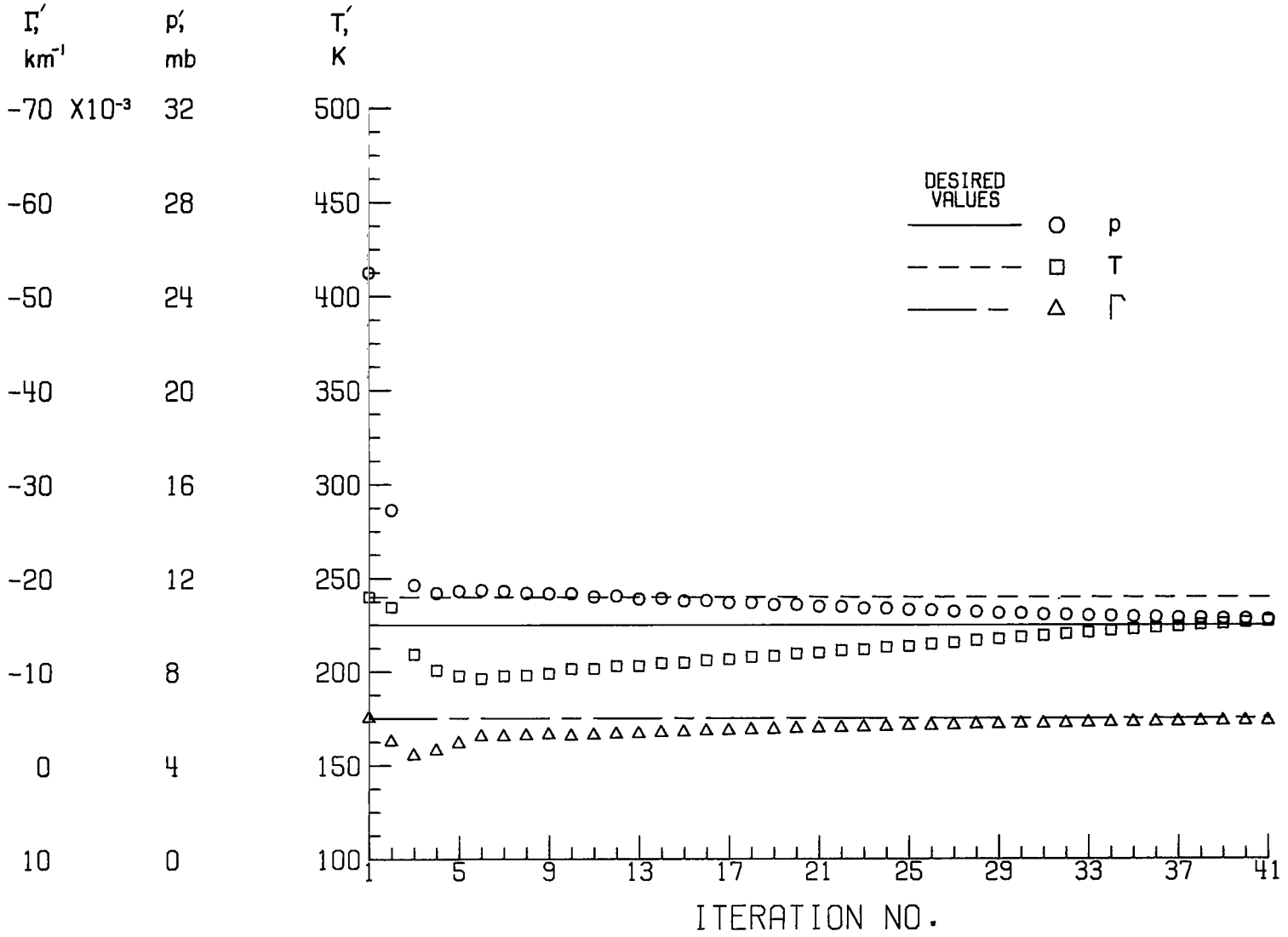

(c) $\lambda = 5500$ Å.

Figure 6.- Continued.

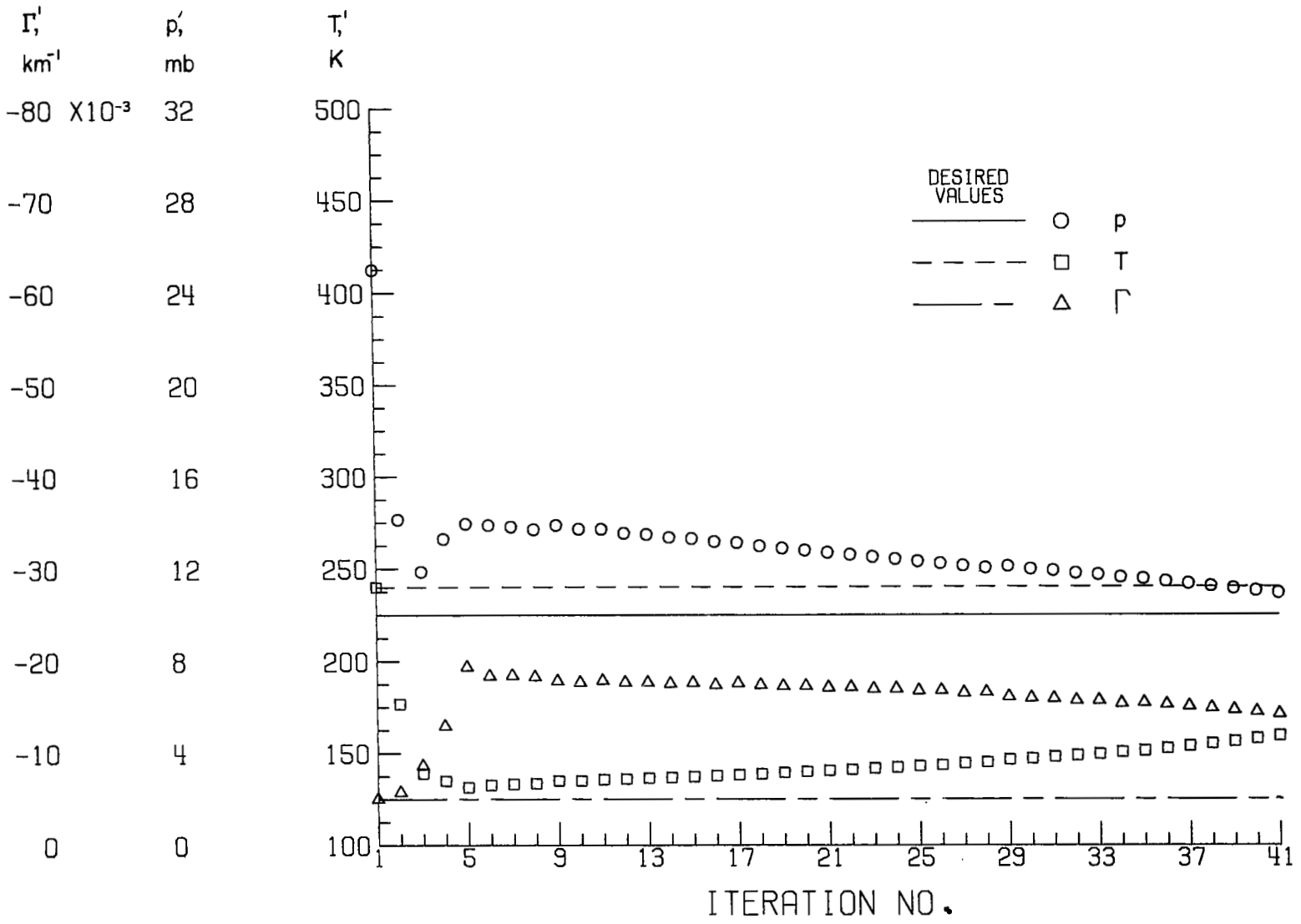

(d) λ = 6500 Å.

Figure 6.- Concluded.

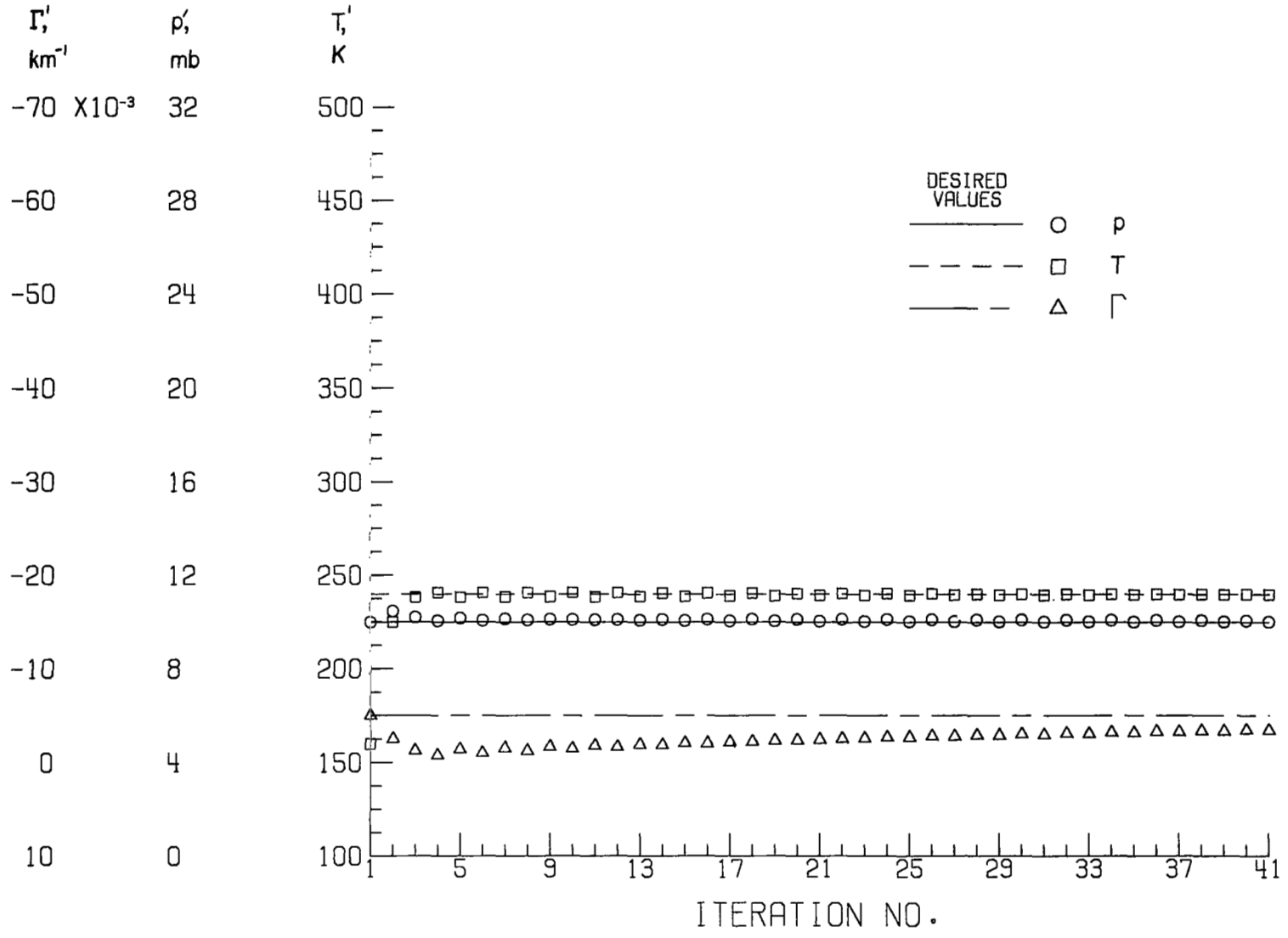

(a) $\lambda = 3500$ Å.

Figure 7.- Convergence plots for $p' = 10$ mb, $T' = 160$ K, and $\Gamma' = -5 \times 10^{-3}$ km^{-1}.

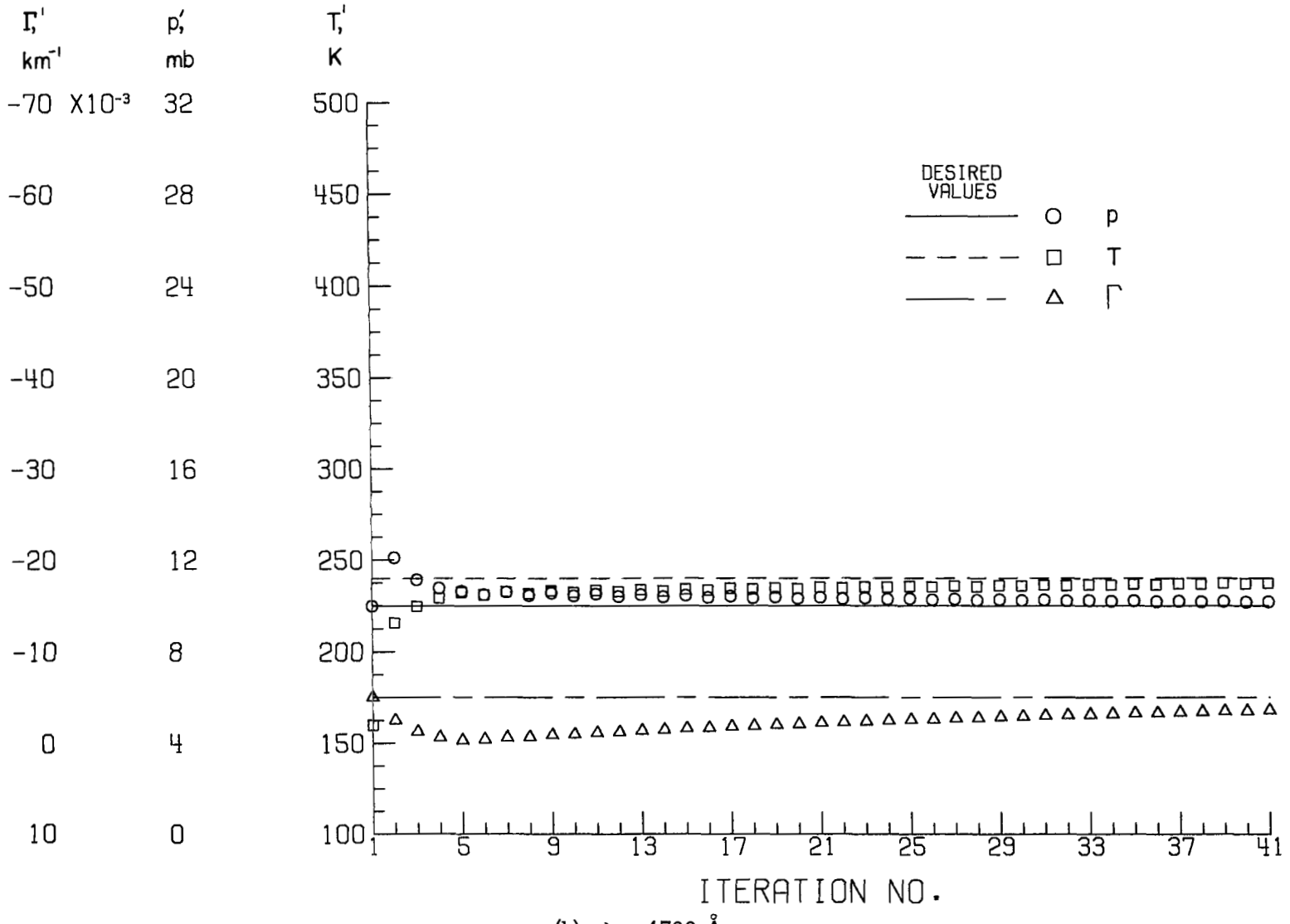

(b) $\lambda = 4700$ Å.

Figure 7.- Continued.

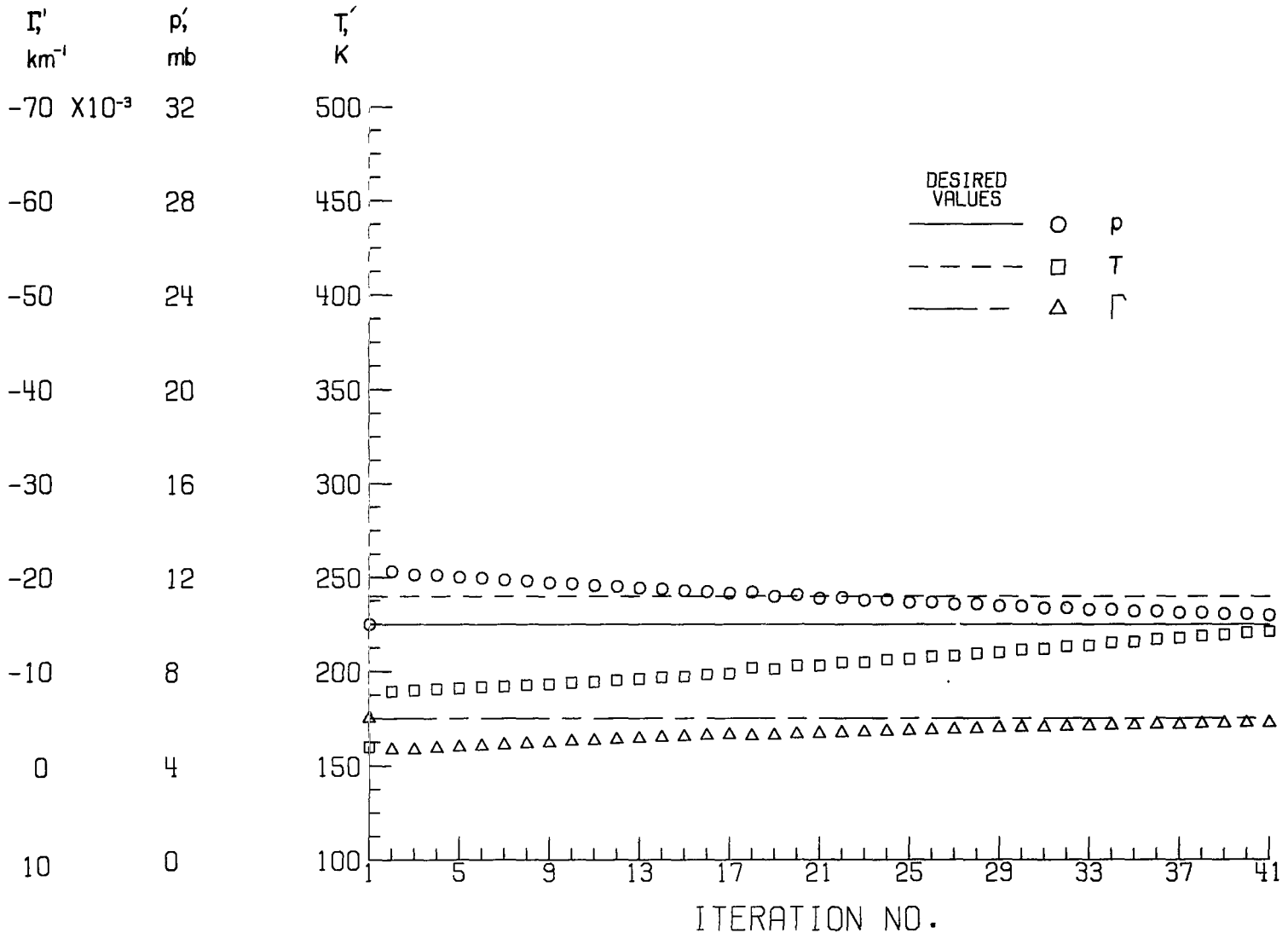

(c) λ = 5500 Å.

Figure 7.- Continued.

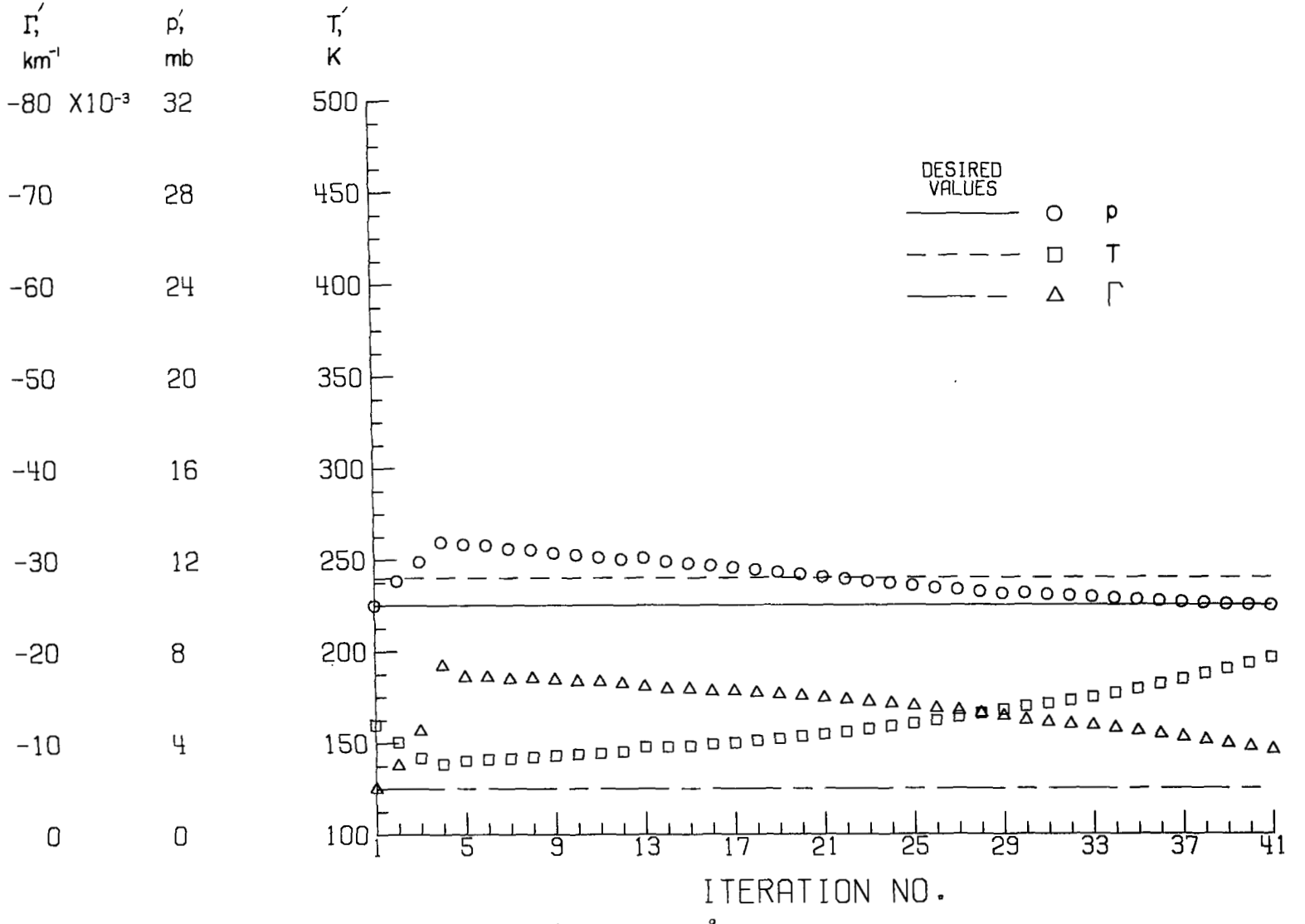

(d) λ = 6500 Å.

Figure 7.- Concluded.

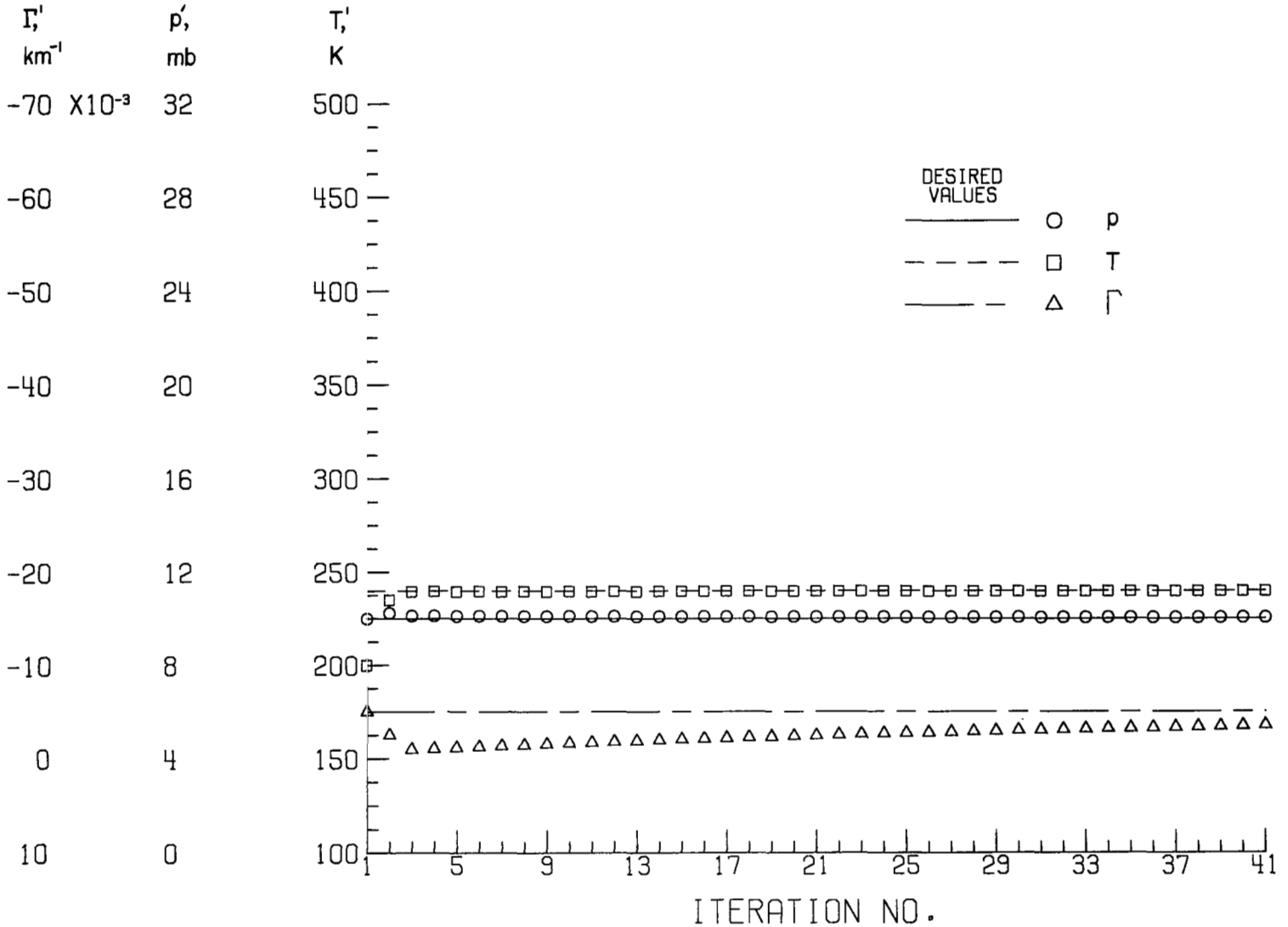

(a) λ = 3500 Å.

Figure 8.- Convergence plots for p' = 10 mb, T' = 200 K, and $\Gamma' = -5 \times 10^{-3}$ km^{-1}.

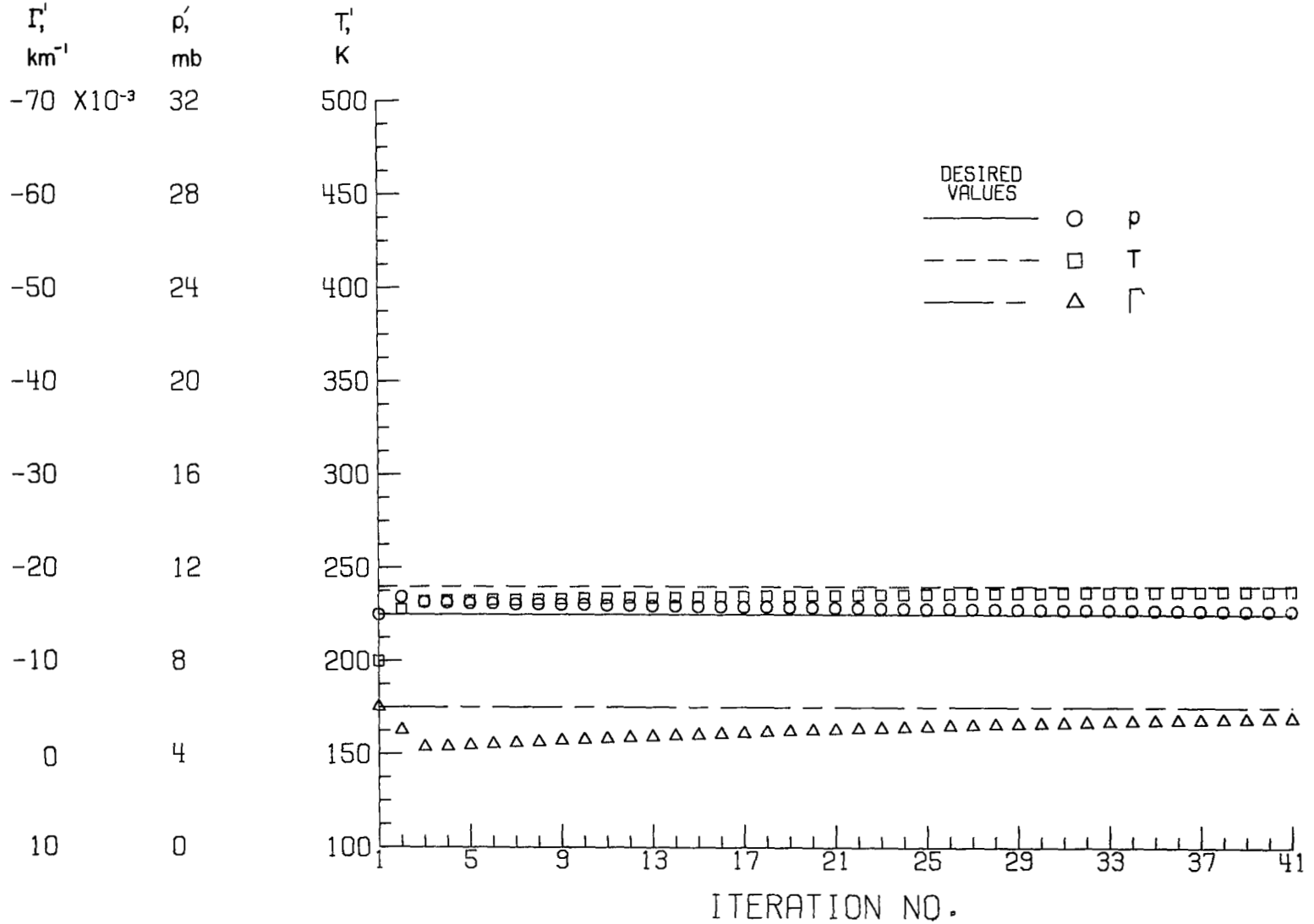

(b) λ = 4700 Å.

Figure 8.- Continued.

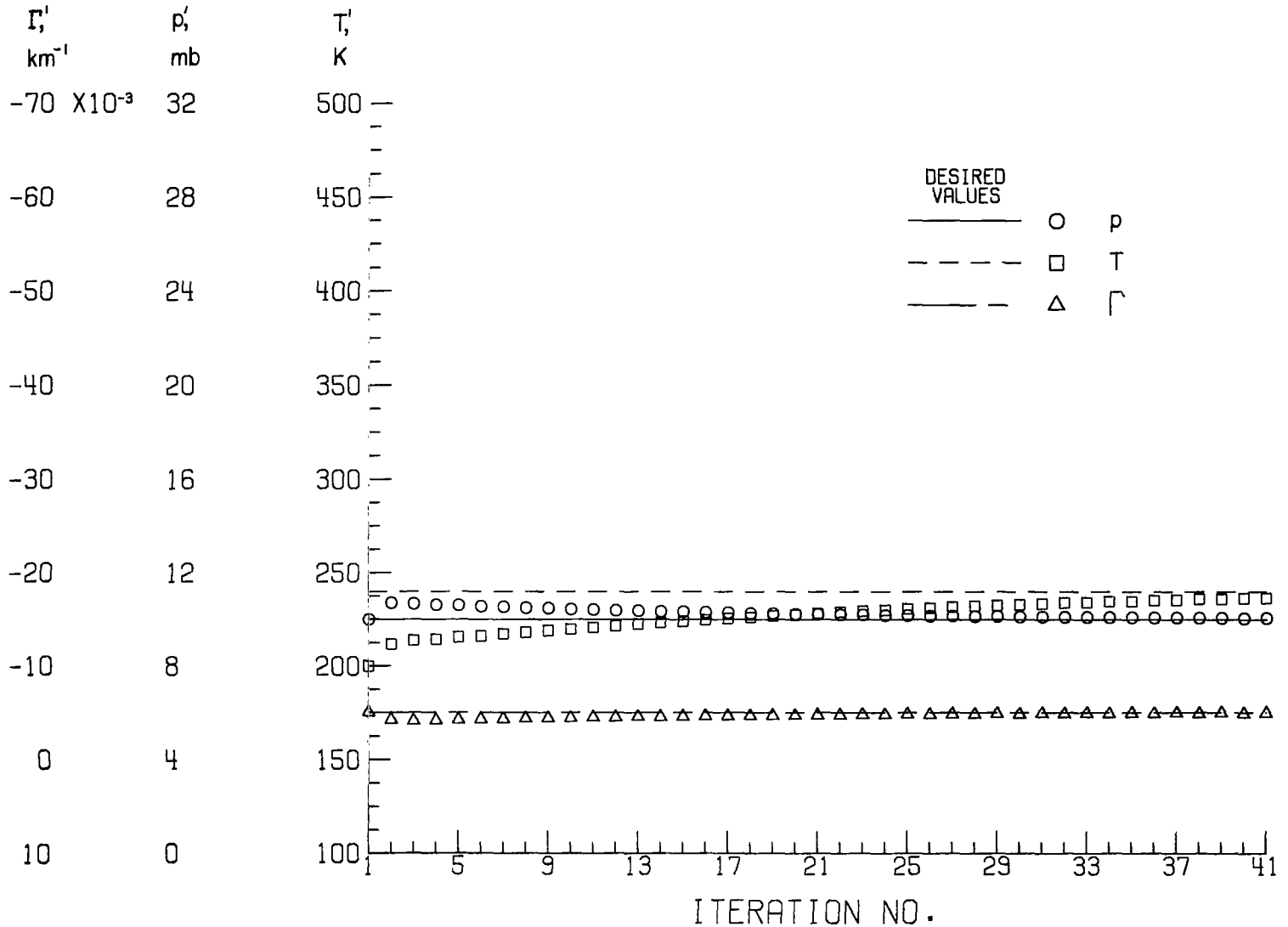

(c) λ = 5500 Å.

Figure 8.- Continued.

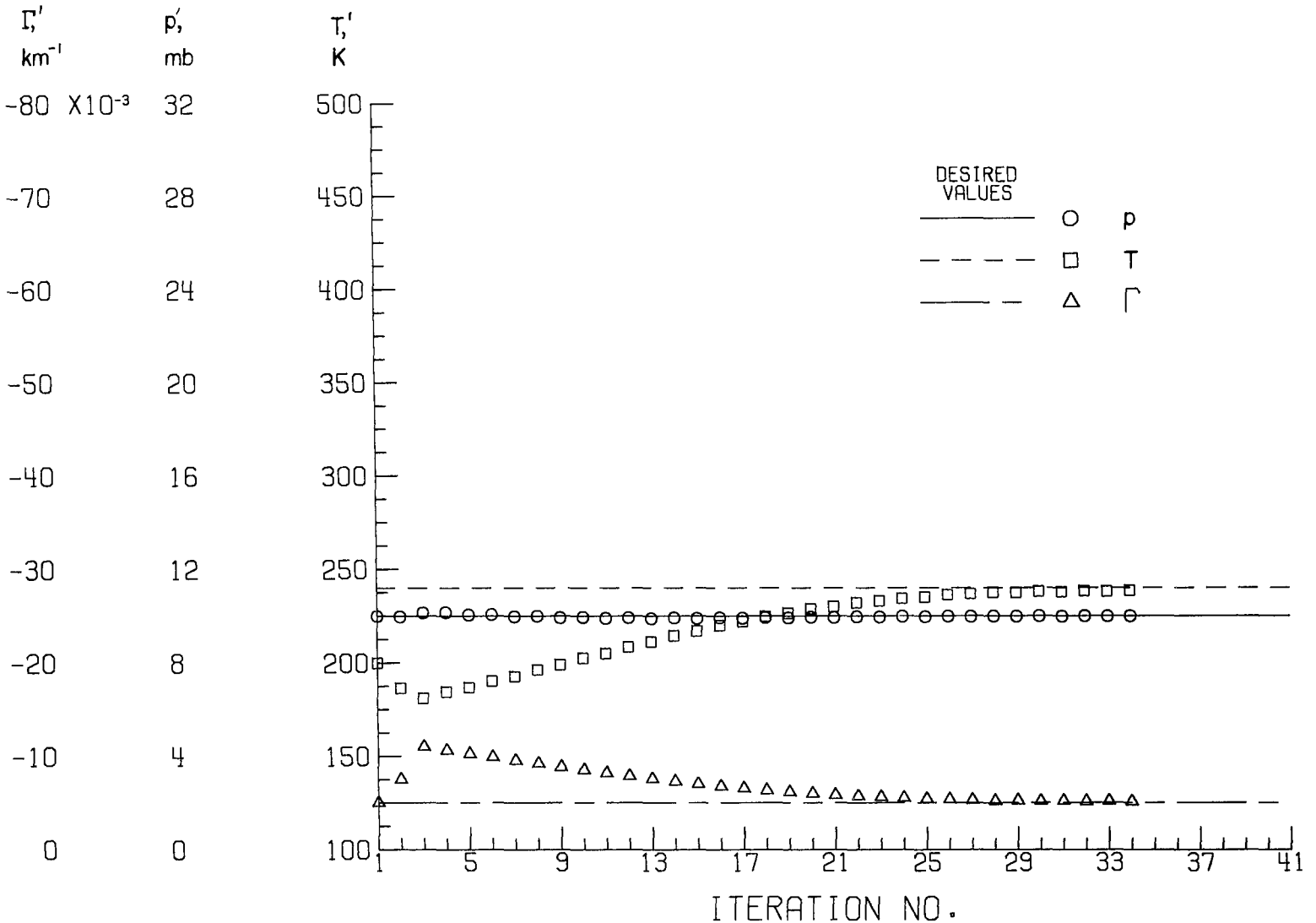

(d) $\lambda = 6500$ Å.

Figure 8.- Concluded.

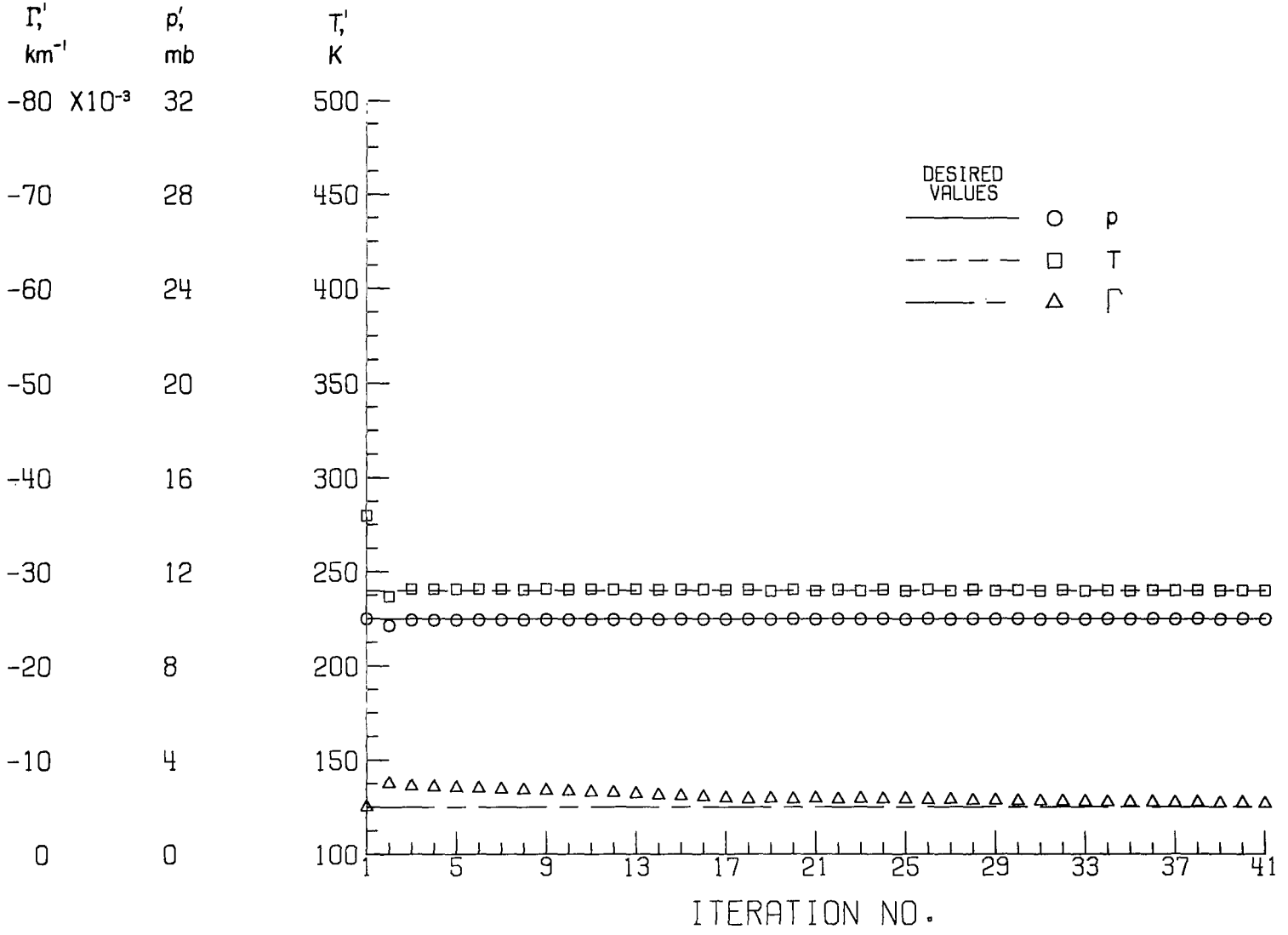

(a) $\lambda = 3500$ Å.

Figure 9.- Convergence plots for $p' = 10$ mb, $T' = 280$ K, and $\Gamma' = -5 \times 10^{-3}$ km^{-1}.

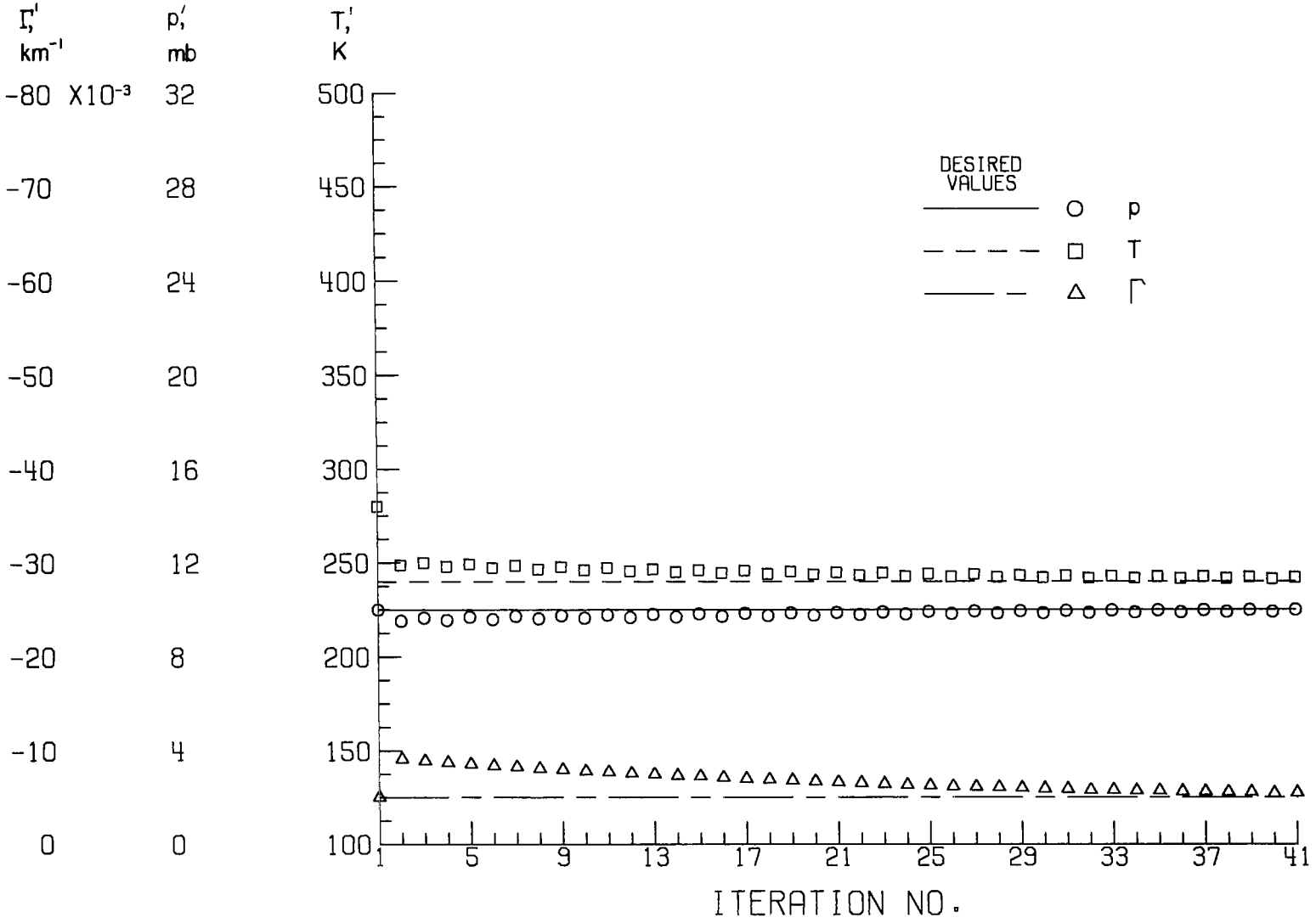

(b) $\lambda = 4700$ Å.

Figure 9.- Continued.

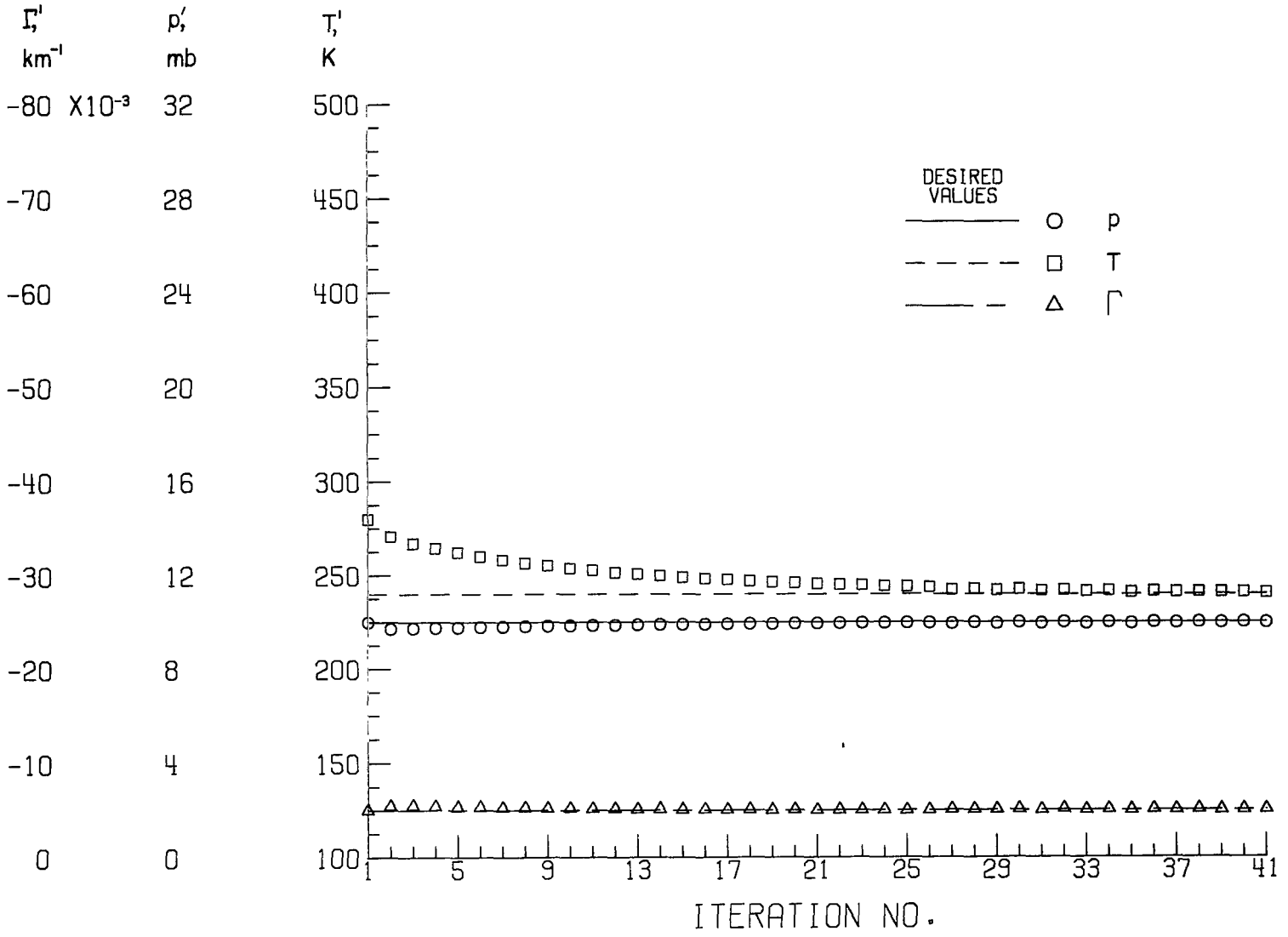

(c) $\lambda = 5500$ Å.

Figure 9.- Continued.

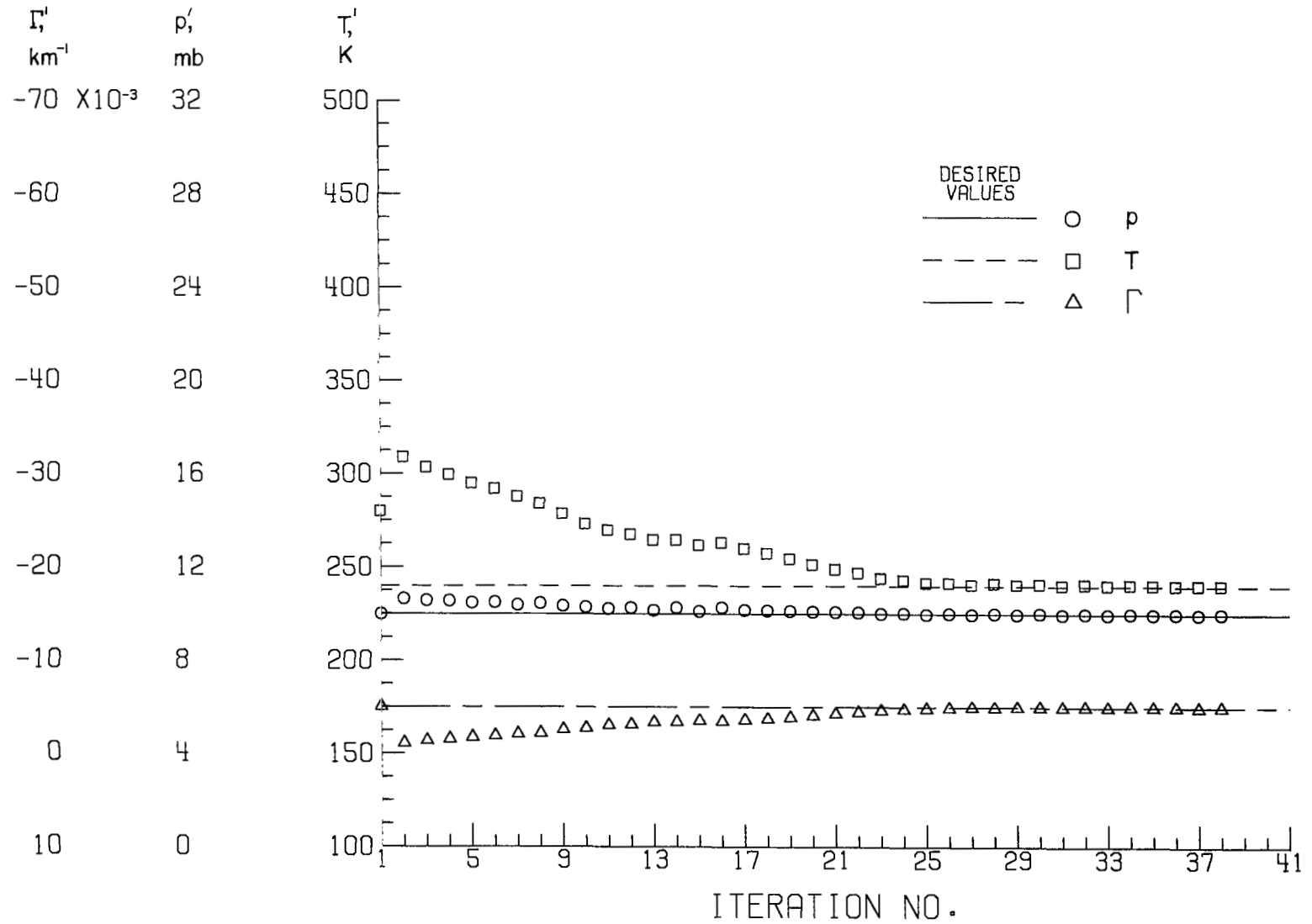

(d) $\lambda = 6500$ Å.

Figure 9.- Concluded.

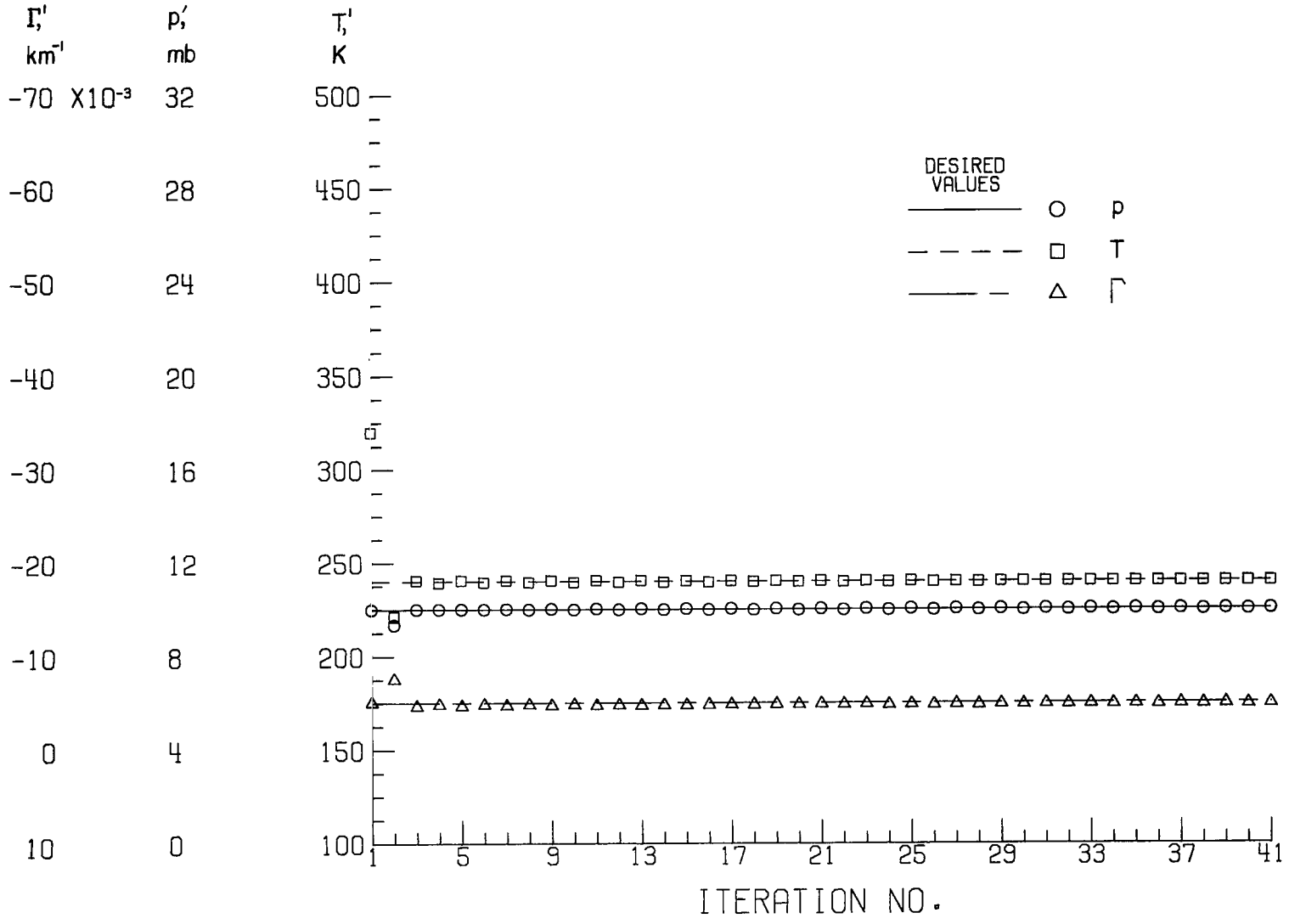

(a) $\lambda = 3500$ Å.

Figure 10.- Convergence plots for p' = 10 mb, T' = 320 K, and $\Gamma' = -5 \times 10^{-3}$ km^{-1}.

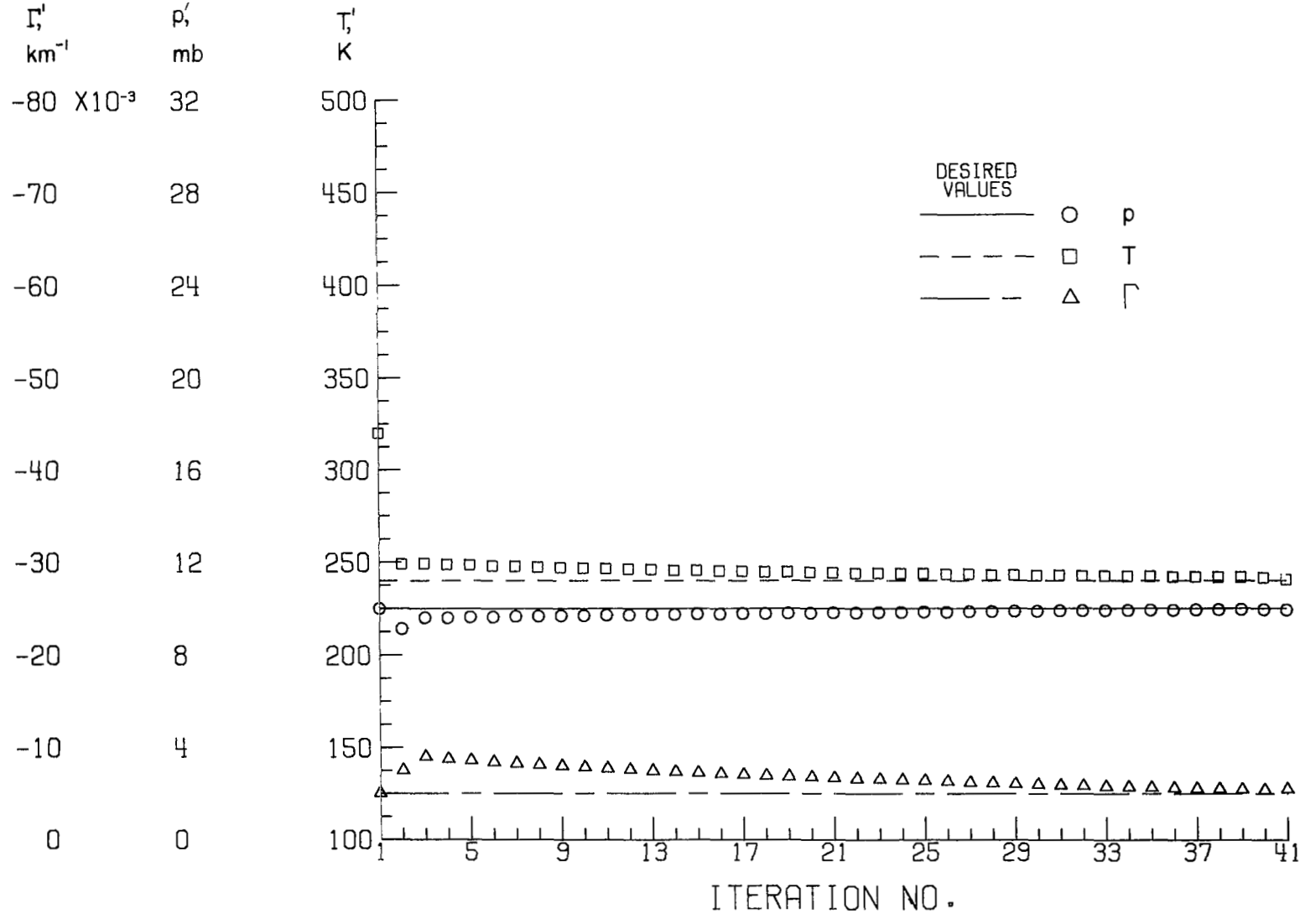

(b) $\lambda = 4700$ Å.

Figure 10.- Continued.

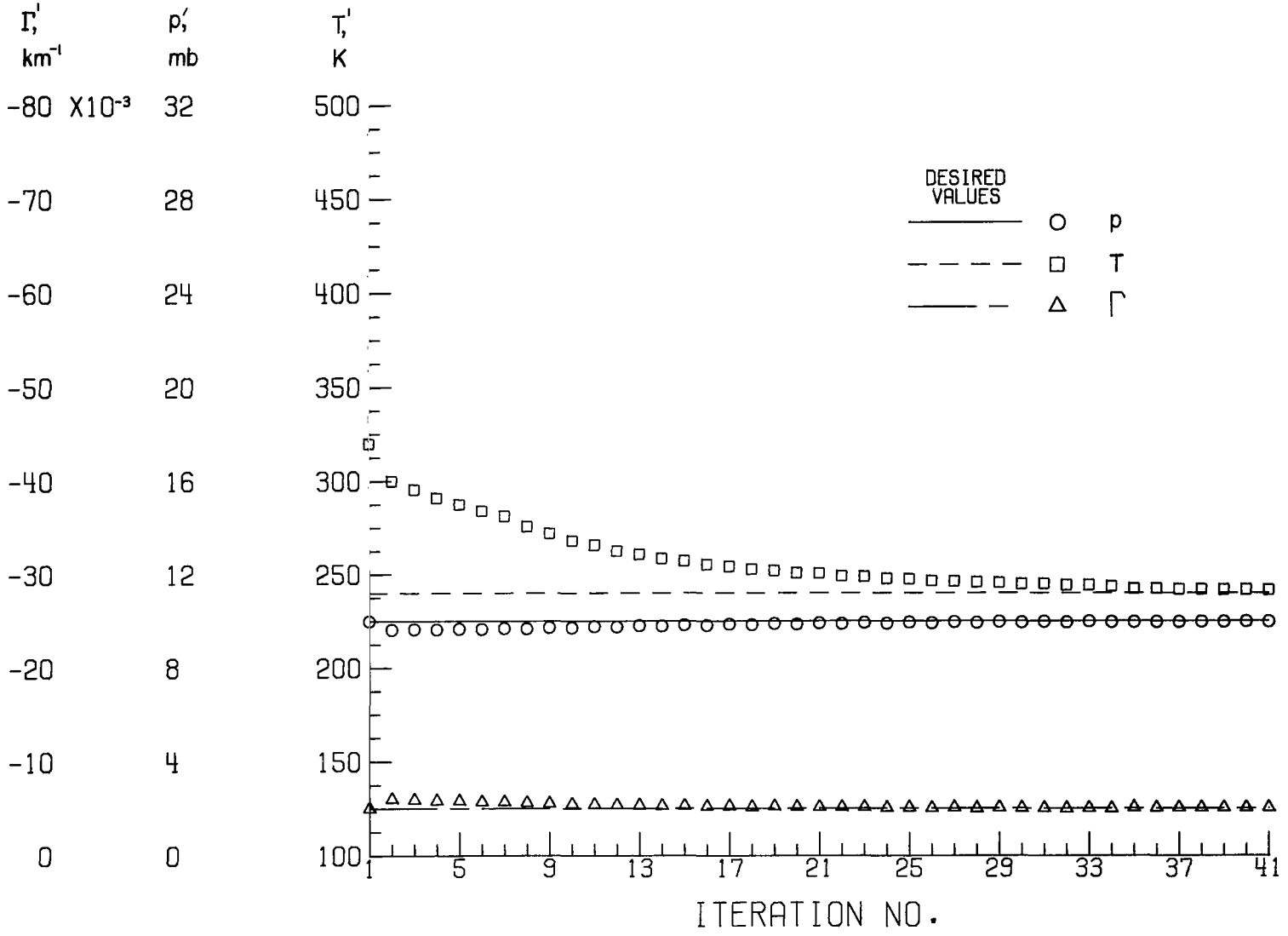

(c) $\lambda = 5500$ Å.

Figure 10.- Continued.

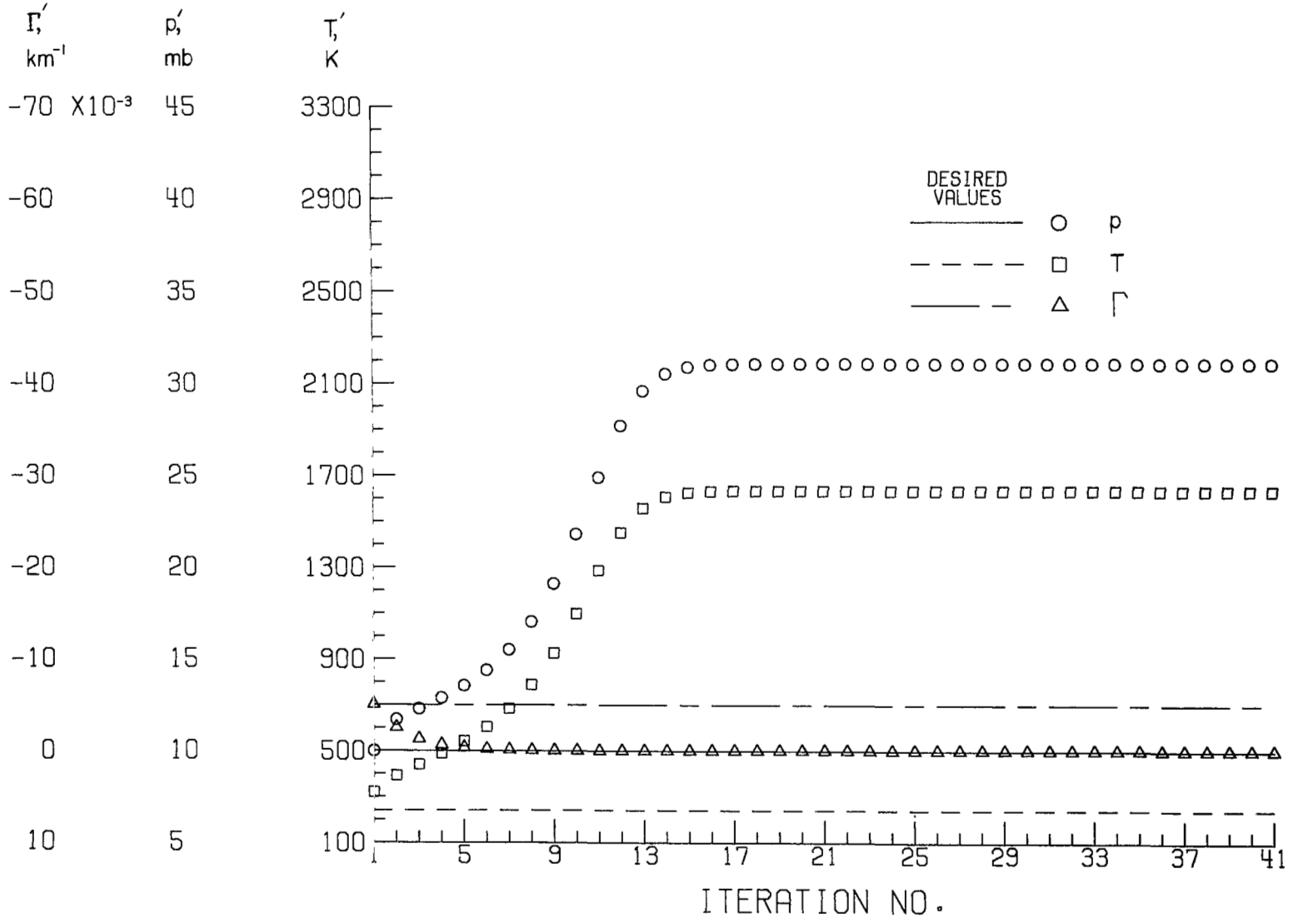

(d) λ = 6500 Å.

Figure 10.- Concluded.

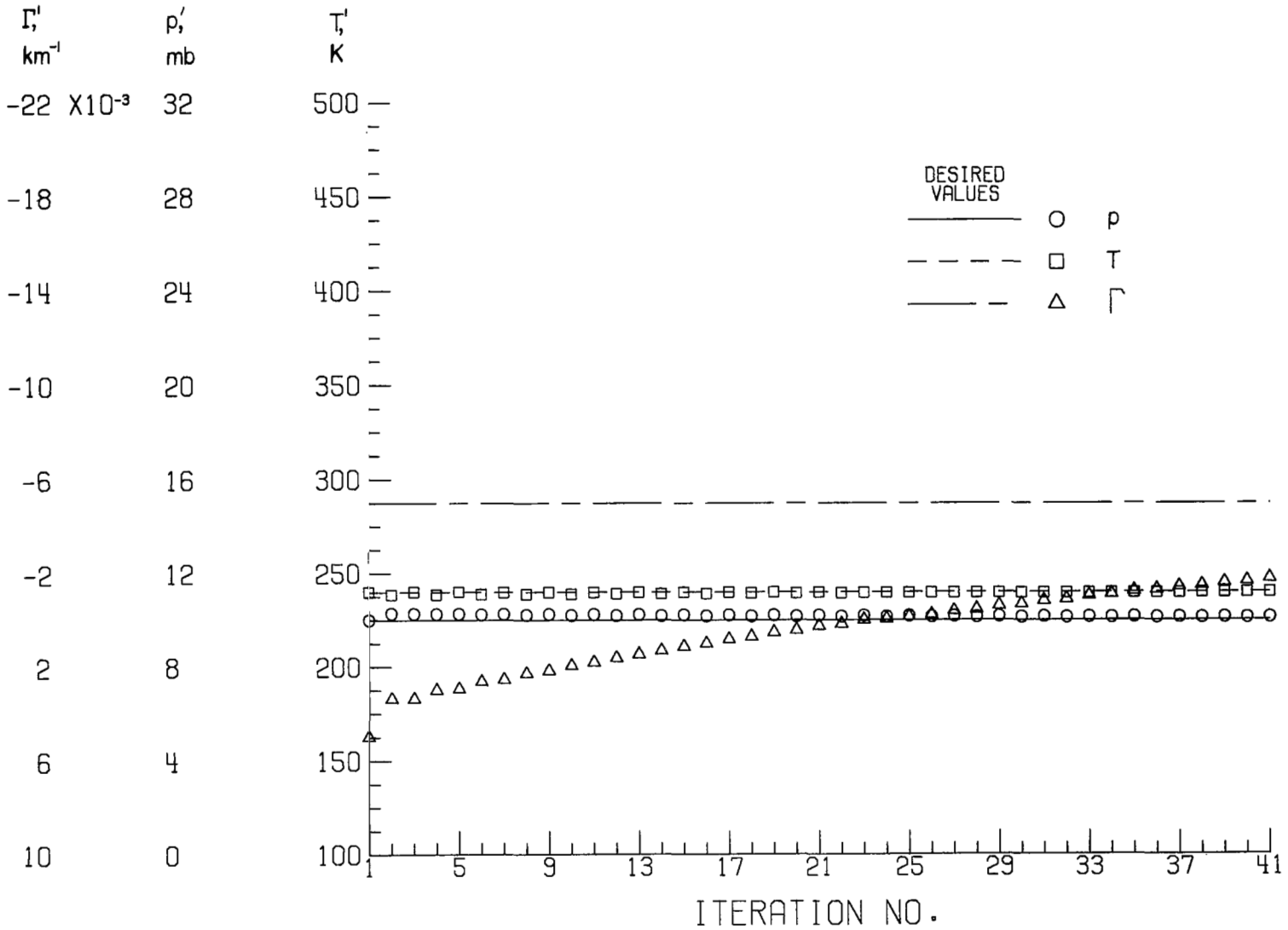

(a) λ = 3500 Å.

Figure 11.- Convergence plots for p' = 10 mb, T' = 240 K, and $\Gamma' = +5 \times 10^{-3}$ km^{-1}.

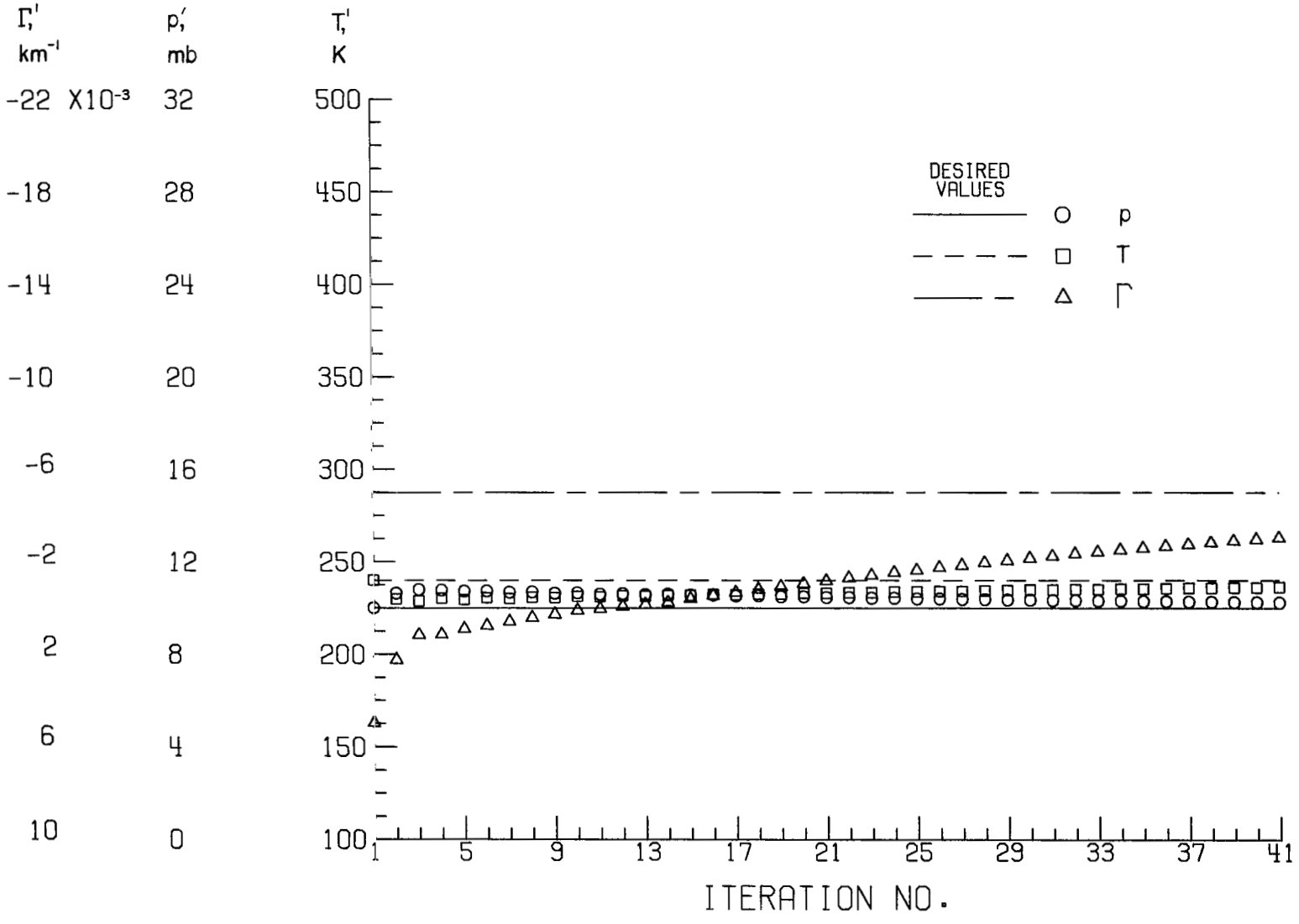

(b) λ = 4700 Å.

Figure 11.- Continued.

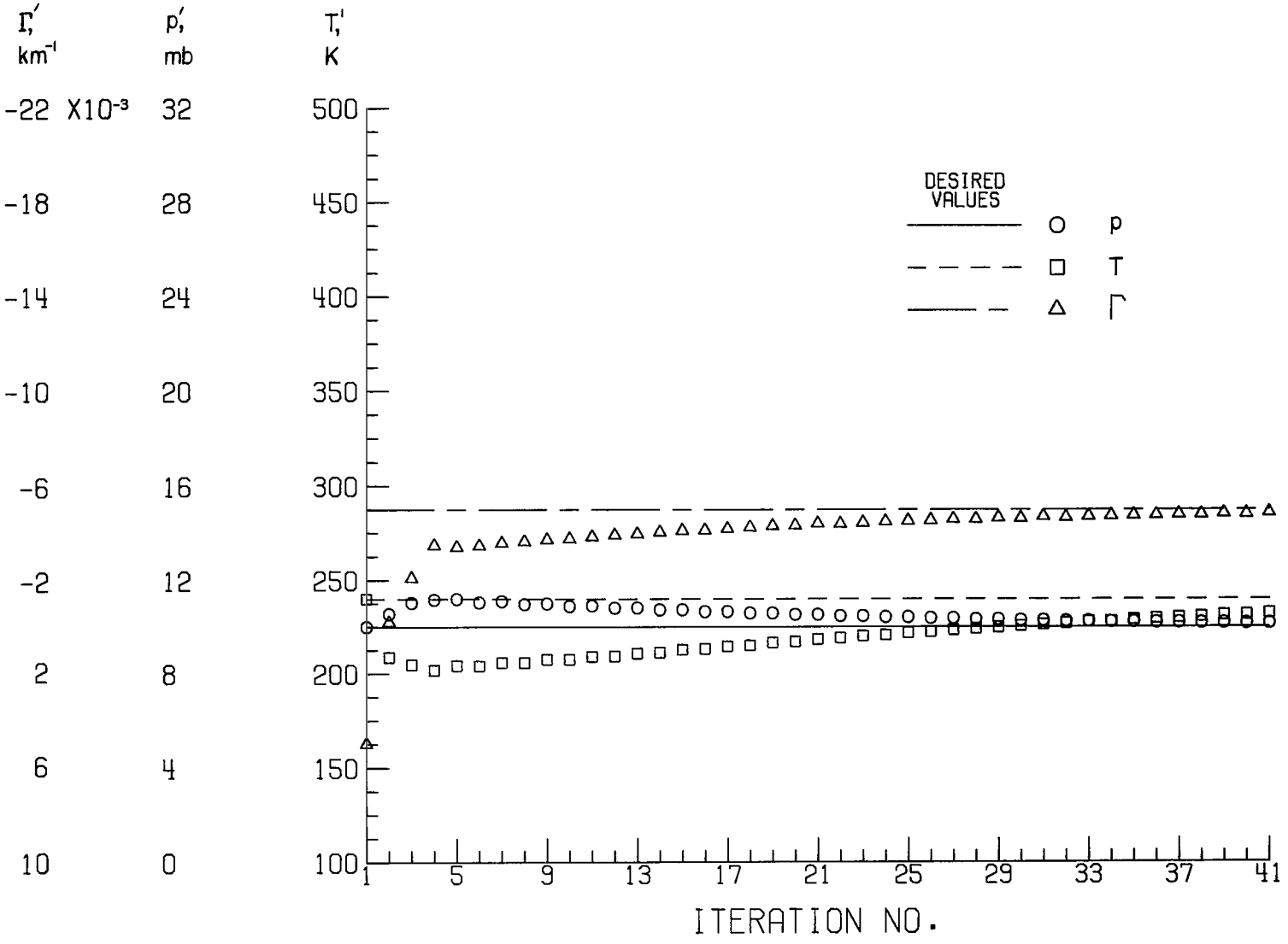

(c) λ = 5500 Å.

Figure 11.- Continued.

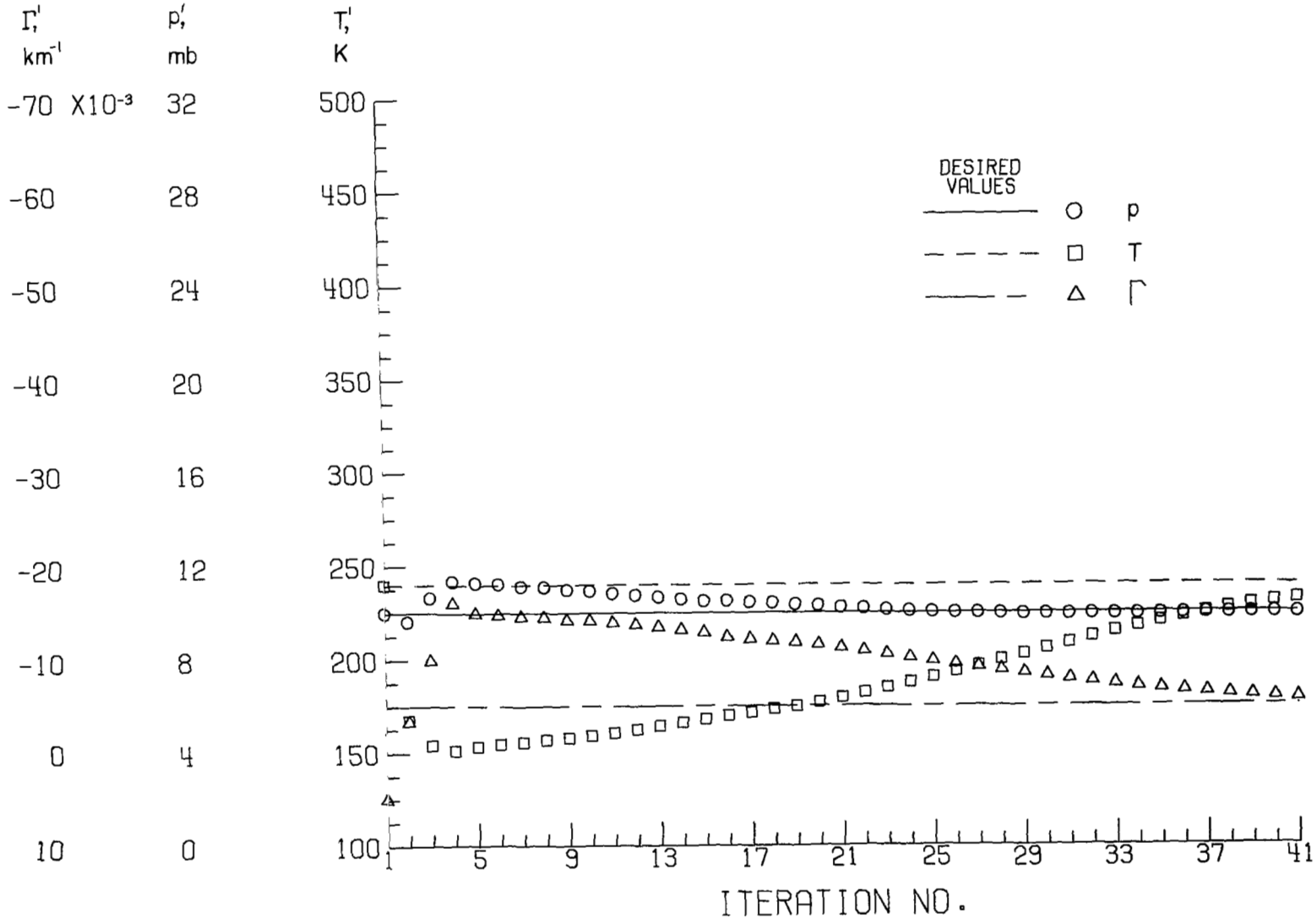

(d) $\lambda = 6500$ Å.

Figure 11.- Concluded.

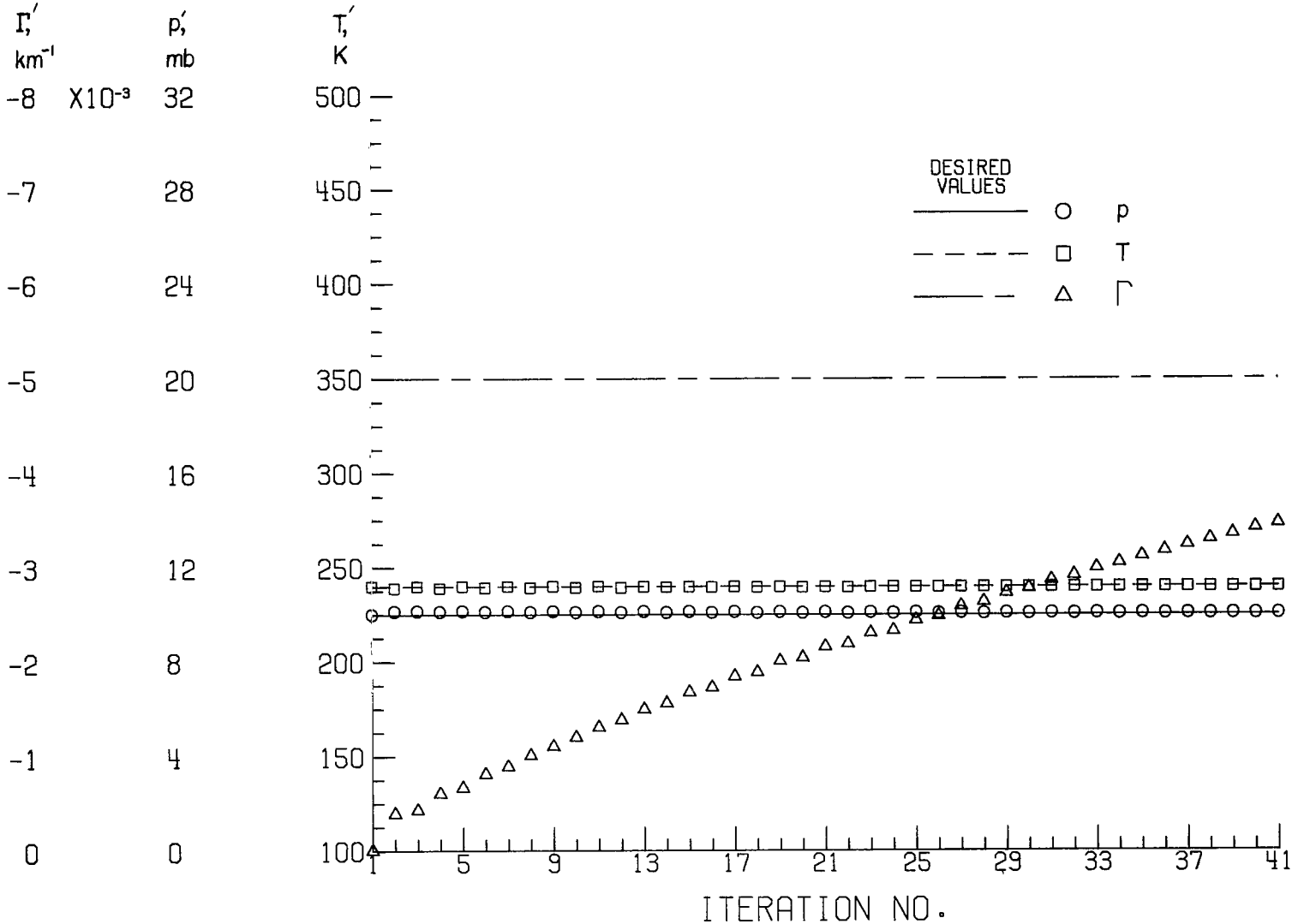

(a) λ = 3500 Å.

Figure 12.- Convergence plots for p' = 10 mb, T' = 240 K, and Γ' = 0.

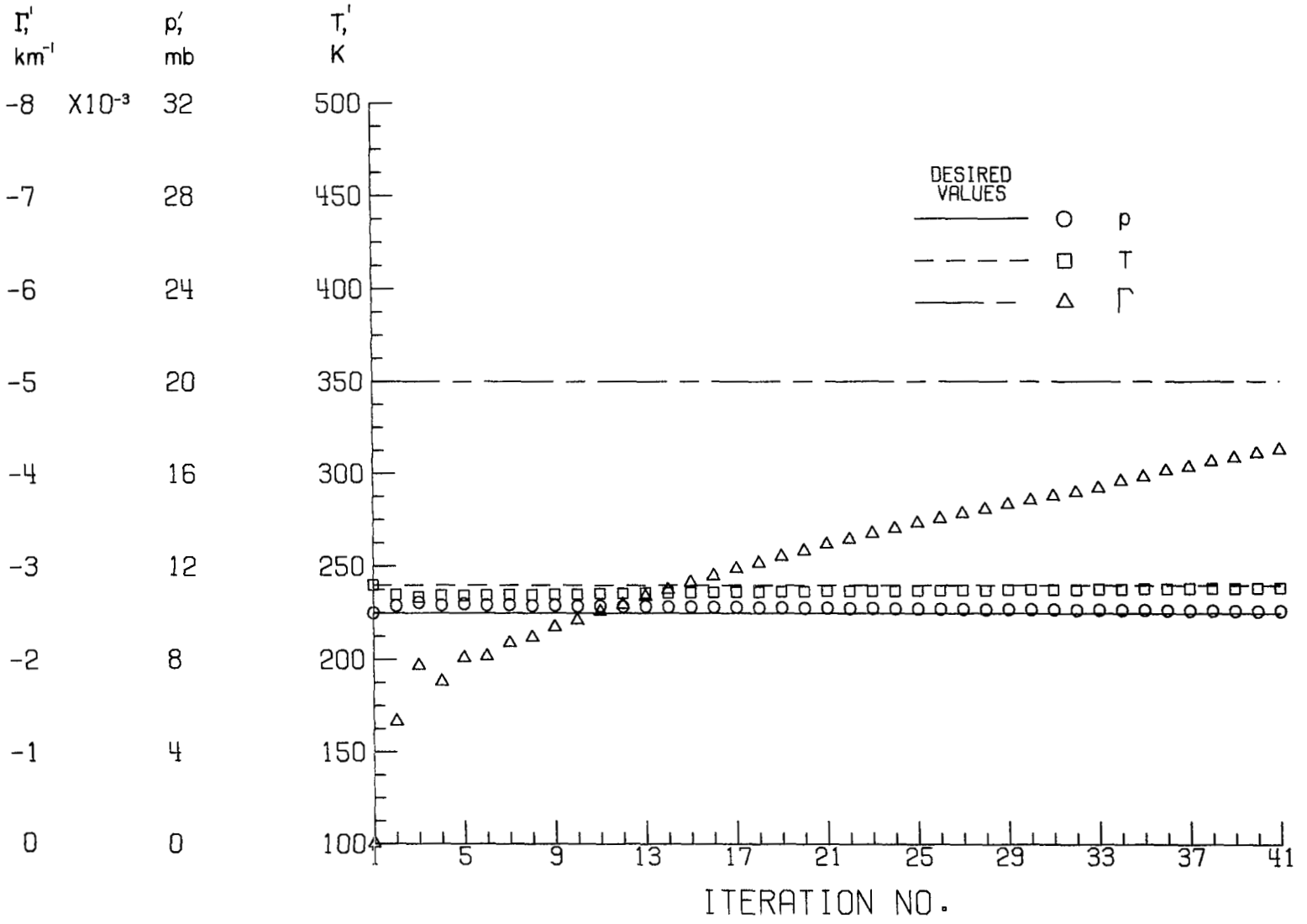

(b) $\lambda = 4700$ Å.

Figure 12.- Continued.

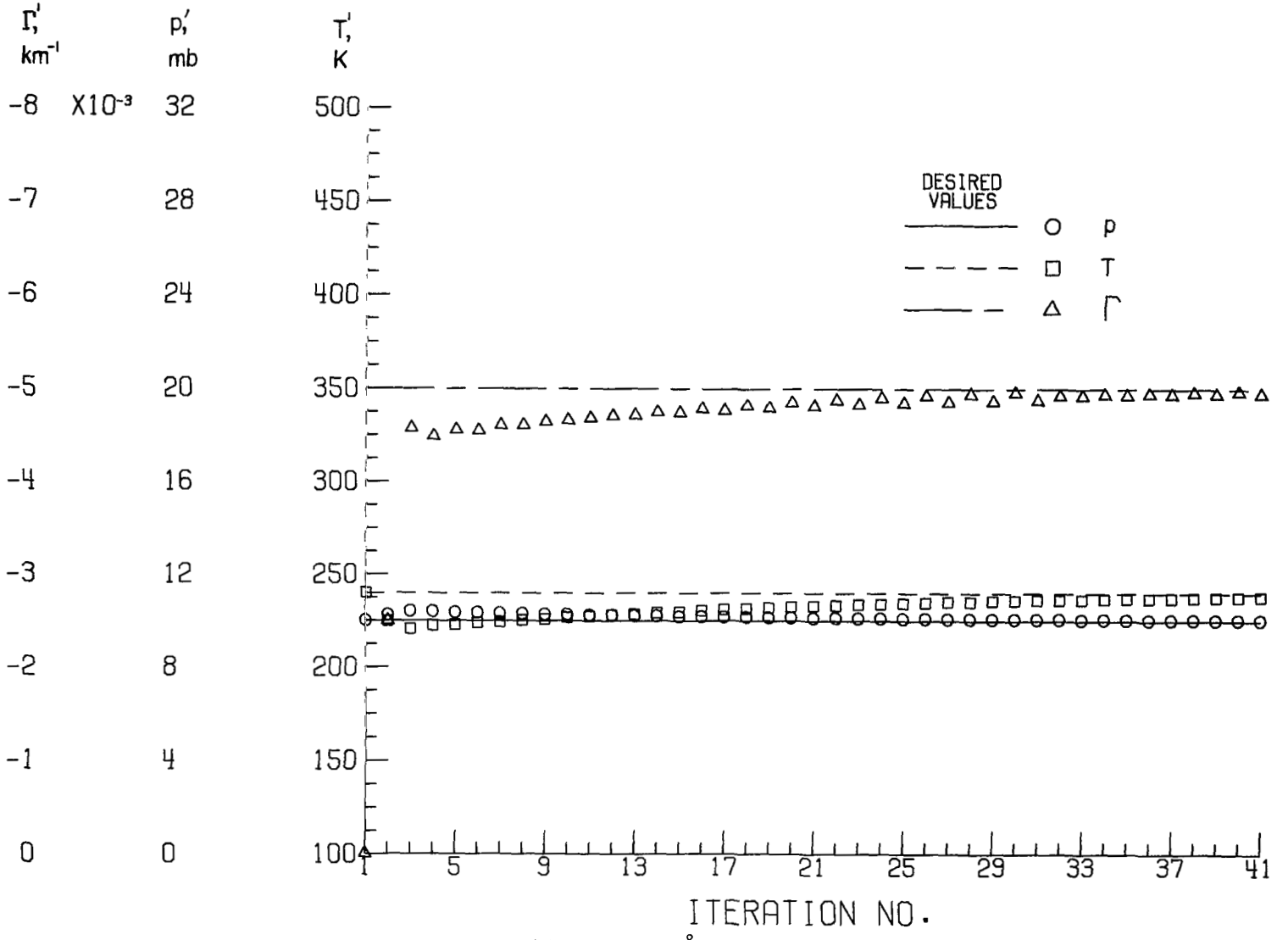

(c) λ = 5500 Å.

Figure 12.- Continued.

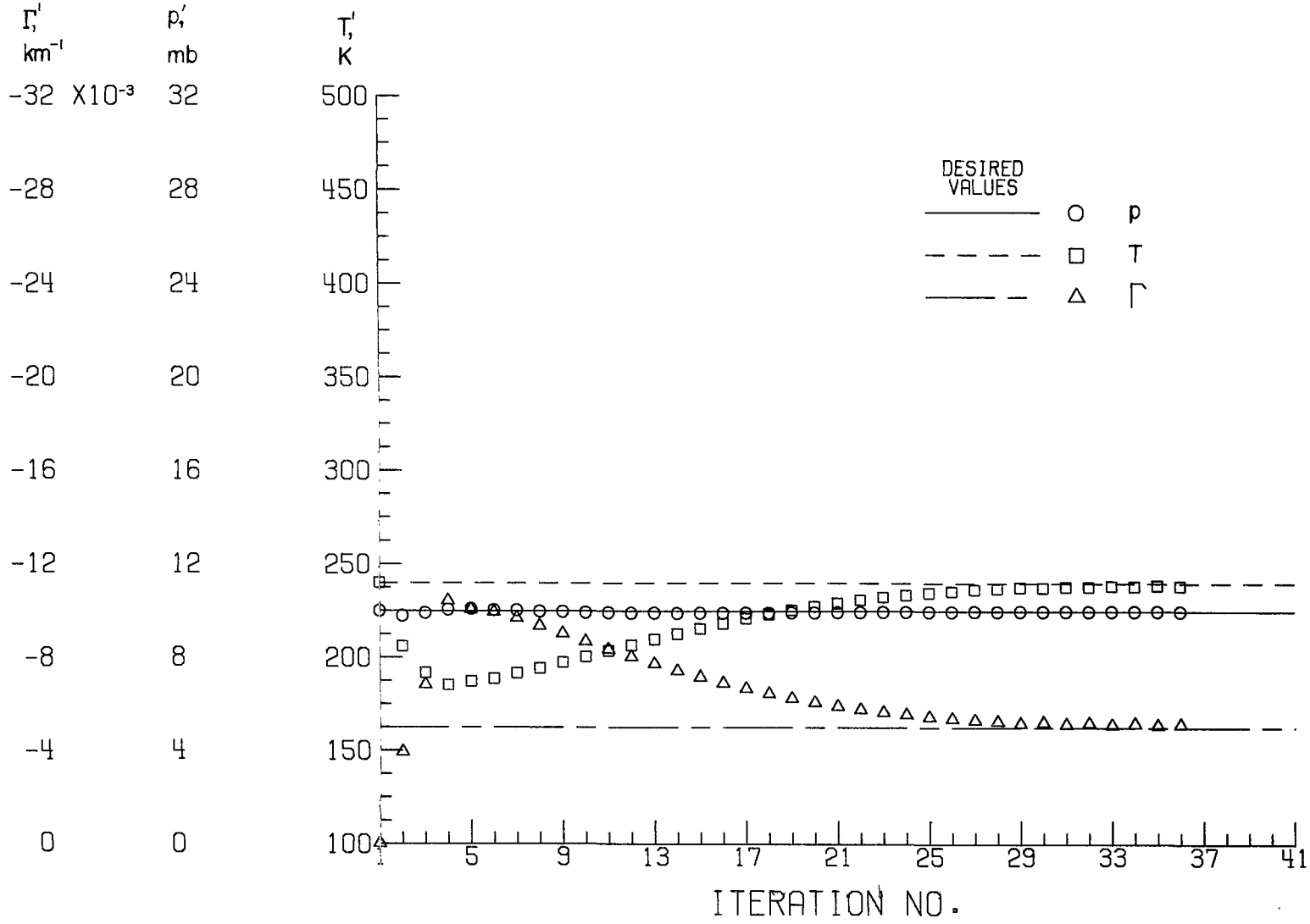

(d) λ = 6500 Å.

Figure 12.- Concluded.

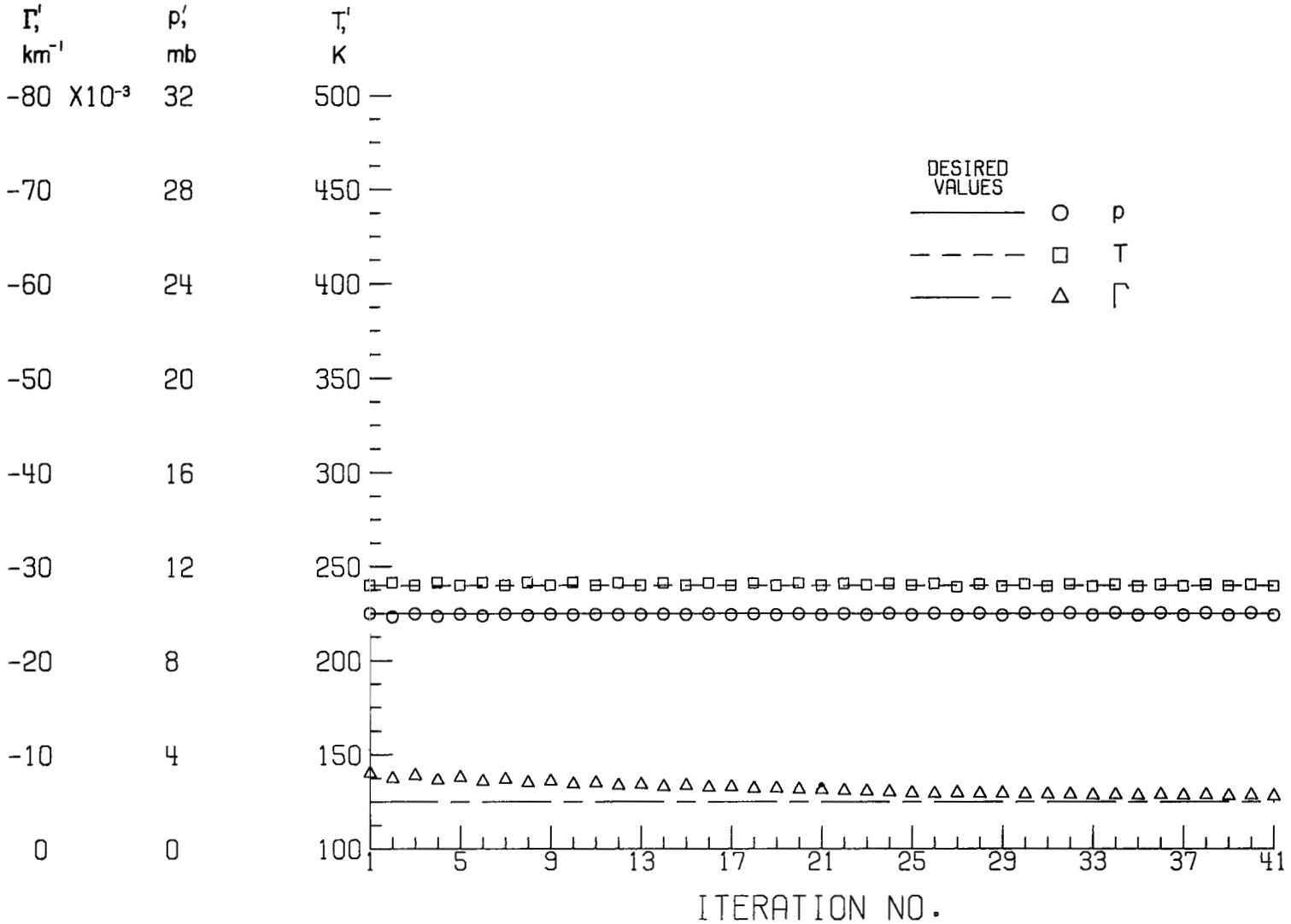

(a) $\lambda = 3500$ Å.

Figure 13.- Convergence plots for $p' = 10$ mb, $T' = 240$ K, and $\Gamma' = -8 \times 10^{-3}$ km^{-1}.

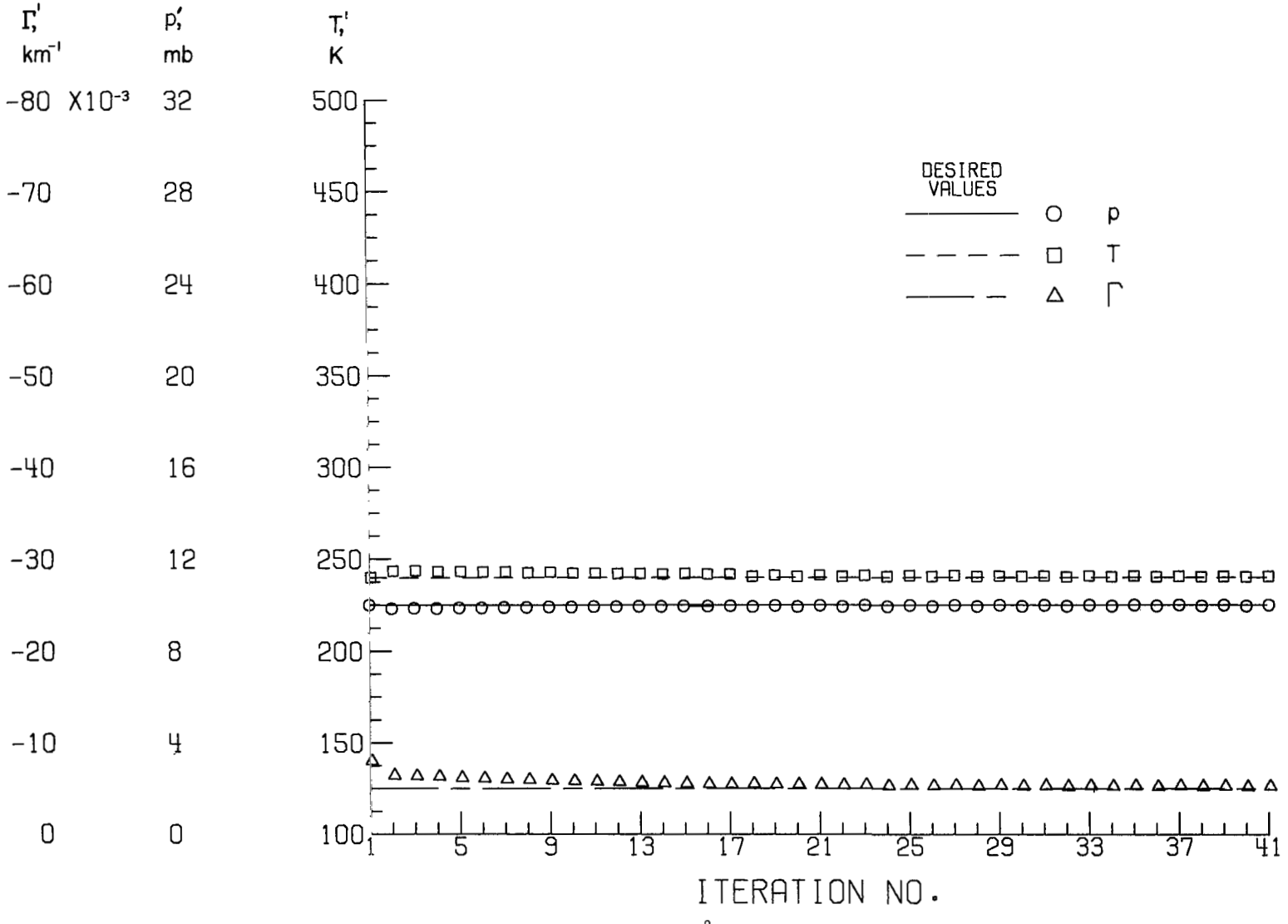

(b) $\lambda = 4700$ Å.

Figure 13.- Continued.

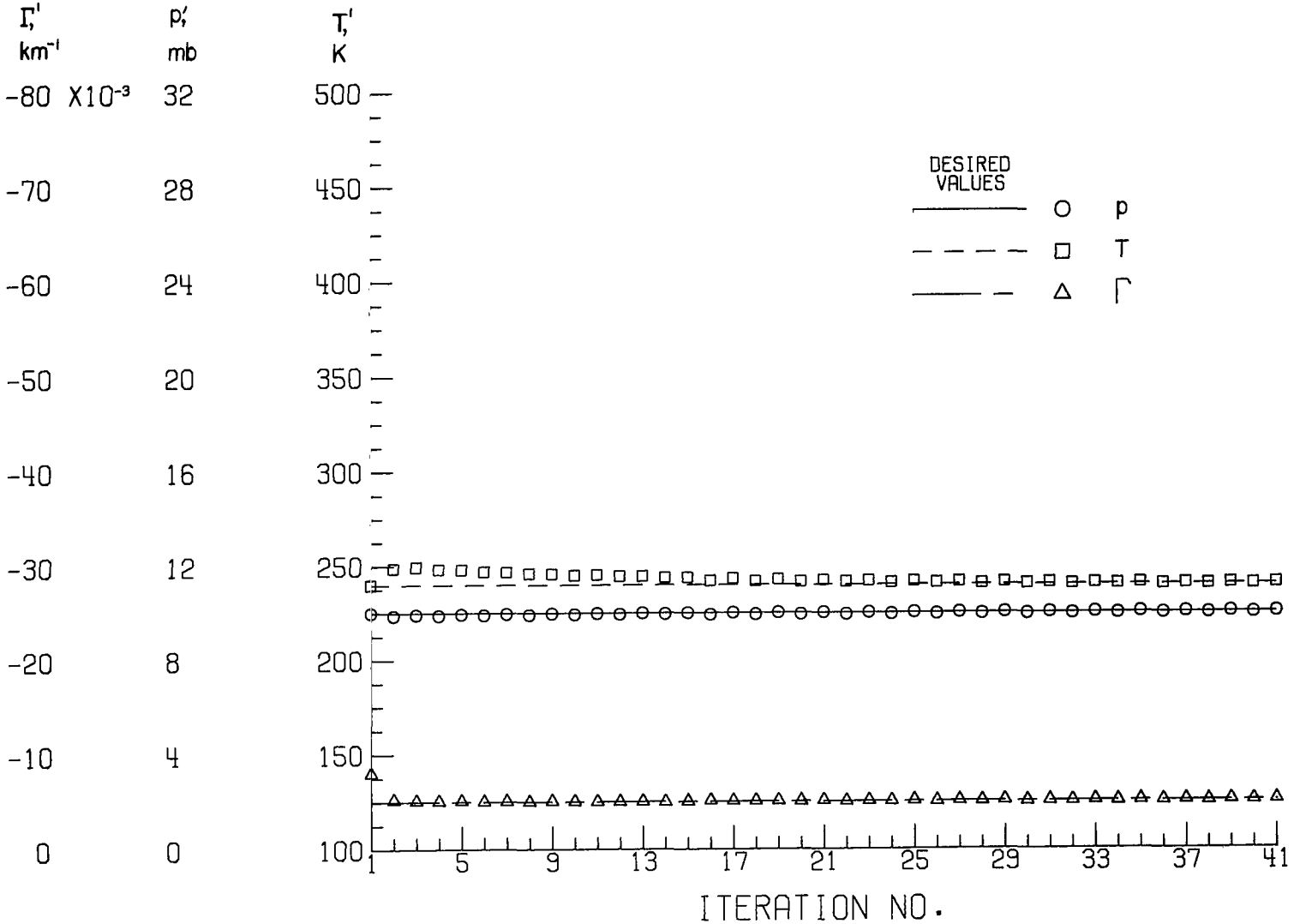

(c) λ = 5500 Å.

Figure 13.- Continued.

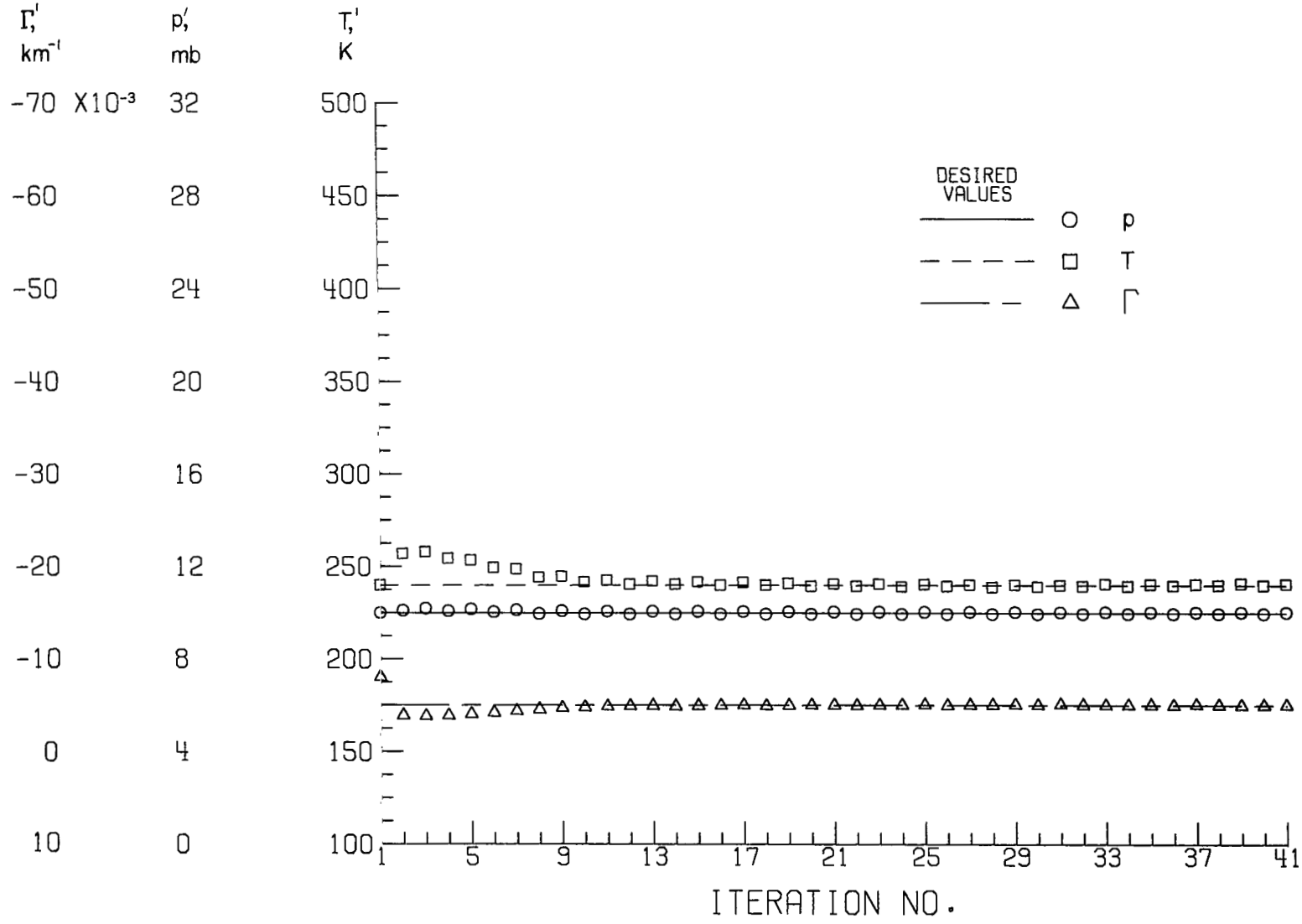

(d) λ = 6500 Å.

Figure 13.- Concluded.

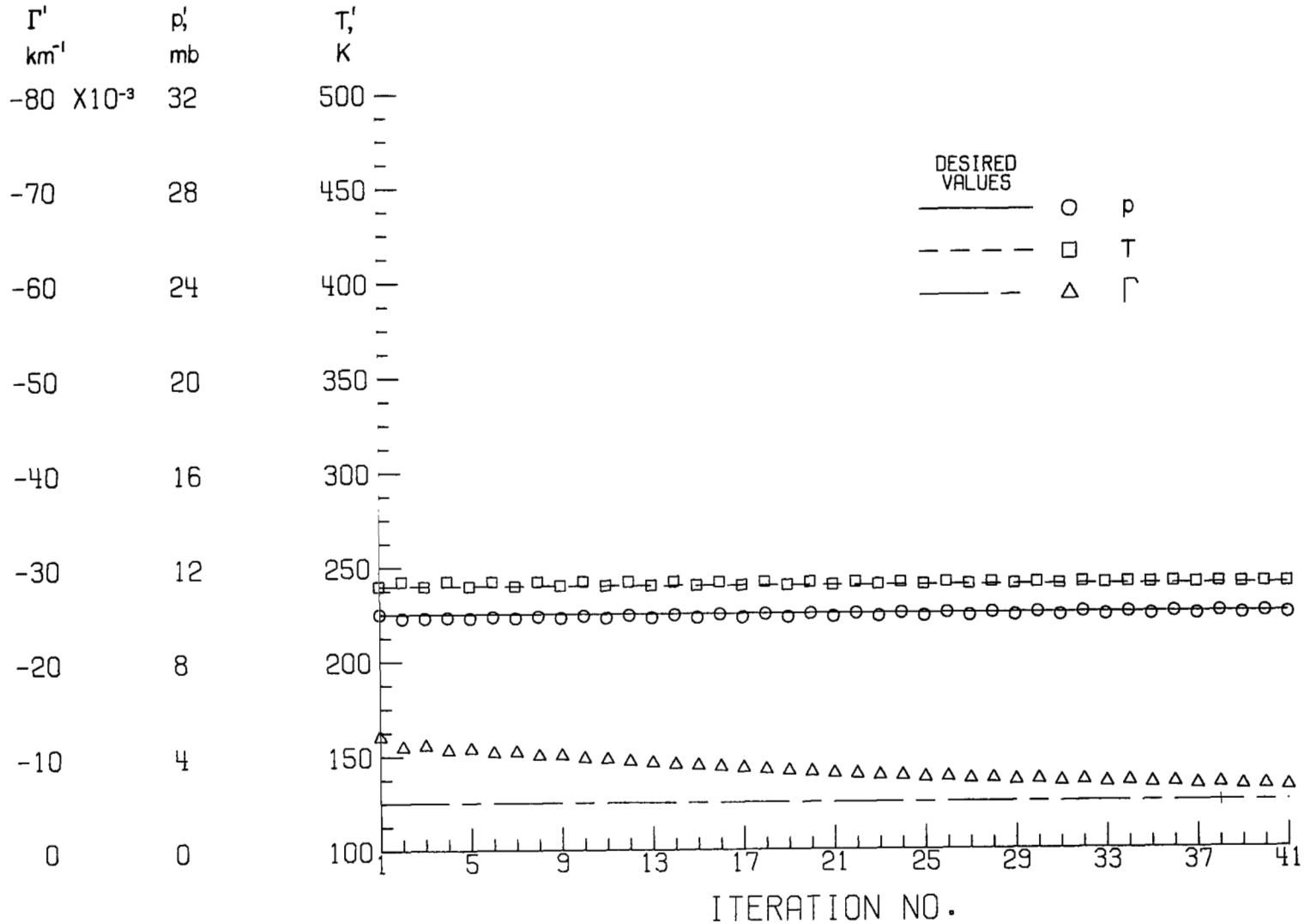

(a) $\lambda = 3500$ Å.

Figure 14.- Convergence plots for $p' = 10$ mb, $T' = 240$ K, $\Gamma' = -12 \times 10^{-3}$ km^{-1}.

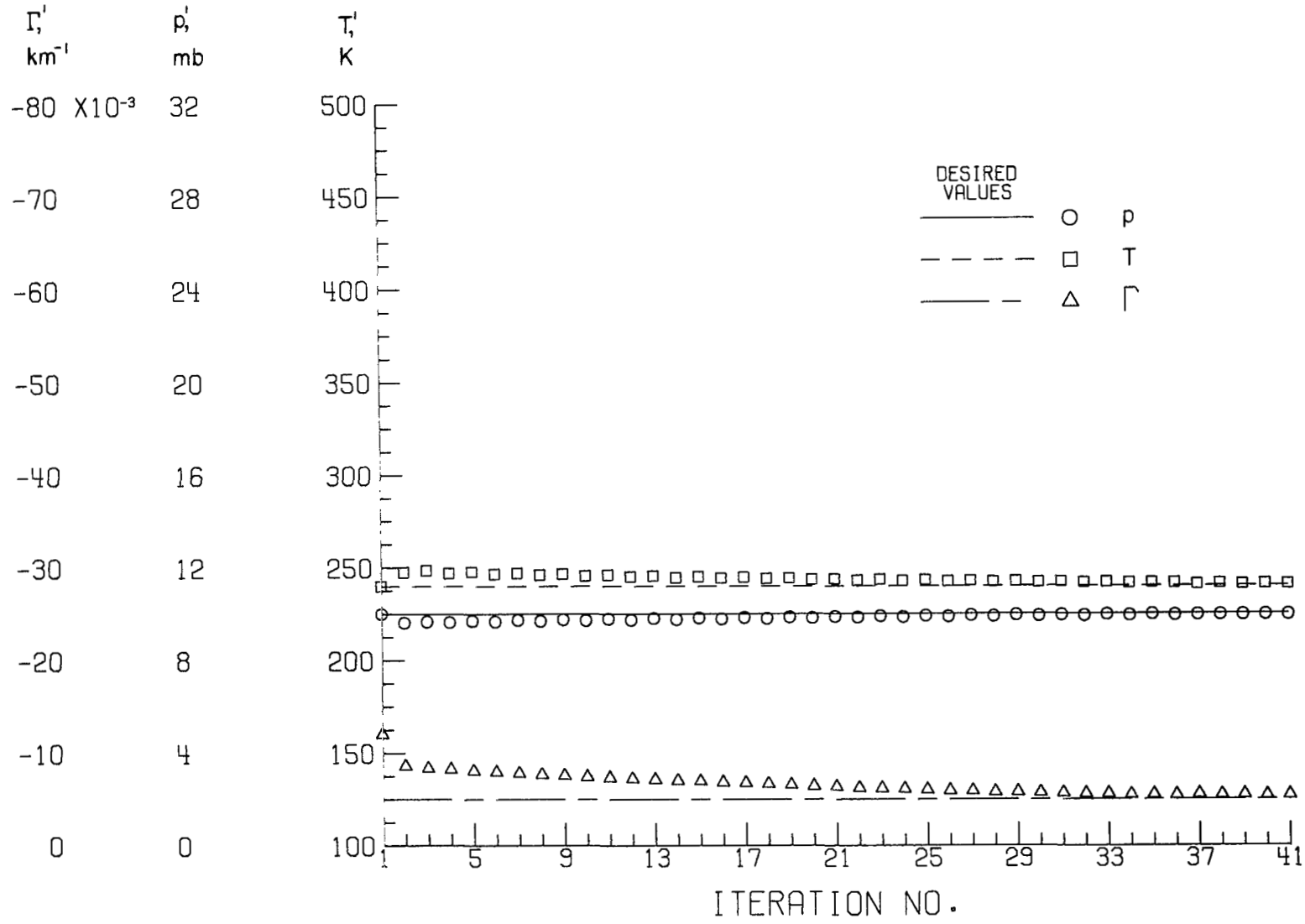

(b) $\lambda = 4700$ Å.

Figure 14.- Continued.

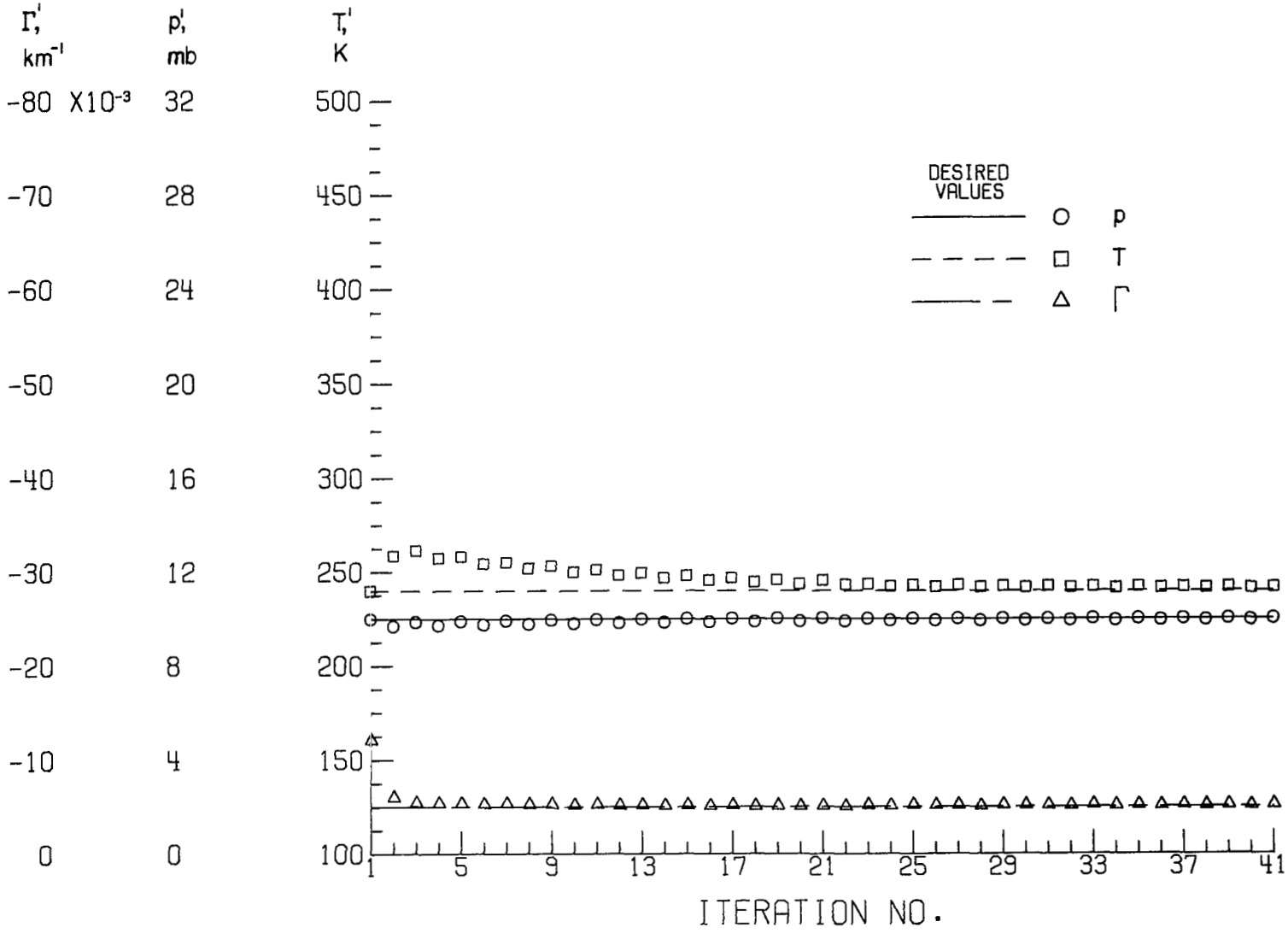

(c) λ = 5500 Å.

Figure 14.- Continued.

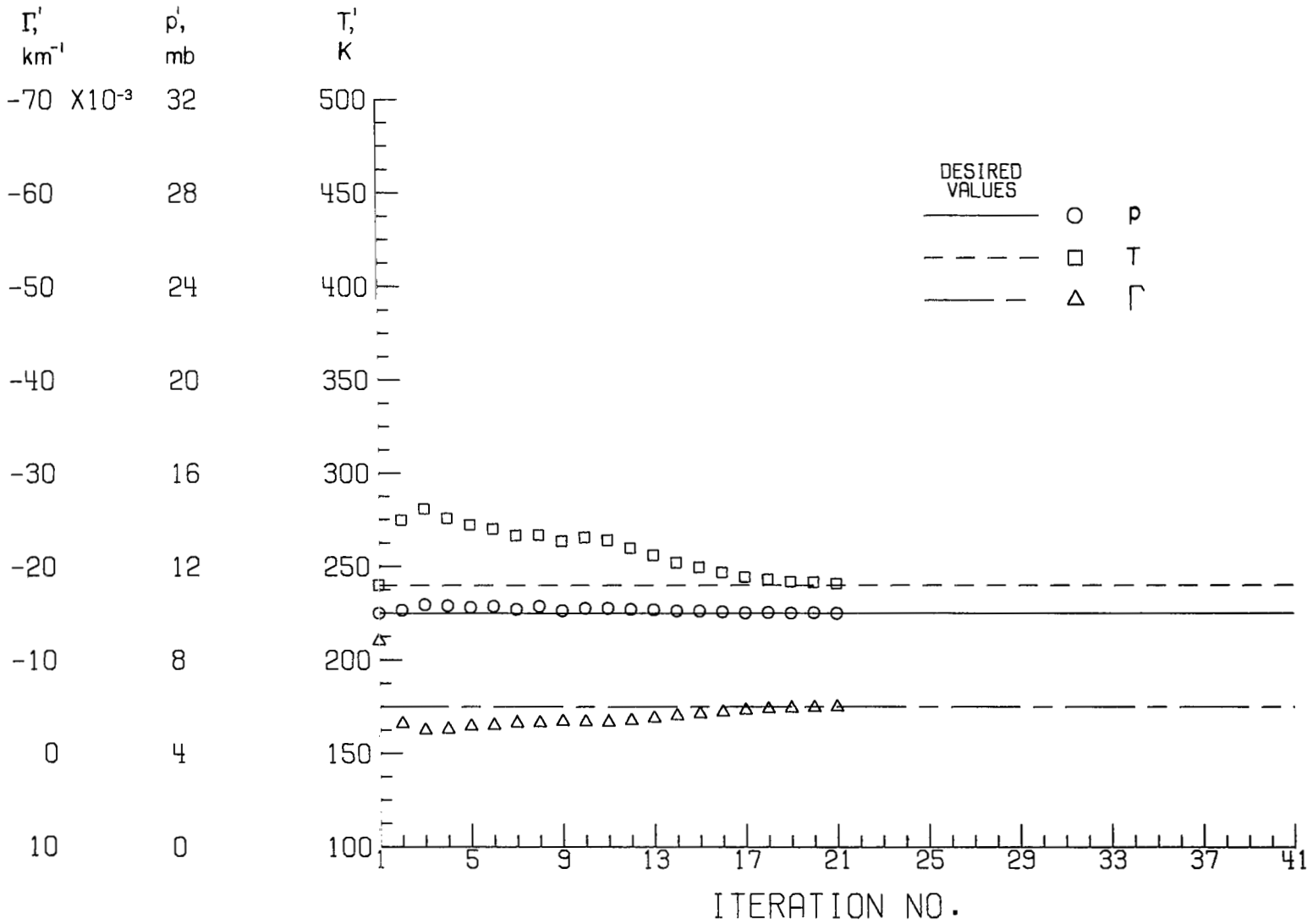

(d) $\lambda = 6500$ Å.

Figure 14.- Concluded.

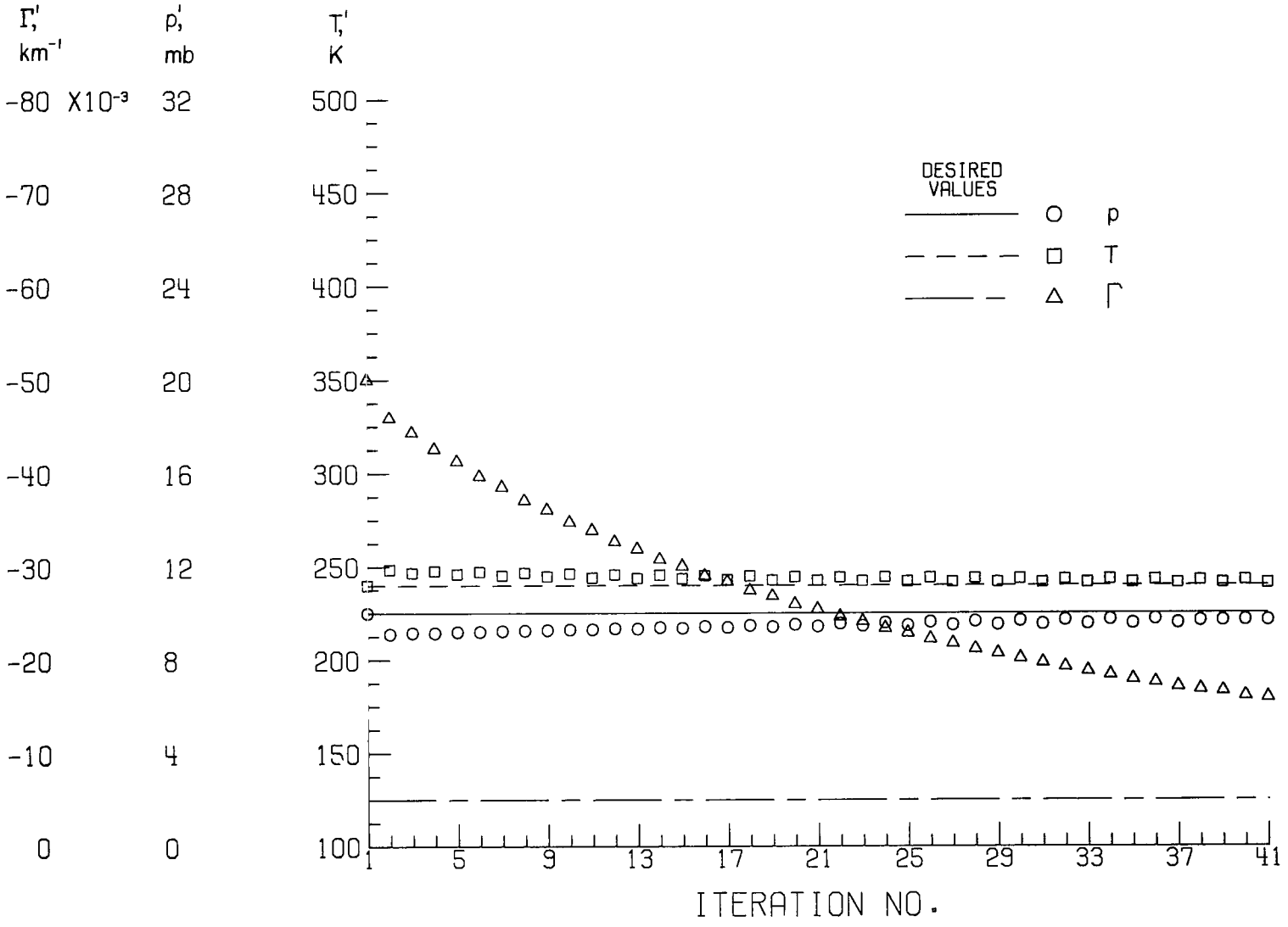

(a) $\lambda = 3500$ Å.

Figure 15.- Convergence plots for $p' = 10$ mb, $T' = 240$ K, and $\Gamma' = -50 \times 10^{-3}$ km^{-1}.

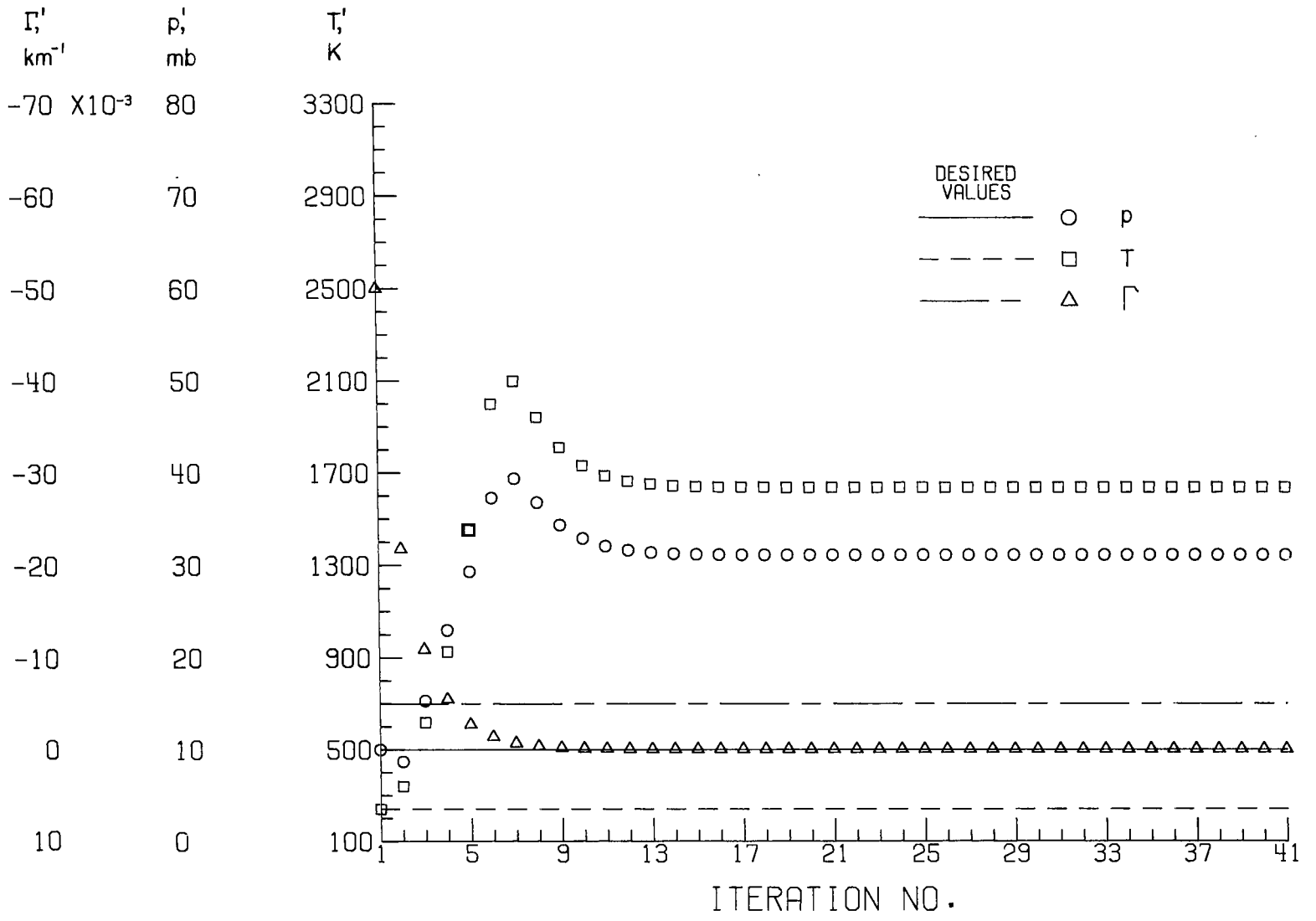

(d) λ = 6500 Å.

Figure 15.- Concluded.

"The aeronautical and space activities of the United States shall be conducted so as to contribute . . . to the expansion of human knowledge of phenomena in the atmosphere and space. The Administration shall provide for the widest practicable and appropriate dissemination of information concerning its activities and the results thereof."

—NATIONAL AERONAUTICS AND SPACE ACT OF 1958

NASA SCIENTIFIC AND TECHNICAL PUBLICATIONS

TECHNICAL REPORTS: Scientific and technical information considered important, complete, and a lasting contribution to existing knowledge.

TECHNICAL NOTES: Information less broad in scope but nevertheless of importance as a contribution to existing knowledge.

TECHNICAL MEMORANDUMS: Information receiving limited distribution because of preliminary data, security classification, or other reasons.

CONTRACTOR REPORTS: Scientific and technical information generated under a NASA contract or grant and considered an important contribution to existing knowledge.

TECHNICAL TRANSLATIONS: Information published in a foreign language considered to merit NASA distribution in English.

SPECIAL PUBLICATIONS: Information derived from or of value to NASA activities. Publications include conference proceedings, monographs, data compilations, handbooks, sourcebooks, and special bibliographies.

TECHNOLOGY UTILIZATION PUBLICATIONS: Information on technology used by NASA that may be of particular interest in commercial and other non-aerospace applications. Publications include Tech Briefs, Technology Utilization Reports and Technology Surveys.

Details on the availability of these publications may be obtained from:

SCIENTIFIC AND TECHNICAL INFORMATION OFFICE

NATIONAL AERONAUTICS AND SPACE ADMINISTRATION

Washington, D.C. 20546